Faculty of Science and Technology, Department of Geosciences

Late glacial and deglacial paleoceanographic and environmental changes at Vestnesa Ridge, Fram Strait

Challenges in reading methane-influenced sedimentary records

—

Kamila Andżela Sztybor

A dissertation for the degree of Philosophiae Doctor – November 2016

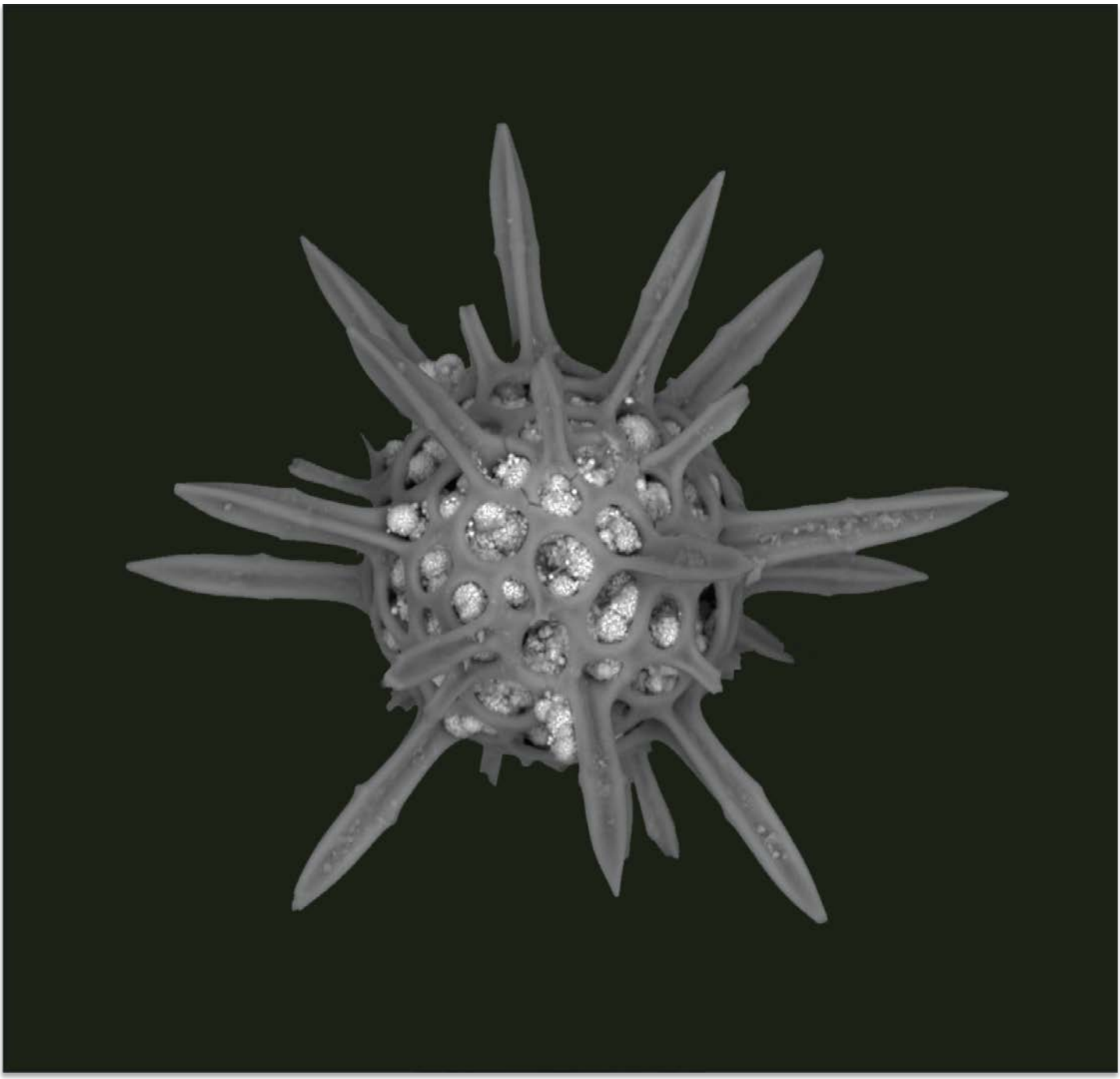

Faculty of Science and Technology, Department of Geosciences,
UiT The Arctic University of Norway

Late glacial and deglacial paleoceanographic and environmental changes at Vestnesa Ridge, Fram Strait: challenges in reading methane-influenced sedimentary records.

Kamila Andżela Sztybor

A dissertation for the degree of Philosophiae Doctor

Tromsø, November 2016

Table of contents

Acknowledgements

First I would like to thank my main supervisor Tine L. Rasmussen for continuous support during my PhD study. Thank you for the enthusiasm, encouragement, pushing me farther then I thought I could go and for not letting me to give up when the bad circumstances occurred. I appreciate your guidance and immense knowledge.

I would like to thank my co-supervisors Jürgen Mienert and Stefan Bünz for giving me the opportunity to join this interesting PhD project.

Thank you to Trine Dahl and Stefan Bünz for introducing me to the Institute of Geology and valuable advices received at the beginning of my stay in Tromsø.

I am thankful to all my friends and colleagues from the department, it was a great pleasure working with you. I thank my office mates Mariana, Calvin, Giacomo, Emmelie and Siri for a pleasant working environment, thank you for your understanding of my situation and why I was not always the most social person and for all your kind words and support. I thank Mohamed for many stimulating, not necessarily scientific discussions during numerous late evenings at work. For technical help and advices related to my work I would like to thank Trine, Matthias, Ingvild, Karina, Margrethe, Steinar, Bjørn Runar, Rolf and Bjørn Ivar. For all the fun I had during trips, cruises, conferences and social events I would like to thank Pati, Kasia, Noortje, Denise, Juho, Steffen, Ulli, Sunil, Sandra, Mohamed, Julia, Chiara, Monica, Mariana, Yulia, Giacomo and Alex.

I am grateful to Kasia and Steffen for having their office and home door always open, the continuous support, sharing with me your time, experience and the delicious homemade food.

I thank Ania, Morten, Ulli, Jesper, Lauri, Sunil and Tommy for being with me in my darkest days and helping me to survive all the stress.
My special thanks go to Ania, I am extremely lucky to move from Poland above the Arctic Circle and still have best friend since high school living in the same town as me. Even though you are very busy with work and family you always find time to help me with my everyday dilemmas, words cannot describe how grateful I am.

I would like to thank Hannah, Lauri, Ilona, Johanna and Tim for distracting me from work on the thesis during skiing, hiking and climbing activities. Thank you for your patience and not giving up on me even though I turned you down so many times, because I had to work.
I am thankful to Ilona and Johanna for all the support and concern in the final phases of our PhDs.

I would like to thank friends in Poland Jovita, Paweł, Wiola and Iwona for not forgetting me and always finding time for me in your busy schedules when I suddenly showed up.

My sincere thanks also goes to Joan Bernhard and Dan McCorkle who provided me guidance and access to the research facilities during my stay at WHOI.

I am grateful to Jan Marcin Węsławski, Marek Zajączkowski and Katarzyna Błachowiak-Samołyk for their support and introducing me to the world of science.

Szczególne podziękowania dedykuję mojej rodzinie, moim rodzicom i siostrze, za ogromne wsparcie w trakcie pisania tej pracy a także na każdym etapie życia. Dziekuję za nieustanną motywację, otuchę, wiare we mnie i za sprawiane że z każdego zakątka na świecie zawsze chętnie wracam do domu.

Preface

This doctoral thesis is the result of PhD study, which started in September 2010. Four years of the PhD study were funded by UiT the Arctic University of Norway, and six months by the Research Council of Norway through its Centre of Excellence funding scheme for CAGE, project number 223259. The last 18 months were carried out without any funding. The Norwegian Research School in Climate Dynamics (ResClim) and CAGE contributed in funding laboratory analyses.

The study included one year assigned for duty work for the Department of Geology. It was finalized during assisting in teaching of courses: GEO-3111 Reconstructing Quaternary marine environments", GEO-3122 "Marine micropaleontology", GEO-3145/8145 "Arctic marine geology and geophysics workshop" and in multiple (stopped counting after 14) cruises. The PhD study included also a three and half month research stay at Woods Hole Oceanographic Institution, USA in autumn 2013. The results of this thesis were presented in national workshops and international conferences. In total 11 countries distributed on four continents were visited during this PhD appointment (Fig. 1).

Figure 1. Places visited during PhD related travels. First three from the left: San Francisco and Cape Cod, USA; Nuuk, Greenland. Rest from the top to the bottom: Longyearbyen, Svalbard; Tromsø, Norway; Torshavn, Faroe Islands; Bergen, Norway, Copenhagen and Aarhus, Denmark; Texel, The Netherlands; Bonn, Germany; Nice, France; Sitges, Spain; Taipei, Taiwan; Wellington, New Zealand. Map from Wikimedia Commons.

This thesis consist of an introduction and three articles:

Sztybor K. and Rasmussen T. L. **Diagenetic disturbances of marine sedimentary records from methane influenced environments in the Fram Strait as indications of variation in seep intensity during the last 35 000 years.** *Boreas, DOI 10.1111/bor.12202*

Sztybor K. and Rasmussen T. L**. Late glacial and deglacial paleoceanographic and environmental changes at Vestnesa Ridge, Fram Strait.** *In review in Paleogeography, Palaeoclimatology, Palaeoecology*

Sztybor K., Rasmussen T. L. and Laier, T. **"Excess sulfur" in sediments from western Svalbard margin as indication for the efficiency of the microbial filter in paleo-Anaerobic oxidation of methane (AOM).** In preparation for submission to Chemical Geology.

1. Introduction and objectives

Methane hydrates are ice-like structure consisting of methane entrapped in a cage of water molecules. The hydrates form and remain stable under specific conditions requiring a sufficient amount of methane and water, high pressure and low temperatures (Sloan, 1998). Such conditions occur mainly on the continental margins and determine the widespread distribution of gas-hydrate systems (Judd and Hovland, 2007) (Fig.2).

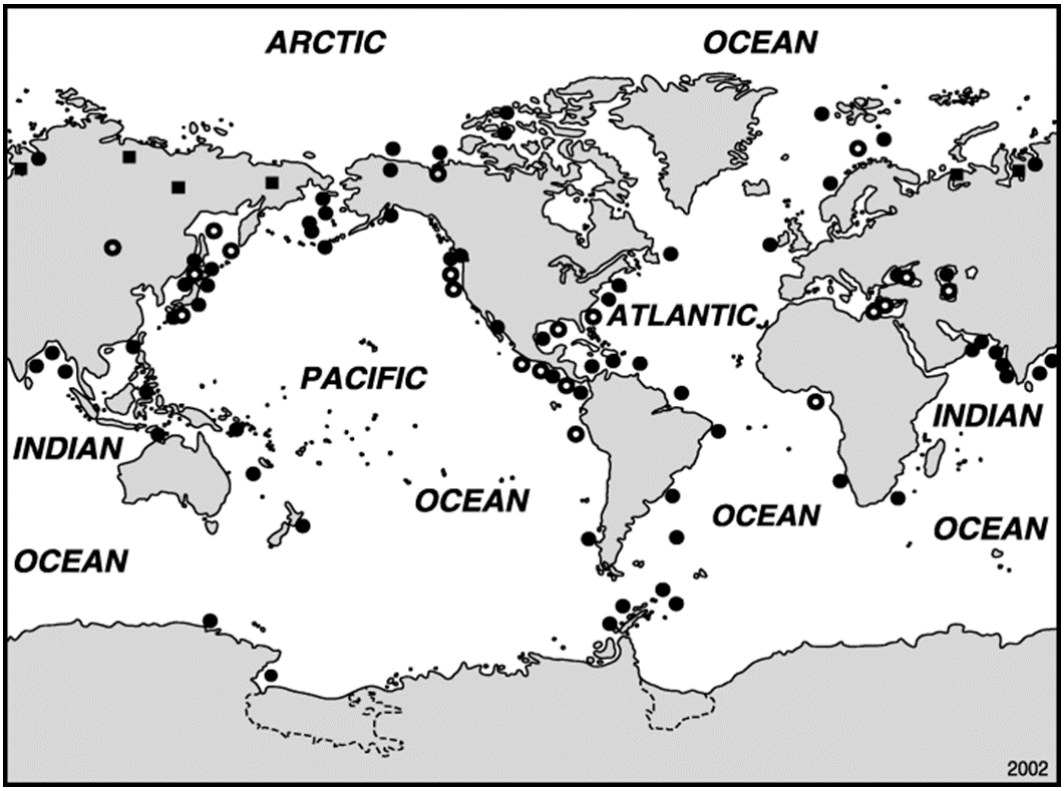

Figure 2. Distribution of known and inferred gas hydrates. Open circles mark locations where gas hydrate has been recovered. Filled circles indicate locations of inferred presence of natural gas hydrate. Squares mark regions for potential gas-hydrate occurrence in Russia (from Kvenvolden, 2000).

The gas hydrates have been estimated to constitute the largest known global carbon reservoir (Kvenvolden, 1988; Kvenvolden et al., 1993) and an important component of the carbon cycle (Dickens, 2001; Kvenvolden, 2002), although the absolute quantity is uncertain (Milkov, 2004). The interests in methane and methane hydrate deposits have increased during the last

three decades from three reasons: 1) the strong greenhouse effect of methane (Howarth et al., 2011), 2) the potential of the gas as future energy source (Collett, 2002; Makogon et al., 2007) and 3) possible geohazards associated with the release of methane from the sea-floor (Maslin et al., 2010). Methane has the potential to accelerate global warming, because one molecule has an almost 25 times stronger greenhouse effect than a molecule of carbon dioxide. In addition, methane change the atmospheric chemistry and increase the radiative forcing (Lelieveld et al., 1998). The decomposition of gas hydrates and release of methane may have caused rapid climate changes in the past (Dickens et al., 1997; Kennett et al., 2003) and could have led to slope instabilities resulting in massive landslides and tsunamis (Mienert and Posewang, 1999; Maslin et al., 2004; Vanneste et al., 2011). In connection with the mentioned hazards, understanding of the sensitivity of gas hydrates to climatic and environmental changes is crucial, especially in the light of ongoing global atmospheric and oceanic warming (IPCC, 2013). Of particular importance are the hydrates in the Arctic region, because the global warming is there more pronounced than at lower latitudes (Graversen et al., 2008 and references therein). Methane plumes rising from the seafloor on the northwestern Svalbard margin have been interpreted as a result of ongoing climatic changes in the Arctic (Westbrook et al., 2009). Quantifying the amount of methane released from the seafloor and the proportion of it that can potentially reach the atmosphere will allow to estimate the impact on the climate and modeling of the global warming in the future.

Deep ocean gas hydrates constitute over 95% of the global hydrate reservoir and have generally low sensitivity to short time climate changes (Ruppel, 2011). Active methane venting currently take place at an Arctic deep-water gas hydrate and free gas reservoir at the Vestnesa Ridge, northwestern Svalbard (Hustoft et al., 2009; Bünz et al., 2012). Little is known about deep-water hydrate deposits and methane seeps in the high Arctic region. A detailed multidisciplinary study is needed in order to improve the understanding of the past

and present methane release, its potential relationship with climatic changes, and its effect on seafloor sediments, water column and the atmosphere.

This PhD thesis focus on: 1) reconstructing past methane release events from an active pockmark at the Vestnesa Ridge, evaluation of reliability of paleo-proxy from methane influenced environment and solid stratigraphy of study area (Paper 1), 2) detailed paleoceanographic and paleoenvironmeantal reconstruction from the study area with the use of proxy resistant to diagenesis– faunal composition of the benthic foraminiferal assemblages (Paper 2) and 3) the use of diagenetic processes in order to estimate the efficiency of microbial filter in the past and quantify the amount of methane escaping to the ocean water (Paper 3).

2. Background

2.1 Cold methane seeps

Cold methane seeps are distributed along continental margins worldwide (Levin, 2005; German et al., 2011) (Fig. 3). They occur at locations where morphological features like faults and fractures provide conduits for methane-rich fluid flow (Paull et al., 1995; Judd and Hovland, 2007). At a typical seep site, methane and reduced compounds (mainly hydrogen sulfide) are available on the seafloor or in shallow sediments (Orphan et al., 2004; Levin, 2005). The reduced compounds sustain rich chemosynthetic communities that together with authigenic carbonates on the seafloor often are used as indicators of presence of fluid flow (Olu et al., 1997; Sibuet and Olu, 1998). At some of the seep–sites obvious venting can be observed as gas bubbles rising from the seabed (e.g. Haeckel et al., 2004). This can be detected by single beam echo-sounding and is referred to as flares (Paull et al., 1995; Heeschen et al., 2003; Veloso et al., 2015). Numerous seeps can also be inferred based on

seafloor mapping that may reveal structures formed by intensive fluid flow (pockmarks, pingos or mud volcanoes) (Judd and Hovland, 2007).

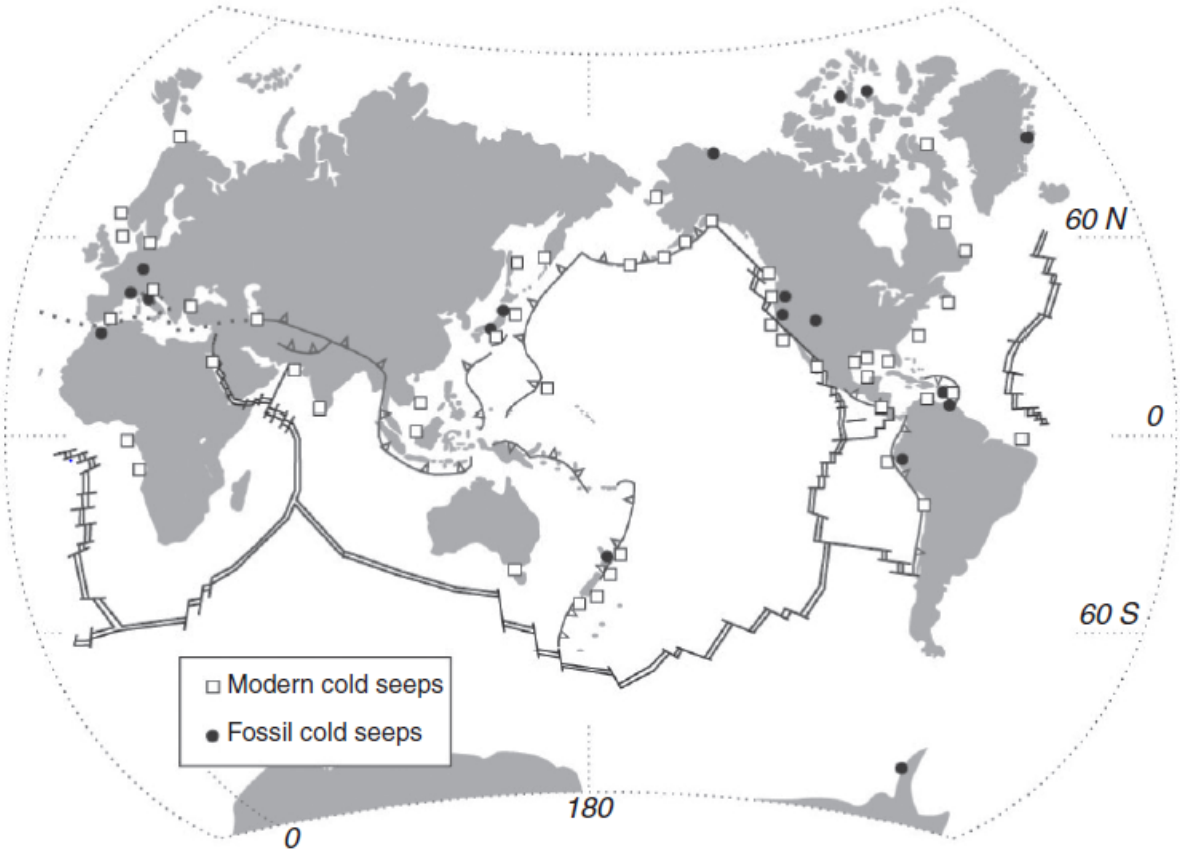

Figure 3. Global distribution of modern and fossil cold seeps (from Levin, 2005).

2.2 Anaerobic oxidation of methane (AOM)

The most important process in a cold seep environment is the anaerobic oxidation of methane (AOM). In this process methane migrating towards the seafloor and sulfate diffusing from the seawater reacts together within the sulphate-methane transition zone (SMTZ) according to the net reaction: $CH_4 + SO_4^{2-} \rightarrow HCO_3^- + HS^- + H_2O$ (e.g. Reeburgh, 1976). This reaction is mediated by a consortium of methane-oxidizing archaea and sulfate-reducing bacteria found in anoxic marine sediments (Boetius et al., 2000; Orphan et al., 2001). The SMTZ is a sediment interval that separates methane-rich and sulphate-depleted sediments below from methane-depleted and sulphate-rich sediments above (Borowski et al., 1996; Snyder et al.,

2007). The products of AOM, bicarbonate and hydrogen sulfide exert a significant influence on the pore water chemistry. The accumulation of bicarbonate elevate the alkalinity and leads to precipitation of authigenic carbonates (Mazzini et al., 2004; Magalhães et al., 2012). High concentration of hydrogen sulphide provides energy for filamentous sulphide-oxidizing bacteria, bivalves and tubeworms hosting chemoautotrophic bacteria (Brooks et al., 1987; MacDonald et al., 1989; Levin, 2005). The phenomenon of patchy distribution (zonation) of the chemosynthetic communities results from heterogeneity within the seep environment (Olu et al., 1997; Sahling et al., 2002). Variations is fluid discharge velocities determine the availability of hydrogen sulfide in the seafloor sediments (Orphan et al., 2004). In addition to serving as the base of the food chain for chemosynthetic communities, the hydrogen sulfide readily converts into iron sulfides and is preserved in the sediments mostly as pyrite (Novosel et al., 2005; Lin et al., 2016b). AOM is estimated to consume the majority of the upward migrating methane and thus, significantly limits the emissions to the water column and atmosphere (Luff and Wallmann, 2003; Sommer et al., 2006). The methane that will manage to bypass the SMTZ will be oxidized aerobically in the water column. In shallow water settings it may reach the atmosphere (McGinnis et al., 2006).

2.3 Evidence of past methane seepage

- Macrofossils

The first examples of fossil seeps were identified one year after the discovery of the first modern cold seep community in the Gulf of Mexico (Paull et al., 1984; Kiel, 2010 and references therein). Seeps fluids attract unique chemosynthetic communities and their fossil analogues were recognized at many locations worldwide (Levin, 2005; German et al., 2011). High alkalinity at seep environments caused by the AOM enhance preservation of carbonate shells. The majority of fossil seep records is based on bivalve shells followed by gastropods, brachiopods and tube worms and the studied records cover time scales spanning from

Devonian to Pliocene (e.g. Campbell and Bottjer, 1995; Kiel and Peckmann, 2007; Kiel, 2010; Vinn et al., 2013).

- Microfossils

Based on studies of modern benthic foraminifera from methane seeps and neighboring areas, the benthic foraminifera assemblages were suggested to be good indicators of methane seepage (Jones, 1993; Akimoto et al., 1994). Further studies supported the idea with results demonstrating that seep areas were dominated by foraminiferal species typical for organic-rich environments (Sen Gupta et al., 1997; Rathburn et al., 2000; Bernhard et al., 2001) and those that are able to survive periods of seafloor hypoxia (Sen Gupta et al., 2007). Seep-related benthic foraminifera assemblages enabled identification of intervals of methane escape in Plio-Pleistocene (Wefer et al., 1994; Bhaumik and Gupta, 2007; Saeidi Ortakand et al., 2016) and Holocene deposits (Wiedicke and Weiss, 2006; Panieri et al., 2014). However, a study of Miocene records from Apennines reveals no difference between seep and non-seep assemblage and points to that "time-averaging" as possible reason of samples homogenization (Barbieri and Panieri, 2004). Influence of post-mortem mixing of foraminiferal tests that may elevate species richness was also suggested by Lobegeier and Sen Gupta (2008).

- Molecular fossils

Strongly depleted ^{13}C values measured in archaeal and bacterial lipids were used to detect the presence of anaerobic methane–oxidizing microbial consortia (Hinrichs et al., 1999; Niemann and Elvert, 2008). Presence of biomarkers diagnostic of aerobic and anaerobic methanotrophy in sediments from the Last Glacial period was interpreted as evidence of methane emission to the water column (Hinrichs, 2001; Uchida et al., 2004) and high rates of AOM in the sediments (Cook et al., 2011), respectively. High abundance of these molecular fossils in seep sediments marks intervals of vigorous methanotrophic activity (Hinrichs et al., 2003). Most likely only the strongest and relatively long-lasting seepage events allow accumulation

of sufficient methanotrophic biomass for detection (Hinrichs et al., 2003; Cook et al., 2011). Studies based on lipid biomarkers extracted from authigenic carbonates documents seepage activity and AOM in Cenozoic and Mesozoic records (Peckmann et al., 1999a; Thiel et al., 1999; Birgel et al., 2006).

- Authigenic minerals

As a result of the increase in alkalinity driven by AOM, methane-derived authigenic carbonates are a common feature of cold seeps. They are typically formed of high-magnesium calcite, aragonite or dolomite and reveals a variety of sizes and shapes ranging from millimeter-size concretions to slabs, pavements, mounds and chimneys (e.g. Aloisi et al., 2000; Gontharet et al., 2007; Feng et al., 2010; Bayon et al., 2013). Ancient cold seep carbonates have been studied at many locations worldwide and are evidences of seeps activities from Devonian to the present (Orpin, 1997; Cavagna et al., 1999; Peckmann et al., 1999b; Campbell et al., 2008). Another product of AOM, hydrogen sulfide, react with iron and enhance pyrite formation in seep sediments. Accumulations of pyrite could be used as indicator of the position of the paleo-SMTZ (Judd and Hovland, 2007; Lim et al., 2011). Depending of the chemistry of the seep fluids precipitation of other authigenic minerals like barite (Greinert et al., 2002; Dickens et al., 2003; Castellini et al., 2006) and gypsum crystals (Pierre et al., 2012; Lin et al., 2016a) may take place.

- Carbon isotopic evidence

Methane has very low carbon isotopic signature, which depending on origin range from –50‰ to –20‰ for thermogenic and from –110‰ to –60‰ for microbial methane (Whiticar, 1999). Bicarbonate produced during the AOM increase the alkalinity of pore water and can significantly decrease the $\delta^{13}C$ values of dissolved inorganic carbon (DIC), which cause precipitation of carbonate minerals with low $\delta^{13}C$ values (Ritger et al., 1987; Aloisi et al., 2000). The low $\delta^{13}C$ values of DIC in pore waters can be recorded in tests of benthic

foraminifera during mineralization or in the form of diagenetic overgrowth (Rathburn et al., 2003; Torres et al., 2003; Consolaro et al., 2015). The $\delta^{13}C$ values of authigenic carbonates and microfossils are the standard and most widely used diagnostic proxy for identifying modern and paleo-seeps deposits (Paull et al., 1992; Kennett, 2000; Hill et al., 2004; Pierre and Fouquet, 2007).

3. Study area

3.1 Oceanography

Vestnesa Ridge is located at the western continental slope of Svalbard in the eastern Fram Strait at water depth between ~1200 and 1300 m (Fig. 4). The northernmost extension of the Norwegian-Atlantic Current - the West Spitsbergen Current (WSC) transports relatively warm and saline water (<3–6 °C and S<39.4 psu) along the western coast of Svalbard through the eastern Fram Strait into the Arctic Ocean (Schauer, 2004; Walczowski et al., 2005). The current transports heat and salt into the Arctic Ocean and maintains ice-free conditions in the eastern Fram Strait throughout most of the year (Aagaard et al., 1987; Schauer, 2004; Walczowski et al., 2005). The WSC is steered by topography, and the entire water column flows northward and reaches maximum speed on the upper slope down to 800 m water depth (Walczowski et al., 2005; Beszczynska-Möller et al., 2012). North of Svalbard the WSC flows as subsurface current and splits into the Yermak Slope Current and the Svalbard Branch (Aagaard et al., 1987; Manley, 1995). In the western Fram Strait, relatively cold and fresh water is transported by the East Greenland Current along the East Greenland margin out of the Arctic, into the North Atlantic Ocean (Aagaard et al., 1987; Beszczynska-Möller et al., 2012). In the central Fram Strait, the dominant water masses, warm Atlantic Water and cold Polar Water mix and generate Arctic water masses (Hop et al., 2006).

At the coring site, the Atlantic layer overlies the cold Greenland Sea Intermediate Water (~ -1 ºC) generated by convection in the Greenland Sea (Aagaard et al., 1985). A thin surface layer influenced by meltwater (10–30 m) occurs above the Atlantic Water (Aagaard et al., 1985; Zamelczyk et al., 2014). Strong bottom current generally prevent preservation of Holocene sediments in the area (Elverhøi et al., 1995; Jessen et al., 2010; Rasmussen et al., 2014).

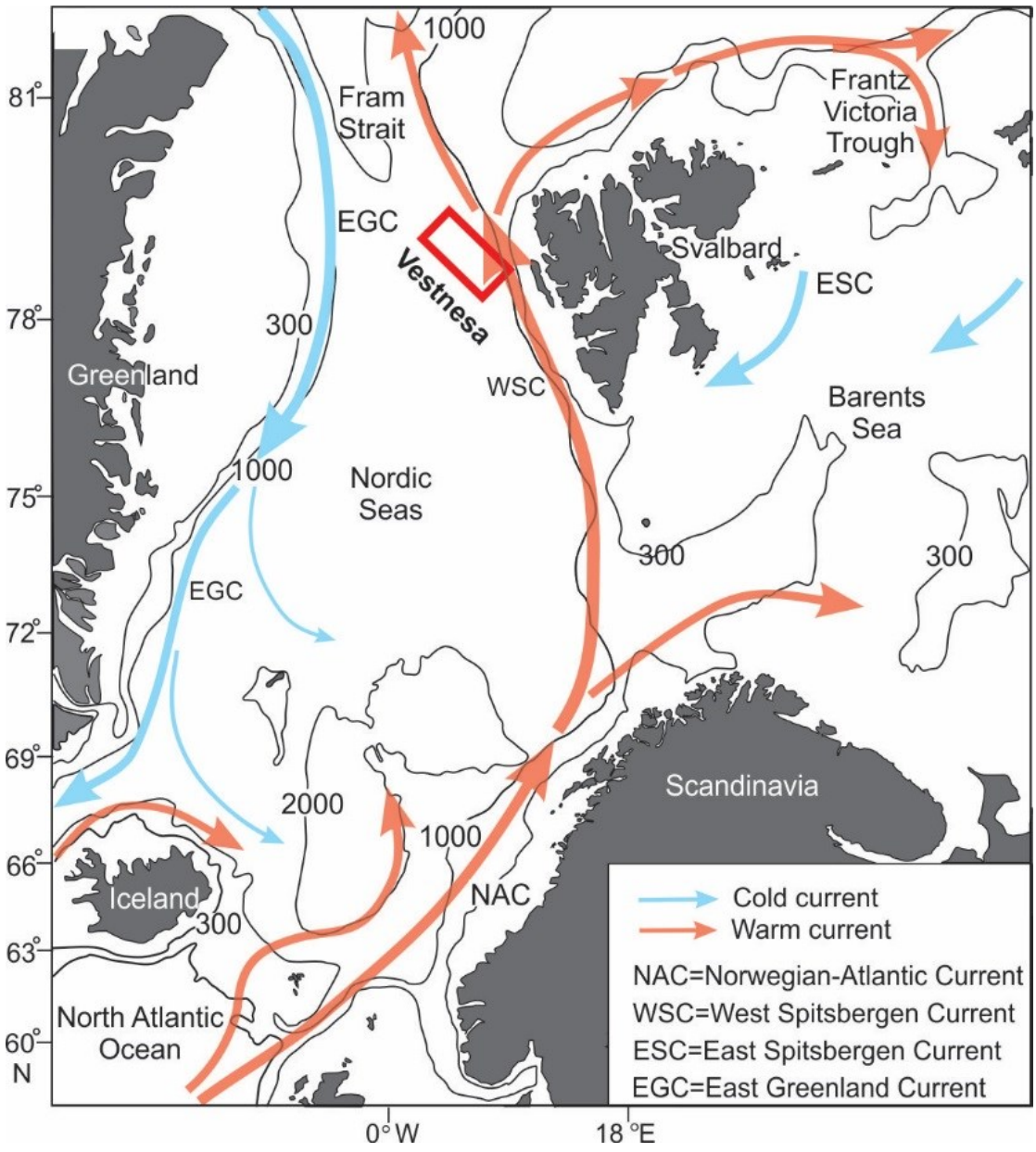

Figure 4. Map of the Nordic Seas and Barents Sea showing the major currents and location of study area, modified from Rasmussen et al. (2007).

3.2 Geology

Vestnesa Ridge is a sediment drift on top of a young, thin and hot oceanic crust (Eiken and Hinz, 1993; Engen et al., 2008). The thick sediment deposits were formed by bottom currents mostly during late Miocene and Pliocene (Eiken and Hinz, 1993). Based on the seismic reflectors the sediments were divided into three major stratigraphic units, YP-1, YP-2 and YP-3 (Eiken and Hinz, 1993), corresponding to post-rift deposits, contourites and Plio-Pleistocene glacial deposits respectively (Hustoft et al., 2009 and references therein). The most recent (Late Quaternary) sediments consist of contourite deposits punctuated by episodic deposition of turbidites (Howe et al., 2008). Presence of gas and gas hydrates in the area was predicted based on bright spots and bottom simulating reflectors in seismic data (Eiken and Hinz, 1993). The crest of Vestnesa Ridge is perforated with pockmarks, the origin of which was suggested to be connected to methane venting (Vogt et al., 1994). The hypothesis was confirmed by extensive geophysical studies (Hustoft et al., 2009; Petersen et al., 2010; Bünz et al., 2012; Plaza-Faverola et al., 2015) that documented methane release from the pockmarks at the eastern part of the ridge and by recovery of methane hydrates in sediment cores (Fisher et al., 2011). Acoustic flares rising from the seafloor are frequently observed on hydroacoustic data (Hustoft et al., 2009; Bünz et al., 2012). Episodes of methane venting at the Vestnesa Ridge may be determined by glacial activity and tectonic stress (Plaza-Faverola et al., 2015).

4. Material and methods

4.1 Sampling and treatment

Investigated sediment cores were taken at Vestnesa Ridge in the eastern Fram Strait (Fig.4) by *RV Jan Mayen* (now *RV Helmer Hanssen*) in June 2010 and July 2012. High-resolution

seismic profiles recorded by an EdgeTech 3300-HM hull-mounted sub-bottom profiler were used to determine the coring positions. CTD (conductivity, temperature, density) data were also collected prior the coring. Three of the cores were retrieved from within an active pockmark (JM10-335GC, HH12-928PC and HH12-929GC), while one core was taken outside the pockmark as a control (Fig. 5).

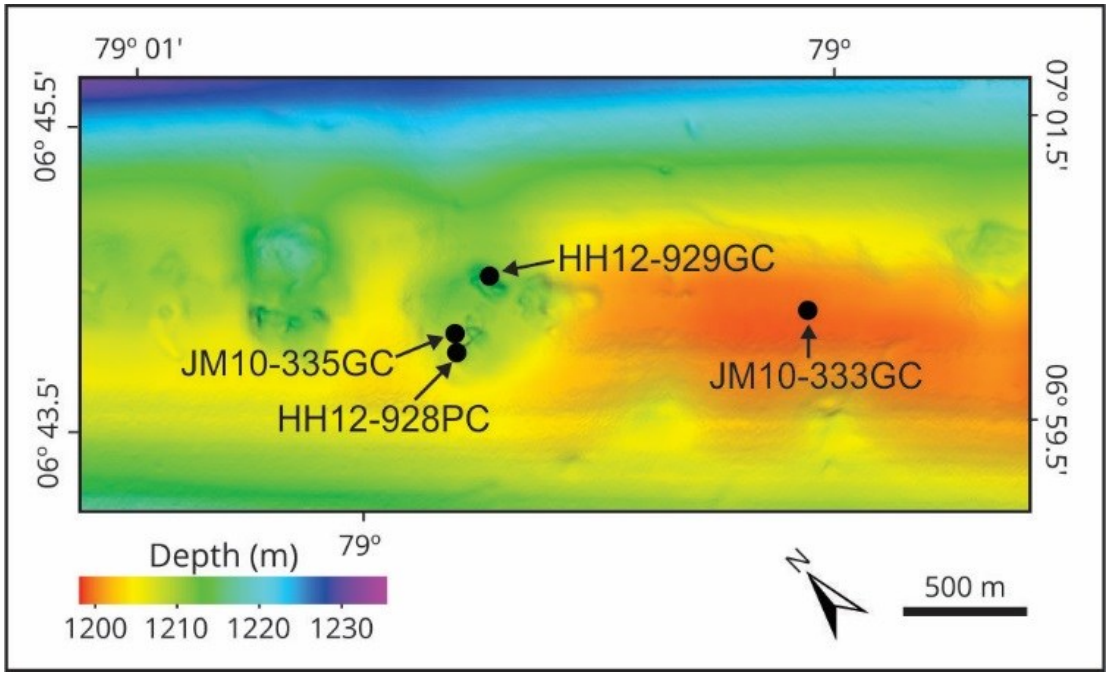

Figure 5. Detailed bathymetric map of the active pockmark on the southern part of Vestnesa ridge with locations of four studied cores. Map was created based on data from Bünz et al. (2012) with help of S. Vadakkepuliyambatta and T. Grytå.

All the cores were cut into 1 m sections and kept in a cooling room (4°C) until further investigations. Density, porosity and magnetic susceptibility were measured in all core sections on a GeoTech Multisensor Core Logger at the Department of Geology, UiT The Arctic University of Norway. Thereafter, each core section was split length-wise into two halves and described for visual changes in color, texture and occurrence of macrofossils. Additionally the reference halves were X-rayed, XRF-scanned and color imaged. Working halves were subsampled at 5 cm intervals in 1 cm thick slices. The sampling interval applies

to all analysis described below. The samples were weighed, freeze dried, weighed and wet-sieved at 0.063, 0.1 and 1 mm sieves. Prior to sieving about 4 g of bulk sediment was taken from each sample for geochemical analyses. Mineral grains in the size fraction > 1 mm were counted as ice-rafted debris (IRD). The concentration of IRD was calculated as number of grains per gram dry weight sediment.

4.2 Geochemical analysis

The weight percentage (wt.%) of total carbon (TC), total organic carbon (TOC) and total sulfur (TS) were measured in bulk sediment samples using a Leco CS-200 induction furnace at the Department of Geology, UiT The Arctic University of Norway. The content (wt.%) of calcium carbonate ($CaCO_3$) was calculated using the equation:

$CaCO_3 = (TC-TOC)*8.333$

4.3 Stable isotope analysis ($\delta^{18}O$ and $\delta^{13}C$)

Stable oxygen and carbon isotopic ratios were measured on well-preserved tests of planktic foraminiferal species *N. pachyderma* and the benthic foraminiferal species *Cassidulina neoteretis* and *Melonis barleeanus*. The measurements were performed on specimens picked from the >0.1 mm fraction from the four sediment cores and analyzed at the Bjerknes Centre for Climate Change, University of Bergen on a Finnigan MAT 253 mass spectrometer with a Kiel IV device. The $\delta^{18}O$ values in core JM10-335GC were corrected for ice volume changes using the sea-level record of Fairbanks (1989).

4.4 Planktic and benthic foraminiferal fauna

Planktic and benthic foraminiferal analyses were performed in the 0.1 to 1 mm size fraction in cores JM10-333GC and JM10-335GC. Approximately 300 benthic and 300 planktic

specimens were picked and identified per sample where possible. The species were identified based on the systematics of Feyling-Hanssen et al. (1971), and Loeblich and Tappan (1988). Benthic foraminiferal species with an affinity to warm bottom water containing *Pullenia bulloides, P. quinqueloba, Eggerella bradyi, Sigmoilopsis schlumbergeri, Bulimina marginata, Gyroidina sp., Gavelinopsis praegeri, Pyrgo serrata, Spirophtalmidium acutimargo* and *Cibicidoides pachyderma* were grouped together as 'Atlantic species' (Rasmussen et al., 1996, 2003; Wollenburg et al., 2001,2004).

The absolute abundances (concentration, number of specimens per gram dry weight sediment) and relative abundances (%) of species were calculated in each sample. The foraminiferal accumulation rates (number/cm^2/year) were calculated following the methods described in Ehrmann and Thiede (1985). Diversity indices were calculated using the PAST software (Hammer et al., 2001).

4.5 Chronology

Chronologies of the investigated cores are based on accelerator mass spectrometry (AMS) ^{14}C dates measured at the Chrono Centre, Queen's University, Belfast (21 samples) and Beta Analytic, London (2 samples). Dated material consisted of monospecific samples of *N. pachyderma* (15 dates), mixed benthic foraminifera (two dates) and bivalve shells (six dates). A reservoir correction of 440 years was applied to all dates (Mangerud and Gulliksen, 1975) and the corrected ages were calibrated to calendar years using the "Fairbanks 0701" calibration curve (Fairbanks et al., 2005). In cores JM10-333GC and JM10-335GC, in addition to radiocarbon dates, stratigraphic tie points from Jessen et al. (2010) including the stacked magnetic susceptibility curve and lithological units were used. Age models were established based on the linear interpolation between dates and tie points.

4.6 Pyrite study

Pyrite particles counts were performed in sample aliquots of the 0.1-1 mm grain-size fractions in cores JM10-333GC and JM10-335GC. The concentrations (number of pyrite particles per gram dry weight) and flux were calculated. Pyrite fluxes were calculated using the formula:

number/g x Mass Accumulation Rate (MAR)

where MAR=Linear Sedimentation Rate (LSR) (cm/ka) x Dry Bulk Density (DBD) (g/cm^3).

The diversity of pyrite textures were documented by using a Hitachi TM3000 scanning electron microscope (SEM) at the Department of Geology, UiT Arctic University of Norway.

5. Summary of papers

Paper 1

Sztybor K. and Rasmussen T. L. **Diagenetic disturbances of marine sedimentary records from methane influenced environments in the Fram Strait as indications of variation in seep intensity during the last 35 000 years.** *Boreas, DOI 10.1111/bor.12202*

In this paper we reconstruct the episodes of past methane release in one of the active pockmarks at Vestnesa Ridge and investigate the effect of seeping of methane on the marine sedimentary record. The study is based on four sediment cores, including three cores taken from within the pockmark with methane venting from the seafloor, and one core taken just outside the pockmark for comparison. The shallow, high-resolution seismic profiles (Chirp) showed acoustic blanking inside the pockmark suggesting gas accumulation at the coring site, while the normal stratification outside the pockmark confirmed that the site was undisturbed and the core could be used for control core.

We carried out a detailed study of diagenetic processes and their imprint on the composition and structure of sediments and foraminiferal shells. The data material comprises stable isotopes, authigenic carbonates, benthic and planktonic foraminifera, biostratigraphy, radiocarbon dates, sedimentary data and magnetic susceptibility. The environmental conditions of seep sediments that stimulate the diagenesis are determined by anaerobic oxidation of methane (AOM). In the process of AOM hydrogen sulfide and high alkalinity are produced. The results show a clear connection between diagenetic processes and the seep environment. We interpret the low and nearly constant magnetic susceptibility values inside the pockmark, in contrast to higher and more variable values from the control core (as well as in other non-seep sites from the Svalbard margin), as a local phenomenon caused by dissolution of magnetic minerals in the reductive environment of seep sediments and formation of paramagnetic minerals. The very low $\delta^{13}C$ values in foraminiferal shells during the Bølling –Allerød interstadials suggest enhanced methane flux that began in the late Heinrich event H1. The recorded low values in both planktic and benthic foraminiferal shells indicate diagenetic overprint by methane-derived authigenic carbonates induced by high alkalinity. Radiocarbon ages of ^{13}C depleted foraminiferal tests are significantly older than those of foraminifera with normal $\delta^{13}C$ values from similar horizons. The higher ages are caused by contamination from methane derived 'old' carbon and the degree of disruption may depend of the seepage intensity. The study emphasize the importance of lithology, biostratigraphy and critical assessment of paleo-proxies in methane influenced sedimentary records in order to reconstruct a reliable stratigraphy.

Paper 2

Sztybor K. and Rasmussen T. L**. Late glacial and deglacial paleoceanographic and environmental changes at Vestnesa Ridge, Fram Strait.** *In review in Palaeogeography, Palaeoclimatology, Palaeoecology*

In this study, we reconstruct the paleoceanography of the Vestnesa Ridge and investigate if the seepage of methane had any impact on the species composition of the benthic foraminiferal faunas and their distribution patterns. For the purpose of the study, we use two sediment cores, one taken from a pockmark with active venting of methane and one taken outside the pockmark for comparison. In these two cores, we focus on the distribution patterns of planktonic and benthic foraminiferal species assemblages, sedimentology and geochemistry of the sediment (total organic carbon and $CaCO_3$ content). The study presents the first detailed record of benthic foraminiferal assemblages in the area. The results show continuous inflow of warm Atlantic water however, during the transition from the glacial maximum to the deglaciation the Atlantic water changed its position in the water column. The change resulted in higher bottom water temperatures during Heinrich event H1 (17,000-15,300 cal yr BP). The warmer bottom water conditions enabled the settlement of 'Atlantic species' of benthic foraminifera (see methods and summary of paper 1) and a community of chemo-synthesizing bivalves. The patterns of diversity, density and the assemblage structure of the benthic foraminifera were the same in both records, indicating that seepage of methane had no influence on the species composition of the foraminiferal faunas. The lack of differences in the benthic foraminiferal faunas of the seep core compared to the non-seep core suggests that the low $\delta^{13}C$ values of foraminiferal tests during the Bølling-Allerød interstadials are a result of diagenesis of the dead specimens. Paleoceanographic conditions were the major factor controlling the benthic foraminiferal assemblage structure, diversity and density.

Paper 3

Sztybor K., Rasmussen T. L. and Laier, T. **"Excess sulfur" in sediments from western Svalbard margin as indication for the efficiency of the microbial filter in paleo-anaerobic oxidation of methane (AOM).** In preparation for submission to Chemical Geology.

In this work we take a closer look at the diagenetic processes at the seep site and try to use the changes in distribution of pyrite particles, total sulfur and total organic carbon in order to estimate the intensity of the paleo-seepage and efficiency of the anaerobic oxidation of methane (AOM) in the past. For the purpose of the study we use the two cores from the previous studies (Papers 1 and 2), one core from a pockmark with methane venting into the water column and the control core from outside the pockmark. The cores were examined in terms of stable isotopes, total organic carbon and sulfur content and carbon-sulfur ratios, magnetic susceptibility, concentration of pyrite particles and their characteristic textures. The results show that although the two cores have similar lithofacies their geochemistry vary significantly. The pockmark core show much higher concentration of pyrite particles, sulfur content and higher sulfur-carbon ratios. The highest sulfur flux correlates with the extremely low $\delta^{13}C$ values in foraminiferal shells reported earlier (Paper 1), which indicate that the sulfate reduction is coupled to the process of AOM.

Total sulfur vs. carbon plots are often used to characterize the type of depositional environments at the seafloor (Berner and Raiswell, 1983; Leventhal, 1983, 1995). In methane seep environments sulfate reduction includes two processes: fermentation of buried organic matter and AOM (e.g. Snyder et al., 2007). Sulfate reduction not connected to higher content of organic material leads to elevated sulfide sulfur in the sediment and disequilibrium from the normal total sulfur/total organic carbon (TS/TOC) ratio (Leventhal, 1995). We interpret

the higher sulfur content and higher TS/TOC ratios in the seep core as a result of diagenetically produced "excess" sulfide in the process of AOM. Moreover, based on the "excess" sulfur fluxes we estimate here for the first time, the efficiency of the microbial filter during the Last Glacial Maximum and the deglaciation. The obtained values corresponds to low and medium methane fluxes at modern seeps. Additionally, we investigated textures of pyrite particles. The framboidal pyrite dominate core intervals with high AOM, while the euhedral pyrite dominate in the low AOM intervals and the entire record of the control core. We interpret this correlation as a possible indicator of two different precipitation mechanisms.

6. Concluding remarks and outlook

In the present PhD study, a multi-core and multi-proxy approach has been used to reconstruct events of past methane release, evaluate the reliability of paleo-proxies from methane influenced environments and to reconstruct paleoceanographic variability in the study area based on high-resolution investigations of four deep-sea cores. Three cores were from an active pockmark with intense release of methane and the fourth was from outside the pockmarks and analyzed as a reference record. The following main findings and suggestions for future work are a result of this thesis:

- High-resolution stable isotope records of foraminiferal shells allowed to identify intervals of low in $\delta^{13}C$ values indicative of presence of a paleo-sulphate-methane transition zone(SMTZ). The low $\delta^{13}C$ values (c. -16 to -7 ‰) recorded in both benthic and planktic foraminifera points to a postmortem, diagenetic origin of the signal. The main problem with using carbon isotopic evidence to detect fossil seepage events is the uncertainty of when the signal was recorded as the position of the paleo-SMTZ in the sediment column is unknown. Based on the presence of chemosynthetic

macrofaunas, magnitude of the $\delta^{13}C$ excursions and correlation between the four records it has been suggested that seepage began to increase during Heinrich event H1 and increased to a maximum in strength during the Bølling-Allerød interstadials. For future studies, use of U-Th datings of the authigenic carbonates could give a more accurate estimation of the time of their formation.

- In this study, special emphasis has been put on producing a solid stratigraphy of the four records. Due to diagenesis in the seep environment the use of common proxies for constructing the age models was impossible (magnetic susceptibility) or limited (AMS^{14}C and $\delta^{18}O$ records). Detailed study of the lithology and biostratigraphy allowed to correlate the records in great details and obtain good age models of the records. One core was unfortunately too disturbed due to very heavily encrustations of the sediment, so that a firm age model could not be reconstructed. The K\Ti ratios from XRF-scanning of the records showed that this proxy known to be fairly resistant to diagenesis has the potential to be a reliable tool for reconstructing age models and assessing the degree of mechanical disturbance of the sedimentary records. Future testing of the K\Ti ratios on multiple sediment cores from seep and control sites from the western Svalbard margin could be an interesting aspect to address in the future.
- Variations in bottom environmental conditions during the Last Glacial and deglaciation have not been investigated before in the study area. Changes in bottom water temperature (BWT) generally are not expected to have any significant impact on deep-sea methane hydrate deposits, but are critical for the benthic micro- and macrofaunas. Although a sufficient flux of hydrogen sulfide is currently available at Vestnesa pockmarks, no living specimens of chemosynthetic bivalves from the family of Vesicomyids have been sampled. Modern oceanographic conditions with a BWT of ~−1°C appears to be too cold for them. Restrictions of their occurrence to a time of

highest paleo-BWT (during Heinrich event H1 17-15.3 ka BP) underlines the importance of knowledge about the paleoceanographic conditions in order to make reliable reconstructions of paleo-seepage of methane. For future studies, measurements of Mg\Ca ratios in shells of benthic foraminifera would enable a detailed absolute temperature reconstruction of bottom and surface waters. Also, developing transfer functions for benthic foraminifera from deep-sea environments for calculation of absolute bottom water temperatures for water depths below 1000 m would constitute and independent tool for comparisons with other temperature proxies.

- Benthic foraminiferal assemblages are generally an excellent tool for reconstructions of past environments and paleoceanography. This study shows that they unfortunately are not good indicator of paleo-seepage of methane. This may be, because the paleoceanographic changes and continuous bottom current activities throughout the investigated time interval was strong enough as to overprint any influence from the methane on the benthic faunas. Another reason may be post-mortem mixing of foraminiferal shells from short-lasting seepage episodes that impair the signal.
- Products of the diagenetic processes induced by anaerobic oxidation of methane (AOM) can change the geochemistry of seep sediments. Seep cores are characterized by higher sulfur content and higher sulfur-carbon ratios (TS\TOC) than the control core from outside seep areas. Correlation between low $\delta^{13}C$ values of foraminiferal shells with high TS\TOC ratios, high TS flux and pyrite content has been interpreted as an indication of enhanced paleo-AOM as the cause of the production of "excess" sulfide. The "excess" sulfur fluxes have been used as a base to estimate of the efficiency of the microbial filter in the past. This may turn out to be a reliable tool for future estimations of paleo-seepage.

- Different dominating pyrite textures observed in core sections with inferred enhanced paleo-AOM, from the low AOM intervals and the control core, may indicate several formation mechanisms. However, this requires further investigation.

Overall, this study contributed to improve our knowledge about high Arctic cold seep environments and the paleoceanographic variability in the eastern Fram Strait from the end of Last Glacial period and until the early Holocene. The results emphasize the great heterogeneity of seep environments and the necessity of multi-core and multi-proxy studies to achieve the best possible understanding of paleo-conditions. The outcome of this study elucidate the imprint of methane seepage on sedimentary records and together with the stratigraphy and paleoceanography of the area provides basis for further geological and geophysical interpretations. Reconstructions of paleo-seepage are important to estimate the contribution of methane to the future climate changes, especially in the light of ongoing global warming and increasing deep-sea temperatures; both trends that are amplified in the Arctic region.

7. References

Aagaard, K., Foldvik, A., Hillman, S.R., 1987. The West Spitsbergen Current: Disposition and water mass transformation. Journal of Geophysical Research, 92(C4): 3778.

Aagaard, K., Swift, J.H., Carmack, E.C., 1985. Thermohaline circulation in the Arctic Mediterranean Seas. Journal of Geophysical Research: Oceans, 90(C3): 4833-4846.

Akimoto, K., Tanaka, T., Hattori, M., Hotta, H., 1994. Recent benthic foraminiferal assemblages from cold seep communities- a contribution to the methane gas indicator., University of Tokyo Tokyo.

Aloisi, G., Pierre, C., Rouchy, J.-M., Foucher, J.-P., Woodside, J., 2000. Methane-related authigenic carbonates of eastern Mediterranean Sea mud volcanoes and their possible relation to gas hydrate destabilisation. Earth and Planetary Science Letters, 184(1): 321-338.

Barbieri, R., Panieri, G., 2004. How are benthic foraminiferal faunas influenced by cold seeps? Evidence from the Miocene of Italy. Palaeogeography, Palaeoclimatology, Palaeoecology, 204(3-4): 257-275.

Bayon, G. et al., 2013. Formation of carbonate chimneys in the Mediterranean Sea linked to deep-water oxygen depletion. Nature Geoscience, 6(9): 755-760.

Berner, R.A., Raiswell, R., 1983. Burial of organic carbon and pyrite sulfur in sediments over phanerozoic time: a new theory. Geochimica et Cosmochimica Acta, 47(5): 855-862.

Bernhard, J.M., Buck, K.R., Barry, J.P., 2001. Monterey Bay cold-seep biota: Assemblages, abundance, and ultrastructure of living foraminifera. Deep Sea Research Part I: Oceanographic Research Papers, 48(10): 2233-2249.
Beszczynska-Möller, A., Fahrbach, E., Schauer, U., Hansen, E., 2012. Variability in Atlantic water temperature and transport at the entrance to the Arctic Ocean, 1997-2010. ICES Journal of Marine Science, 69(5): 852-863.
Bhaumik, A.K., Gupta, A.K., 2007. Evidence of methane release from Blake Ridge ODP Hole 997A during the Plio-Pleistocene: Benthic foraminifer fauna and total organic carbon. Current Science, 92(2): 192-199.
Birgel, D. et al., 2006. Lipid biomarker patterns of methane-seep microbialites from the Mesozoic convergent margin of California. Organic Geochemistry, 37(10): 1289-1302.
Boetius, A. et al., 2000. A marine microbial consortium apparently mediating anaerobic oxidation of methane. Nature, 407(6804): 623-626.
Borowski, W.S., Paull, C.K., Ussler, W., 1996. Marine pore-water sulfate profiles indicate in situ methane flux from underlying gas hydrate. Geology, 24(7): 655-658.
Brooks, J.M. et al., 1987. Deep-Sea Hydrocarbon Seep Communities: Evidence for Energy and Nutritional Carbon Sources. Science, 238(4830): 1138-1142.
Bünz, S., Polyanov, S., Vadakkepuliyambatta, S., Consolaro, C., Mienert, J., 2012. Active gas venting through hydrate-bearing sediments on the Vestnesa Ridge, offshore W-Svalbard. Marine Geology, 332-334: 189-197.
Campbell, K.A., Bottjer, D.J., 1995. Brachiopods and chemosymbiotic bivalves in Phanerozoic hydrothermal vent and cold seep environments. Geology, 23(4): 321-324.
Campbell, K.A. et al., 2008. Hydrocarbon seep-carbonates of a Miocene forearc (East Coast Basin), North Island, New Zealand. Sedimentary Geology, 204(3-4): 83-105.
Castellini, D.G., Dickens, G.R., Snyder, G.T., Ruppel, C.D., 2006. Barium cycling in shallow sediment above active mud volcanoes in the Gulf of Mexico. Chemical Geology, 226(1–2): 1-30.
Cavagna, S., Clari, P., Martire, L., 1999. The role of bacteria in the formation of cold seep carbonates: geological evidence from Monferrato (Tertiary, NW Italy). Sedimentary Geology, 126(1–4): 253-270.
Collett, T.S., 2002. Energy resource potential of natural gas hydrates. AAPG bulletin, 86(11): 1971-1992.
Consolaro, C. et al., 2015. Carbon isotope (δ13C) excursions suggest times of major methane release during the last 14 kyr in Fram Strait, the deep-water gateway to the Arctic. Climate of the Past, 11(4): 669-685.
Cook, M.S., Keigwin, L.D., Birgel, D., Hinrichs, K.-U., 2011. Repeated pulses of vertical methane flux recorded in glacial sediments from the southeast Bering Sea. Paleoceanography, 26(2): n/a-n/a.
Dickens, G.R., 2001. Modeling the Global Carbon Cycle with a Gas Hydrate Capacitor: Significance for the Latest Paleocene Thermal Maximum, Natural Gas Hydrates: Occurrence, Distribution, and Detection. American Geophysical Union, pp. 19-38.
Dickens, G.R., Castillo, M.M., Walker, J.C.G., 1997. A blast of gas in the latest Paleocene: Simulating first-order effects of massive dissociation of oceanic methane hydrate. Geology, 25(3): 259-262.
Dickens, G.R., Fewless, T., Thomas, E., Bralower, T.J., 2003. Excess barite accumulation during the Paleocene-Eocene thermal Maximum: Massive input of dissolved barium from seafloor gas hydrate reservoirs. Geological Society of America Special Papers, 369: 11-23.

Ehrmann, W.U., Thiede, J., 1985. History of mesozoic and cenozoic sediment fluxes to the-North Atlantic Ocean. Contributions to Sedimentary Geology, 15: 1-109.
Eiken, O., Hinz, K., 1993. Contourites in the Fram Strait. Sedimentary Geology, 82(1): 15-32.
Elverhøi, A. et al., 1995. The Growth and Decay of the Late Weichselian Ice Sheet in Western Svalbard and Adjacent Areas Based on Provenance Studies of Marine Sediments. Quaternary Research, 44(3): 303-316.
Engen, Ø., Faleide, J.I., Dyreng, T.K., 2008. Opening of the Fram Strait gateway: A review of plate tectonic constraints. Tectonophysics, 450(1-4): 51-69.
Fairbanks, R.G., 1989. A 17,000-year glacio-eustatic sea level record: influence of glacial melting rates on the Younger Dryas event and deep-ocean circulation. Nature, 342(6250): 637-642.
Fairbanks, R.G. et al., 2005. Radiocarbon calibration curve spanning 0 to 50,000 years BP based on paired 230Th/234U/238U and 14C dates on pristine corals. Quaternary Science Reviews, 24(16–17): 1781-1796.
Feng, D., Chen, D., Peckmann, J., Bohrmann, G., 2010. Authigenic carbonates from methane seeps of the northern Congo fan: Microbial formation mechanism. Marine and Petroleum Geology, 27(4): 748-756.
Feyling-Hanssen, R.W., Jørgensen, J.A., Knudsen, K.L., Lykke-Andersen, A.-L., 1971. Late Quaternary Foraminifera from Vendsyssel, Denmark and Sandnes, Norway. Geological Society of Denmark.
Fisher, R.E. et al., 2011. Arctic methane sources: Isotopic evidence for atmospheric inputs. Geophysical Research Letters, 38(21): n/a-n/a.
German, C.R., Ramirez-Llodra, E., Baker, M.C., Tyler, P.A., Committee, C.S.S., 2011. Deep-water chemosynthetic ecosystem research during the census of marine life decade and beyond: a proposed deep-ocean road map. PLoS One, 6(8): e23259.
Gontharet, S. et al., 2007. Nature and origin of diagenetic carbonate crusts and concretions from mud volcanoes and pockmarks of the Nile deep-sea fan (eastern Mediterranean Sea). Deep Sea Research Part II: Topical Studies in Oceanography, 54(11-13): 1292-1311.
Graversen, R.G., Mauritsen, T., Tjernstrom, M., Kallen, E., Svensson, G., 2008. Vertical structure of recent Arctic warming. Nature, 451(7174): 53-56.
Greinert, J., Bollwerk, S.M., Derkachev, A., Bohrmann, G., Suess, E., 2002. Massive barite deposits and carbonate mineralization in the Derugin Basin, Sea of Okhotsk: precipitation processes at cold seep sites. Earth and Planetary Science Letters, 203(1): 165-180.
Haeckel, M., Suess, E., Wallmann, K., Rickert, D., 2004. Rising methane gas bubbles form massive hydrate layers at the seafloor. Geochimica et Cosmochimica Acta, 68(21): 4335-4345.
Hammer, Ø., Harper, D.A.T., Ryan, P.D., 2001. PAST: Paleontological Statistics Software Package for Education and Data Analysis, Palaeontologia Electronica.
Heeschen, K.U., Tréhu, A.M., Collier, R.W., Suess, E., Rehder, G., 2003. Distribution and height of methane bubble plumes on the Cascadia Margin characterized by acoustic imaging. Geophysical Research Letters, 30(12): n/a-n/a.
Hill, T.M., Kennett, J.P., Valentine, D.L., 2004. Isotopic evidence for the incorporation of methane-derived carbon into foraminifera from modern methane seeps, Hydrate Ridge, Northeast Pacific. Geochimica et Cosmochimica Acta, 68(22): 4619-4627.
Hinrichs, K.-U., 2001. A molecular recorder of methane hydrate destabilization. Geochemistry, Geophysics, Geosystems, 2(1): 1029.
Hinrichs, K.-U., Hayes, J.M., Sylva, S.P., Brewer, P.G., DeLong, E.F., 1999. Methane-consuming archaebacteria in marine sediments. Nature, 398(6730): 802-805.

Hinrichs, K.-U., Hmelo, L.R., Sylva, S.P., 2003. Molecular Fossil Record of Elevated Methane Levels in Late Pleistocene Coastal Waters. Science, 299(5610): 1214-1217.
Hop, H. et al., 2006. Physical and biological characteristics of the pelagic system across Fram Strait to Kongsfjorden. Progress in Oceanography, 71(2–4): 182-231.
Howarth, R.W., Santoro, R., Ingraffea, A., 2011. Methane and the greenhouse-gas footprint of natural gas from shale formations. Climatic Change, 106(4): 679.
Howe, J.A., Shimmield, T.M., Harland, R.E.X., Eyles, N., 2008. Late Quaternary contourites and glaciomarine sedimentation in the Fram Strait. Sedimentology, 55(0): 179-200.
Hustoft, S., Bünz, S., Mienert, J., Chand, S., 2009. Gas hydrate reservoir and active methane-venting province in sediments on <20 Ma young oceanic crust in the Fram Strait, offshore NW-Svalbard. Earth and Planetary Science Letters, 284(1-2): 12-24.
IPCC, 2013. Climate Change 2013: The Physical Science Basis. Contribution of Working Group I to the Fifth Assessment Report of the Intergovernmental Panel on Climate Change. Cambridge University Press, Cambridge, United Kingdom and New York, NY, USA, 1535 pp.
Jessen, S.P., Rasmussen, T.L., Nielsen, T., Solheim, A., 2010. A new Late Weichselian and Holocene marine chronology for the western Svalbard slope 30,000–0 cal years BP. Quaternary Science Reviews, 29(9-10): 1301-1312.
Jones, R.W., 1993. Preliminary Observations on Benthonic Foramininera Associated with Biogenic Gas Seep in the North Sea. In: Jenkins, D.G. (Ed.), Applied Micropalaeontology. Springer Netherlands, Dordrecht, pp. 69-91.
Judd, A., Hovland, M., 2007. Seabed fluid flow: the impact on geology, biology and the marine environment. Cambridge University Press.
Kennett, J.P., 2000. Carbon Isotopic Evidence for Methane Hydrate Instability During Quaternary Interstadials. Science, 288(5463): 128-133.
Kennett, J.P., Cannariato, K.G., Hendy, I.L., Behl, R.J., 2003. Methane Hydrates in Quaternary Climate Change: The Clathrate Gun Hypothesi. Wiley Online Library.
Kiel, S., 2010. The vent and seep biota: Aspects from microbes to ecosystems, 33. Springer Science & Business Media.
Kiel, S., Peckmann, J., 2007. Chemosymbiotic bivalves and stable carbon isotopes indicate hydrocarbon seepage at four unusual Cenozoic fossil localities. Lethaia, 40(4): 345-357.
Kvenvolden, K.A., 1988. Origins of Methane in the Earth Methane hydrate — A major reservoir of carbon in the shallow geosphere? Chemical Geology, 71(1): 41-51.
Kvenvolden, K.A., 2002. Methane hydrate in the global organic carbon cycle. Terra Nova, 14(5): 302-306.
Kvenvolden, K.A., Ginsburg, G.D., Soloviev, V.A., 1993. Worldwide distribution of subaquatic gas hydrates. Geo-Marine Letters, 13(1): 32-40.
Lelieveld, J.O.S., Crutzen, P.J., Dentener, F.J., 1998. Changing concentration, lifetime and climate forcing of atmospheric methane. Tellus B, 50(2): 128-150.
Leventhal, J.S., 1983. An interpretation of carbon and sulfur relationships in Black Sea sediments as indicators of environments of deposition. Geochimica et Cosmochimica Acta, 47(1): 133-137.
Leventhal, J.S., 1995. Carbon-sulfur plots to show diagenetic and epigenetic sulfidation in sediments. Geochimica et Cosmochimica Acta, 59(6): 1207-1211.
Levin, L.A., 2005. Ecology of cold seep sediments: Interactions of fauna with flow, chemistry and microbes. In: Gibson, R.N., Atkinson, R.J.A., Gordon, J.D.M. (Eds.), Oceanography and Marine Biology - an Annual Review, Vol. 43. Oceanography and Marine Biology. Crc Press-Taylor & Francis Group, Boca Raton, pp. 1-46.

Lim, Y.C., Lin, S., Yang, T.F., Chen, Y.-G., Liu, C.-S., 2011. Variations of methane induced pyrite formation in the accretionary wedge sediments offshore southwestern Taiwan. Marine and Petroleum Geology, 28(10): 1829-1837.
Lin, Q., Wang, J., Algeo, T.J., Su, P., Hu, G., 2016a. Formation mechanism of authigenic gypsum in marine methane hydrate settings: Evidence from the northern South China Sea. Deep Sea Research Part I: Oceanographic Research Papers, 115: 210-220.
Lin, T.J. et al., 2016b. Linkages between mineralogy, fluid chemistry, and microbial communities within hydrothermal chimneys from the Endeavor Segment, Juan de Fuca Ridge. Geochemistry, Geophysics, Geosystems: n/a-n/a.
Lobegeier, M.K., Sen Gupta, B.K., 2008. FORAMINIFERA OF HYDROCARBON SEEPS, GULF OF MEXICO. The Journal of Foraminiferal Research, 38(2): 93-116.
Loeblich, A.R., Tappan, H.N., 1988. Foraminiferal genera and their classification. Van Nostrand Reinhold Co.
Luff, R., Wallmann, K., 2003. Fluid flow, methane fluxes, carbonate precipitation and biogeochemical turnover in gas hydrate-bearing sediments at Hydrate Ridge, Cascadia Margin: numerical modeling and mass balances. Geochimica et Cosmochimica Acta, 67(18): 3403-3421.
MacDonald, I.R. et al., 1989. Gulf of Mexico hydrocarbon seep communities. Marine Biology, 101(2): 235-247.
Magalhães, V.H. et al., 2012. Formation processes of methane-derived authigenic carbonates from the Gulf of Cadiz. Sedimentary Geology, 243-244: 155-168.
Makogon, Y.F., Holditch, S.A., Makogon, T.Y., 2007. Natural gas-hydrates — A potential energy source for the 21st Century. Journal of Petroleum Science and Engineering, 56(1–3): 14-31.
Mangerud, J., Gulliksen, S., 1975. Apparent radiocarbon ages of recent marine shells from Norway, Spitsbergen, and Arctic Canada. Quaternary Research, 5(2): 263-273.
Manley, T.O., 1995. Branching of Atlantic Water within the Greenland-Spitsbergen Passage: An estimate of recirculation. Journal of Geophysical Research: Oceans, 100(C10): 20627-20634.
Maslin, M. et al., 2010. Gas hydrates: past and future geohazard? Philosophical Transactions of the Royal Society A: Mathematical, Physical and Engineering Sciences, 368(1919): 2369-2393.
Maslin, M., Owen, M., Day, S., Long, D., 2004. Linking continental-slope failures and climate change: Testing the clathrate gun hypothesis. Geology, 32(1): 53-56.
Mazzini, A. et al., 2004. Methane-related authigenic carbonates from the Black Sea: geochemical characterisation and relation to seeping fluids. Marine Geology, 212(1-4): 153-181.
McGinnis, D.F., Greinert, J., Artemov, Y., Beaubien, S.E., Wüest, A., 2006. Fate of rising methane bubbles in stratified waters: How much methane reaches the atmosphere? Journal of Geophysical Research, 111(C9).
Mienert, J., Posewang, J., 1999. Evidence of shallow- and deep-water gas hydrate destabilizations in North Atlantic polar continental margin sediments. Geo-Marine Letters, 19(1): 143-149.
Milkov, A.V., 2004. Global estimates of hydrate-bound gas in marine sediments: how much is really out there? Earth-Science Reviews, 66(3-4): 183-197.
Niemann, H., Elvert, M., 2008. Diagnostic lipid biomarker and stable carbon isotope signatures of microbial communities mediating the anaerobic oxidation of methane with sulphate. Organic Geochemistry, 39(12): 1668-1677.
Novosel, I., Spence, G.D., Hyndman, R.D., 2005. Reduced magnetization produced by increased methane flux at a gas hydrate vent. Marine Geology, 216(4): 265-274.

Olu, K. et al., 1997. Cold seep communities as indicators of fluid expulsion patterns through mud volcanoes seaward of the Barbados accretionary prism. Deep Sea Research Part I: Oceanographic Research Papers, 44(5): 811-841.
Orphan, V.J. et al., 2001. Comparative analysis of methane-oxidizing archaea and sulfate-reducing bacteria in anoxic marine sediments. Appl Environ Microbiol, 67(4): 1922-34.
Orphan, V.J. et al., 2004. Geological, geochemical, and microbiological heterogeneity of the seafloor around methane vents in the Eel River Basin, offshore California. Chemical Geology, 205(3-4): 265-289.
Orpin, A.R., 1997. Dolomite chimneys as possible evidence of coastal fluid expulsion, uppermost Otago continental slope, southern New Zealand. Marine Geology, 138(1): 51-67.
Panieri, G. et al., 2014. Late Holocene foraminifera of Blake Ridge diapir: Assemblage variation and stable-isotope record in gas-hydrate bearing sediments. Marine Geology, 353: 99-107.
Paull, C.K. et al., 1992. Indicators of methane-derived carbonates and chemosynthetic organic carbon deposits; examples from the Florida Escarpment. PALAIOS, 7(4): 361-375.
Paull, C.K. et al., 1984. Biological Communities at the Florida Escarpment Resemble Hydrothermal Vent Taxa. Science, 226(4677): 965-967.
Paull, C.K., Ussler, W., Borowski, W.S., Spiess, F.N., 1995. Methane-rich plumes on the Carolina continental rise: Associations with gas hydrates. Geology, 23(1): 89-92.
Peckmann, J. et al., 1999a. Cold seep deposits of Beauvoisin (Oxfordian; southeastern France) and Marmorito (Miocene; northern Italy): microbially induced authigenic carbonates. International Journal of Earth Sciences, 88(1): 60-75.
Peckmann, J., Walliser, O.H., Riegel, W., Reitner, J., 1999b. Signatures of hydrocarbon venting in a Middle Devonian Carbonate Mound (Hollard Mound) at the Hamar Laghdad (Antiatlas, Morocco). Facies, 40(1): 281-296.
Petersen, C.J., Bünz, S., Hustoft, S., Mienert, J., Klaeschen, D., 2010. High-resolution P-Cable 3D seismic imaging of gas chimney structures in gas hydrated sediments of an Arctic sediment drift. Marine and Petroleum Geology, 27(9): 1981-1994.
Pierre, C. et al., 2012. Authigenic carbonates from active methane seeps offshore southwest Africa. Geo-Marine Letters, 32(5-6): 501-513.
Pierre, C., Fouquet, Y., 2007. Authigenic carbonates from methane seeps of the Congo deep-sea fan. Geo-Marine Letters, 27(2-4): 249-257.
Plaza-Faverola, A. et al., 2015. Role of tectonic stress in seepage evolution along the gas hydrate-charged Vestnesa Ridge, Fram Strait. Geophysical Research Letters, 42(3): 733-742.
Rasmussen, T.L., Thomsen, E., Labeyrie, L., van Weering, T.C.E., 1996. Circulation changes in the Faeroe-Shetland Channel correlating with cold events during the last glacial period (58–10 ka). Geology, 24(10): 937.
Rasmussen, T.L., Thomsen, E., Nielsen, T., 2014. Water mass exchange between the Nordic seas and the Arctic Ocean on millennial timescale during MIS 4-MIS 2. Geochemistry, Geophysics, Geosystems, 15(3): 530-544.
Rasmussen, T.L. et al., 2007. Paleoceanographic evolution of the SW Svalbard margin (76°N) since 20,000 14C yr BP. Quaternary Research, 67(1): 100-114.
Rasmussen, T.L., Thomsen, E., Troelstra, S.R., Kuijpers, A., Prins, M.A., 2003. Millennial-scale glacial variability versus Holocene stability: changes in planktic and benthic foraminifera faunas and ocean circulation in the North Atlantic during the last 60 000 years. Marine Micropaleontology, 47(1–2): 143-176.

Rathburn, A.E., Levin, L.A., Held, Z., Lohmann, K.C., 2000. Benthic foraminifera associated with cold methane seeps on the northern California margin: Ecology and stable isotopic composition. Marine Micropaleontology, 38(3–4): 247-266.
Rathburn, A.E. et al., 2003. Relationships between the distribution and stable isotopic composition of living benthic foraminifera and cold methane seep biogeochemistry in Monterey Bay, California. Geochemistry, Geophysics, Geosystems, 4(12): 1106.
Reeburgh, W.S., 1976. Methane consumption in Cariaco Trench waters and sediments. Earth and Planetary Science Letters, 28(3): 337-344.
Ritger, S., Carson, B., Suess, E., 1987. Methane-derived authigenic carbonates formed by subduction-induced pore-water expulsion along the Oregon/Washington margin. Geological Society of America Bulletin, 98(2): 147.
Ruppel, C., 2011. Methane hydrates and contemporary climate change. Nature Education Knowledge, 3(10): 29.
Saeidi Ortakand, M., Hasegawa, S., Matsumoto, R., Matsuda, H., 2016. Correlating biostratigraphy and palaeoceanographic changes during late Quaternary at cold seeps with gas hydrate-free areas of the Japan Sea using foraminifera paleoecology. Island Arc, 25(1): 55-71.
Sahling, H., Rickert, D., Lee, R.W., Linke, P., Suess, E., 2002. Macrofaunal community structure and sulfide flux at gas hydrate deposits from the Cascadia convergent margin, NE Pacific. Marine Ecology Progress Series, 231: 121-138.
Schauer, U., 2004. Arctic warming through the Fram Strait: Oceanic heat transport from 3 years of measurements. Journal of Geophysical Research, 109(C6).
Sen Gupta, B.K., Platon, E., Bernhard, J.M., Aharon, P., 1997. Foraminiferal colonization of hydrocarbon-seep bacterial mats and underlying sediment, Gulf of Mexico slope. The Journal of Foraminiferal Research, 27(4): 292-300.
Sen Gupta, B.K., Smith, L.E., Lobegeier, M.K., 2007. Attachment of Foraminifera to vestimentiferan tubeworms at cold seeps: Refuge from seafloor hypoxia and sulfide toxicity. Marine Micropaleontology, 62(1): 1-6.
Sibuet, M., Olu, K., 1998. Biogeography, biodiversity and fluid dependence of deep-sea cold-seep communities at active and passive margins. Deep Sea Research Part II: Topical Studies in Oceanography, 45(1–3): 517-567.
Sloan, E.D., 1998. Gas Hydrates: Review of Physical/Chemical Properties. Energy & Fuels, 12(2): 191-196.
Snyder, G.T. et al., 2007. Pore water profiles and authigenic mineralization in shallow marine sediments above the methane-charged system on Umitaka Spur, Japan Sea. Deep Sea Research Part II: Topical Studies in Oceanography, 54(11-13): 1216-1239.
Sommer, S. et al., 2006. Efficiency of the benthic filter: Biological control of the emission of dissolved methane from sediments containing shallow gas hydrates at Hydrate Ridge. Global Biogeochemical Cycles, 20(2): n/a-n/a.
Thiel, V. et al., 1999. Highly isotopically depleted isoprenoids: molecular markers for ancient methane venting. Geochimica et Cosmochimica Acta, 63(23–24): 3959-3966.
Torres, M.E. et al., 2003. Is methane venting at the seafloor recorded by δ13C of benthic foraminifera shells? Paleoceanography, 18(3): n/a-n/a.
Uchida, M., Shibata, Y., Ohkushi, K.i., Ahagon, N., Hoshiba, M., 2004. Episodic methane release events from Last Glacial marginal sediments in the western North Pacific. Geochemistry, Geophysics, Geosystems, 5(8): n/a-n/a.
Vanneste, M. et al., 2011. Hinlopen-Yermak landslide, Arctic Ocean—geomorphology, landslide dynamics and tsunami simulations. Mass-transport deposits in deepwater settings. SEPM Society for Sedimentary Geology Spec Publ, 96.

Veloso, M., Greinert, J., Mienert, J., De Batist, M., 2015. A new methodology for quantifying bubble flow rates in deep water using splitbeam echosounders: Examples from the Arctic offshore NW-Svalbard. Limnology and Oceanography: Methods, 13(6): 267-287.
Vinn, O., Kupriyanova, E.K., Kiel, S., 2013. Serpulids (Annelida, Polychaeta) at Cretaceous to modern hydrocarbon seeps: Ecological and evolutionary patterns. Palaeogeography, Palaeoclimatology, Palaeoecology, 390: 35-41.
Vogt, P.R., Crane, K., Sundvor, E., Max, M.D., Pfirman, S.L., 1994. Methane-generated(?) pockmarks on young, thickly sedimented oceanic crust in the Arctic: Vestnesa ridge, Fram strait. Geology, 22(3): 255-258.
Walczowski, W., Piechura, J., Osinski, R., Wieczorek, P., 2005. The West Spitsbergen Current volume and heat transport from synoptic observations in summer. Deep Sea Research Part I: Oceanographic Research Papers, 52(8): 1374-1391.
Wefer, G., Heinze, P.M., Berger, W.H., 1994. Clues to ancient methane release. Nature, 369(6478): 282-282.
Westbrook, G.K. et al., 2009. Escape of methane gas from the seabed along the West Spitsbergen continental margin. Geophysical Research Letters, 36(15): L15608.
Whiticar, M.J., 1999. Carbon and hydrogen isotope systematics of bacterial formation and oxidation of methane. Chemical Geology, 161(1–3): 291-314.
Wiedicke, M., Weiss, W., 2006. Stable carbon isotope records of carbonates tracing fossil seep activity off Indonesia. Geochemistry, Geophysics, Geosystems, 7(11): n/a-n/a.
Wollenburg, J.E., Knies, J., Mackensen, A., 2004. High-resolution paleoproductivity fluctuations during the past 24 kyr as indicated by benthic foraminifera in the marginal Arctic Ocean. Palaeogeography, Palaeoclimatology, Palaeoecology, 204(3–4): 209-238.
Wollenburg, J.E., Kuhnt, W., Mackensen, A., 2001. Changes in Arctic Ocean paleoproductivity and hydrography during the last 145 kyr: The benthic foraminiferal record. Paleoceanography, 16(1): 65-77.
Zamelczyk, K., Rasmussen, T.L., Husum, K., Godtliebsen, F., Hald, M., 2014. Surface water conditions and calcium carbonate preservation in the Fram Strait during marine isotope stage 2, 28.8-15.4 kyr. Paleoceanography, 29(1): 1-12.

Paper 1

Diagenetic disturbances of marine sedimentary records from methane influenced environments in the Fram Strait as indications of variation in seep intensity during the last 35 000 years

Kamila Sztybor and Tine Lander Rasmussen

Boreas, DOI 10.1111/bor.12202

BOREAS An international journal of Quaternary research

Diagenetic disturbances of marine sedimentary records from methane-influenced environments in the Fram Strait as indications of variation in seep intensity during the last 35 000 years

KAMILA SZTYBOR AND TINE L. RASMUSSEN

BOREAS

Sztybor, K. & Rasmussen, T. L.: Diagenetic disturbances of marine sedimentary records from methane-influenced environments in the Fram Strait as indications of variation in seep intensity during the last 35 000 years. *Boreas*. 10.1111/bor.12202. ISSN 0300-9483.

The effect of seeping of methane on marine sediment records has been studied in four gravity cores from Vestnesa Ridge, Svalbard margin. The area shows acoustic signs in the form of flares indicating active methane gas seepage. For a better understanding of the timing and variability of the flux of methane in the past and the effects on potential proxies, a detailed study of the diagenetic processes that may affect the composition and structure of both sediments and foraminiferal shells is needed. Here we discuss deep-sea records from methane-influenced environments in three cores from an active and very heterogeneous seep-area (pockmark) and one core from outside the pockmark for background. The results include the distribution and stable isotopes of authigenic carbonates and of benthic and planktonic foraminifera, magnetic susceptibility, AMS-^{14}C dates, sedimentary data and biostratigraphy. Extremely low δ^{13}C values recorded in both benthic and planktonic foraminifera during the Bølling-Allerød interstadials indicate possible increased methane flux beginning at late Heinrich event H1. The recorded low values are mainly a result of diagenetic overprint by methane-derived authigenic carbonates. The δ^{18}O signals of authigenic carbonates are close to those of foraminiferal calcite and thus the δ^{18}O records remain a valid stratigraphical tool in methane seep sites, except in the case of severely encrusted samples. In addition, the records from the active pockmark show nearly constant values of low magnetic susceptibility in contrast to higher and more variable magnetic susceptibility values from the control station and other published records from normal sediments west of Svalbard. This phenomenon is probably caused by dissolution of magnetic minerals in the reducing environmental conditions of methane seep sediments, associated with anaerobic oxidation of methane and formation of paramagnetic minerals (pyrite). This process enables magnetic susceptibility to be used as a common diagnostic tool for identifying methane-related palaeo-reductive environments.

Kamila Sztybor (kamila.sztybor@uit.no) and Tine L. Rasmussen, CAGE - Centre for Arctic Gas Hydrate, Environment and Climate, Department of Geology, UiT The Arctic University of Norway, Tromsø N-9037, Norway; *received 16th February 2016, accepted 4th July 2016.*

Continental margins worldwide store large amounts of methane in the form of gas hydrate, free gas and dissolved gas (Kvenvolden 1988; Kvenvolden *et al.* 1993; Milkov 2004). Methane in marine reservoirs comes from degradation of organic matter via microbial methanogenesis or thermogenesis (Whiticar 1999). The methane stored in marine sediments is an important component of the global carbon cycle and can influence both the atmosphere and ocean carbon pool (Judd *et al.* 2002; Kvenvolden 2002; Dickens 2003).

Cold seeps (Hovland & Judd 1988) occur at many locations on continental margins, where faults and fracture networks provide conduits for deep-sourced methane-rich fluids to advect toward the sea floor (Paull *et al.* 1995; Pohlman *et al.* 2009). Intensive fluid expulsions can change the morphology of the ocean floor by forming pockmarks, pingos or mud volcanoes (Judd & Hovland 2007). These structures are often associated with release of free gas into the water column (e.g. Paull *et al.* 1995; Suess *et al.* 1999). Methane-rich fluid flow can also be inferred by the presence of chemosynthetic biological communities and authigenic carbonates on the sea floor (Paull *et al.* 1984; Hovland & Thomsen 1989; Sibuet & Olu 1998; Orphan *et al.* 2004; Naehr *et al.* 2007).

Methane from deeper sources diffusing or advecting towards the sea floor passes through the sulphate-methane transition zone (SMTZ) that separates sulphate-bearing and methane-depleted sediments above from sulphate-depleted and methane-rich sediments below (Borowski *et al.* 1996; Roberts 2001). Here, methane is oxidized through a process of anaerobic oxidation of methane (AOM; Orcutt *et al.* 2004; Treude *et al.* 2005). Any advecting methane that passes the SMTZ can leave marine sediments by direct venting into the water column, where it is oxidized aerobically (Hinrichs *et al.* 2003; Orphan *et al.* 2004). In the process of AOM a consortium of archaea and sulphate-reducing bacteria convert methane and sulphate to bicarbonate and hydrogen sulphide (Reeburgh 1976; Hinrichs *et al.* 1999; Boetius *et al.* 2000). Hydrogen sulphide can further support rich chemosynthetic communities on the sea floor (Hovland & Thomsen 1989; MacDonald *et al.* 1990; Barry *et al.* 1996; Levin 2005). The high content of bicarbonate in the subsea-floor environment increases the alkalinity of the pore water and leads to precipitation of authigenic carbonates (Jørgensen 1992; Paull *et al.* 1992; Borowski *et al.* 1996; Snyder *et al.* 2007; Ussler & Paull 2008). At this horizon dissolved bicarbonate generated from AOM

DOI 10.1111/bor.12202

contains the isotopic signature of methane, which is strongly depleted in ^{13}C relative to seawater dissolved inorganic carbon (DIC) (Paull *et al.* 1992; Orphan *et al.* 2004; Ussler & Paull 2008; Chen *et al.* 2010). The isotopic ratio of DIC at the depth of the SMTZ can also be affected by the DIC of fluids from greater depths migrating upwards and the bicarbonate produced from fermentation of buried organic matter (Luff & Wallmann 2003; Snyder *et al.* 2007; Chen *et al.* 2010; Chatterjee *et al.* 2011).

Enhanced methane flux would cause a shallower position of the SMTZ close to or at the sea floor (Borowski *et al.* 1996; Luff & Wallmann 2003; Bhatnagar *et al.* 2011). At numerous locations where advection brings methane very close to the sea floor, the SMTZ and authigenic carbonates were observed at or near the sediment surface (Niemann *et al.* 2006; Hensen *et al.* 2007; Nöthen & Kasten 2011; Magalhães *et al.* 2012). Strong methane flux also causes higher rates of sulphate reduction and higher alkalinity as a result of intensive AOM closer to the sea floor (Treude *et al.* 2003; Snyder *et al.* 2007; Chatterjee *et al.* 2011). Benthic foraminifera record the low $\delta^{13}C$ values of the DIC in the pore waters and thus record the presence of anaerobically oxidized methane in sediments during mineralization of their tests and/or through post-mortem diagenetic processes (Torres *et al.* 2003; Martin *et al.* 2010; Consolaro *et al.* 2015).

Vestnesa Ridge in the eastern Fram Strait (Fig. 1) represents one of the northernmost known deep-water gas hydrate provinces in the Arctic (Hustoft *et al.* 2009; Bünz *et al.* 2012). The eastern part of the ridge is characterized by the presence of pockmarks and flares (Fig. 1B, C). Previous studies from Vestnesa Ridge have focused on variations in the release of methane based on isotope measurements in benthic

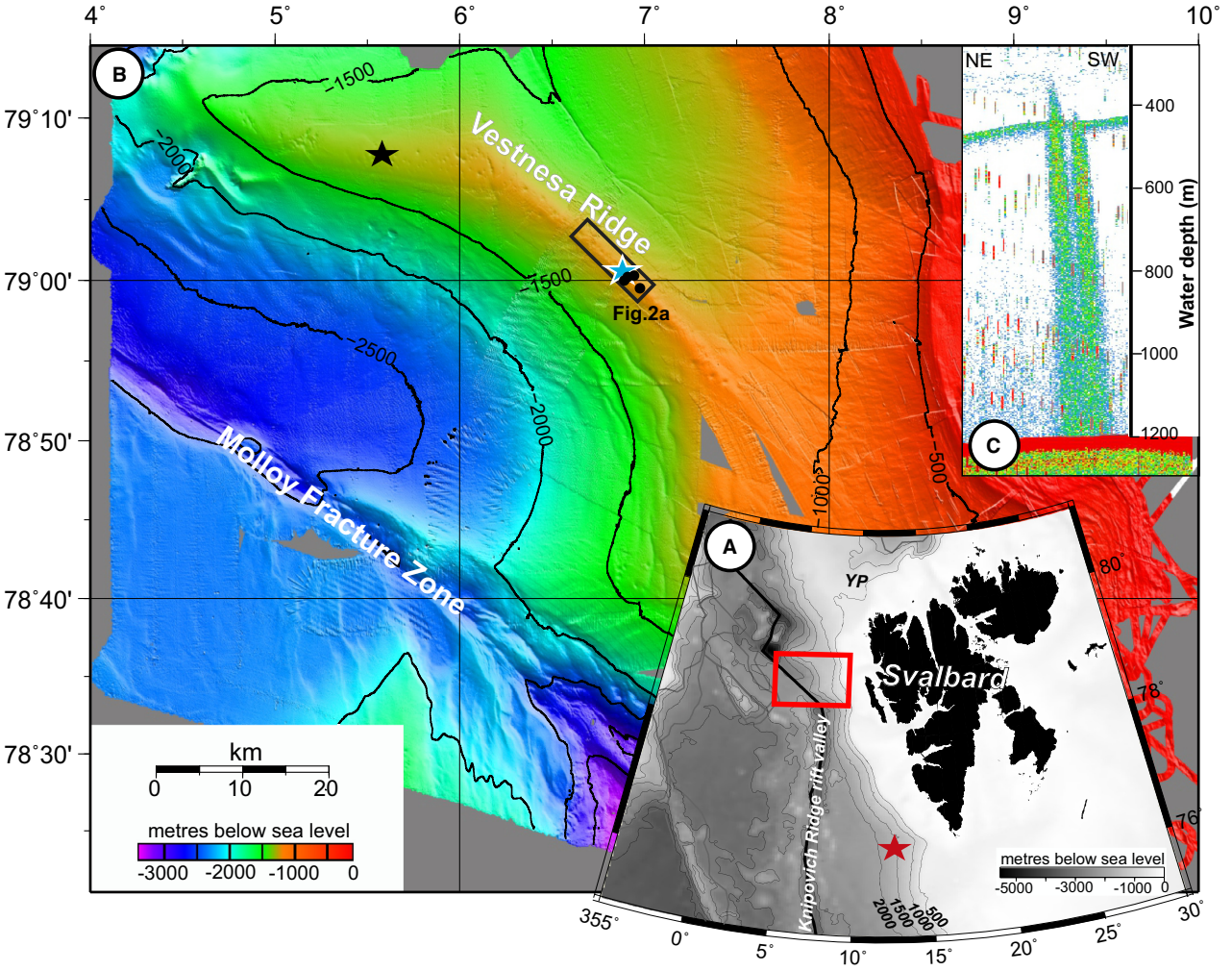

Fig. 1. A. Bathymetric map (IBCAO; Jakobsson *et al.* 2000) of the West Svalbard margin. Red box indicates the location of the investigated area of Vestnesa Ridge. Red star shows position of core JM03-373PC from Rasmussen *et al.* (2007). B. Swath bathymetry map of Vestnesa Ridge. Black box indicates location of the pockmark field with recently observed gas flares. Black circles mark cores from this study, black star = core JM10-330GC from Consolaro *et al.* (2015), blue star = core JR211-26GC from Panieri *et al.* (2014). C. 38 kHz echogram showing an example of a gas flare recorded from the studied pockmark in 2014 and reaching more than 800 m above the sea floor.

foraminifera and comprised single records of either a short time interval (Consolaro *et al.* 2015) or without a solid stratigraphy (Panieri *et al.* 2014) (Figs 1B, 2). Thus a new comprehensive data analysis, which aims towards a reliable chronostratigraphy is needed.

In this paper, we present results from three cores from a single pockmark, where each core represents different degrees of disturbance from seeping of methane. We also studied an important control record from outside the pockmark from normal sediments unaffected by methane release for comparison with the pockmark records (stratigraphical control core). The purpose of our investigation is to study the heterogeneity of the methane seep environment, with focus on the timing and impact on the sedimentary record and various proxies of the variable flux of methane in the past.

Study area

Oceanography

The Vestnesa Ridge is located at the northwestern Svalbard margin in the eastern Fram Strait (~79°N) at a water depth of ~1200–1300 m (Fig. 1A). Relatively warm and saline water (<3–6 °C and S<39.4 psu) is transported by the West Spitsbergen Current along the western Svalbard margin and through the Fram Strait to the Arctic Ocean (Schauer *et al.* 2004; Walczowski *et al.* 2005). Cold, low-salinity water is transported by the East Greenland Current along the East Greenland margin into the North Atlantic Ocean (Aagaard *et al.* 1987; Beszczynska-Möller *et al.* 2012). At the coring site a relatively thin surface layer influenced by meltwater (10–30 m) occurs above the Atlantic Water (until ~500 m), which overlies the cold Greenland Sea Intermediate Water (~−0.9 °C) generated by convection in the Greenland Sea (Aagaard *et al.* 1985). The entire water column flows northward with maximum current speed on the upper slope down to 800 m water depth (Walczowski *et al.* 2005; Beszczynska-Möller *et al.* 2012).

Geology

Vestnesa Ridge is an about 100-km-long, elongated sediment drift located on <20 -Myr-old, thin and hot oceanic crust of the Eurasian Plate (Engen *et al.* 2008) (Fig. 1B). The crest of the sediment drift is

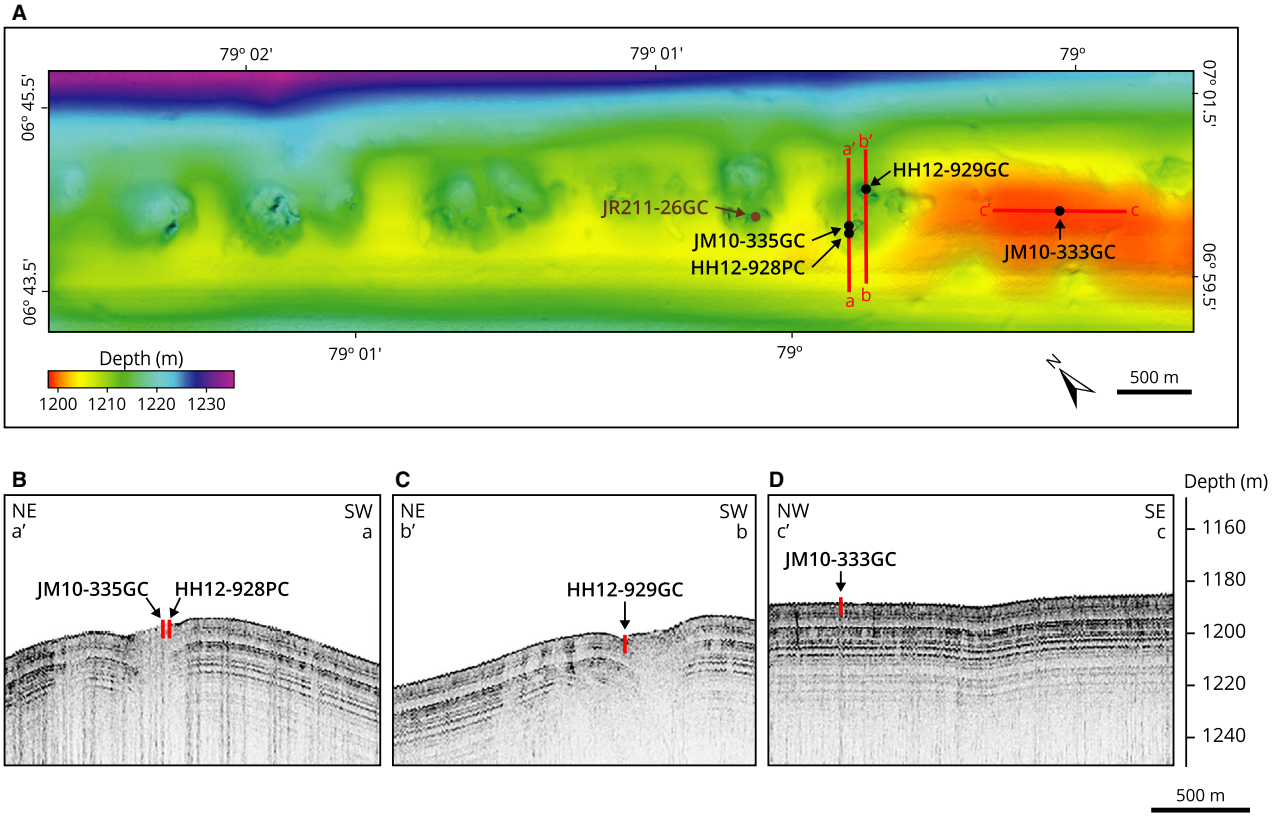

Fig. 2. A. Detailed bathymetric map of pockmark field on southern part of Vestnesa Ridge with locations of the four studied gravity cores and three seismic profiles. Cores JM10-335GC, HH12-928PC and HH12-929GC were collected from an active pockmark and core JM10-333GC from outside the pockmark as a control. Location of core JR211-26GC (Panieri *et al.* 2014) is also indicated. B. Chirp profile a–a'. C. Chirp profile b–b' from the pockmark showing chimney structure. D. Chirp profile c–c' outside the pockmark with normal layering of sediments.

Table 1. Core positions and water depth of cores shown in Figs 1 and 2.

Core ID	Latitude N	Longitude E	Water depth (m)
JM10-333GC	78°59.785′	06°58.044′	1200
JM10-335GC	79°00.173′	06°55.335′	1197
HH12-928PC	79°00.155′	06°55.250′	1206
HH12-929GC	79°00.220′	06°56.007′	1211

perforated with pockmarks (Vogt *et al.* 1994; Hustoft *et al.* 2009). It is adjacent to the eastern spreading segment of the Molloy Ridge and consists of ~5-km-thick sediments deposited after the final continental break-up of Eurasia and North America (Eiken & Hinz 1993; Ritzmann *et al.* 2004). The post-rift deposits are overlain by contourites, Plio-Pleistocene glaciomarine sediments and glacially derived material from the Kongsfjorden Trough Mouth Fan (Eiken & Hinz 1993; Vorren & Laberg 1997). The upper succession consists of silty turbidites and contourites of Late Weichselian and Holocene age (Howe *et al.* 2008). Presence of gas and gas hydrate accumulations in the area has been reported based on conventional (Eiken & Hinz 1993; Vanneste *et al.* 2005; Hustoft *et al.* 2009) and high-resolution P-Cable seismic studies (Petersen *et al.* 2010; Bünz *et al.* 2012; Plaza-Faverola *et al.* 2015). The pockmark field on the eastern part of the ridge (Fig. 1B) is characterized by vigorous gas release from the seabed. Flares rising from pockmarks are frequently observed on single-beam 38 kHz echo-sounder data and may reach >800 m heights into the water column (Fig. 1C; Hustoft *et al.* 2009; Bünz *et al.* 2012).

Material and methods

Before coring in June 2010 and July 2012, high-resolution seismic profiles were recorded, using an EdgeTech 3300-HM hull-mounted sub-bottom profiler. Coring positions were determined based on the profiles (Fig. 2A, B). Sediments are stratified outside the pockmark, while acoustically transparent within the pockmark (Fig. 2B).

Two gravity cores JM10-335GC and JM10-333GC were collected from 1200 m water depth on the Vestnesa Ridge in June 2010 during a cruise with RV 'Jan Mayen' (now RV 'Helmer Hanssen'; Table 1, Figs 1, 2). Core JM10-335GC was taken from inside a pockmark, from within a rising gas flare, as observed on the echo-sounder during core collection. Core JM10-333GC was taken outside the pockmark as a control core to retrieve hemipelagic sediments unaffected by seeping of methane. Two additional cores were taken in July 2012 from inside the same pockmark during a cruise with RV 'Helmer Hanssen' (piston core HH12-928PC and gravity core HH12-929GC; Table 1). Piston core HH12-928PC targeted the old position of JM10-335GC to obtain a longer stratigraphical record. Due to strong currents and wind, the ship drifted away from the exact position (Fig. 2A, B, Table 1) and the sediment corer accidentally hit hard ground (Fig. 3A). Despite the bent core tube, more than 2 m of sediments was collected. Gravity core HH12-929GC was taken from within the pockmark at the deepest location, which is about 10 m deeper than the pockmark rim. This core collected gas hydrates and the sediments within the core tube expanded. The core sections were cut to remove the voids, and gas hydrates were observed at the top and bottom of each small core section in the lower part of the core. The reconstructed sediment-log indicates that the hydrates occurred from 1.45 m to the core bottom (Fig. 3B). Gas flares were observed on the echo-sounder during the retrieval of both cores HH12-928PC and HH12-929GC.

Before opening of the cores, density and magnetic susceptibility were measured every centimetre with a loop sensor mounted on a GeoTek Multi Sensor Core Logger. Thereafter, the cores were split, X-rayed, XRF-scanned and visually described. A lithological log was established by combining X-ray and grain-size distributions with XRF-scanning results and visual descriptions (Fig. 4).

The cores were subsequently subsampled at 5-cm intervals in 1-cm-thick slices. The samples were weighed, freeze dried and wet-sieved through 0.063, 0.100 and 1.0 mm sieves. The residues were dried at 40 °C. Benthic and planktonic foraminifera were counted in the size fraction 0.100–1.0 mm. A total number of >300 benthic and >300 planktonic specimens of foraminifera were picked for each sample, counted and identified to species level. In this paper, we present only data of the percent occurrence of benthic species from the 'Atlantic species group': *Eggerella bradyi*, *Sigmoilopsis schlumbergeri*, *Bulimina marginata*, *Gyroidina* spp., *Gavelinopsis praegeri*, *Pyrgo serrata*, *Spirophtalmidium acutimargo*, *Pullenia bulloides*, and *P. quinqueloba* (Rasmussen *et al.* 1996, 2007; Wollenburg *et al.* 2001).

Seventeen AMS ^{14}C dates were obtained at the Chrono Centre, Queen's University, Belfast, UK, and two dates at Beta Analytic, London, UK (Table 2). Fifteen dates were measured on monospecific samples of *N. pachyderma* sinistral, two on mixed benthic foraminifera and two dates were measured on bivalve shells. In addition, four dates in core HH12-928PC were measured on bivalve shells cleaned of carbonate crusts, with oxygen and carbon isotopes measured on sample aliquots (Table 3). All dates were corrected using a reservoir effect of 440 years (Mangerud & Gulliksen 1975) and calibrated to calendar (cal.) years BP using the 'Fairbanks 0701' calibration curve (Fairbanks *et al.* 2005).

Oxygen and carbon isotopes were measured on well-preserved specimens of the planktonic foraminiferal

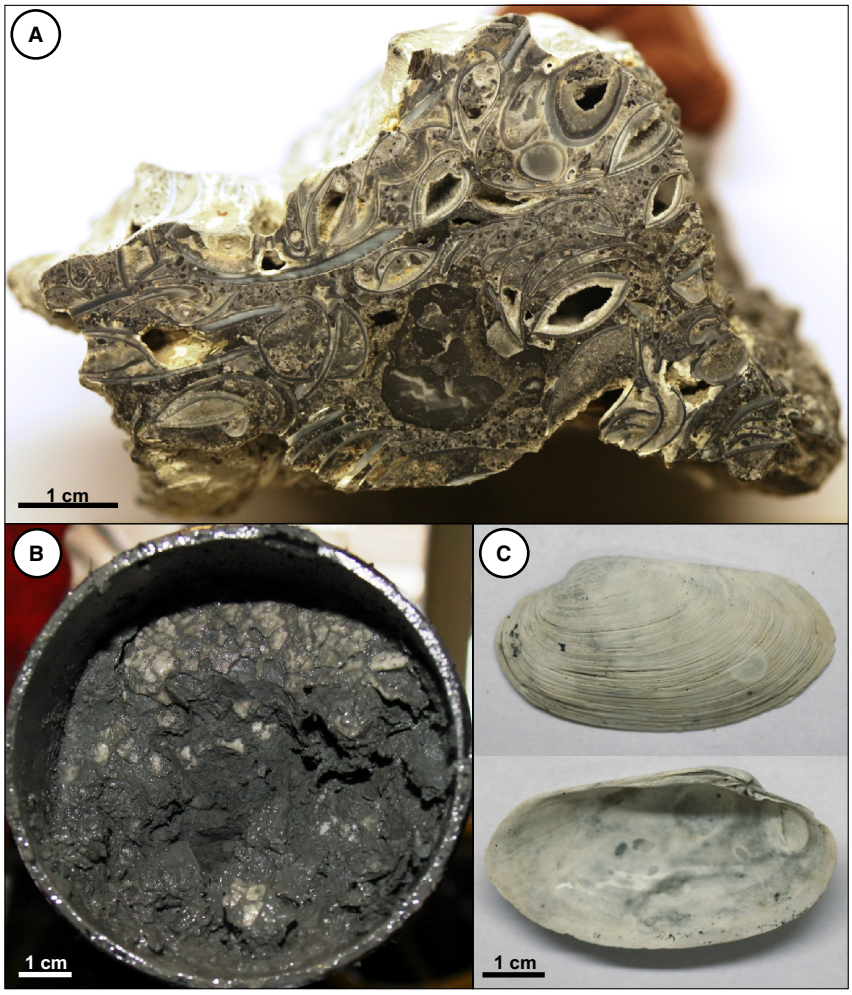

Fig. 3. A. Carbonate from the top of core HH12-928PC (piece of aragonitic pavement). B. Methane hydrates sampled in core HH12-929GC. C. Vesicomyid bivalve species from the shell horizon in core JM10-335GC.

species *N. pachyderma* and on the benthic foraminiferal species *Cassidulina neoteretis* and *Melonis barleeanus*. Samples were cleaned using alcohol in an ultrasonic bath. Five-cm-resolution stable isotope records for cores JM10-335GC and HH12-929 and 5–10 cm resolution for core HH12-928PC (Fig. 5) were generated using a Finnigan MAT 253 mass spectrometer with a Kiel IV device at the Bjerknes Centre for Climate Change, University of Bergen. Stable isotopes on selected carbonates from cores HH12-928PC and JM10-335GC were also measured (Table 4). Reported precision was ±0.08‰ for $\delta^{18}O$ and ±0.04‰ for $\delta^{13}C$. The oxygen isotope records were not corrected for isotopic disequilibrium. The $\delta^{18}O$ record for core JM10-335GC was corrected for ice-volume changes using the sea-level curve of Fairbanks (1989).

Two samples from the surface carbonate pavement from the site of core HH12-928GC were XRD-analysed at the Department of Geoscience, Aarhus University, Denmark (Supporting Information Table S1 and Fig. S1).

Results

Lithology, magnetic susceptibility, AMS ^{14}C dates and stable isotopes

Core JM10-333GC: control core east of the pockmark. – The sediments consist primarily of soft, fine-grained, homogenous green-grey hemipelagic clayey silt, with some intervals containing large dropstones (Fig. 4A). The upper ~50 cm of the core consists of hemipelagic clayey, silty deposits with high concentrations of ice-rafted debris (IRD). Below 50 cm downcore, a 65-cm-thick layer of fine laminated clay with low magnetic susceptibility (MS) values is found. Between 265 and 285 cm, a coarse-grained, dark brown layer of unsorted sediments with high density and low MS values is found. This layer is clearly visible in the colour scan. Both the laminated layer and the coarse-grained layer were clearly visible on the X-ray photographs, which formed the basis of the drawing of the lithological log (see Material and methods). The

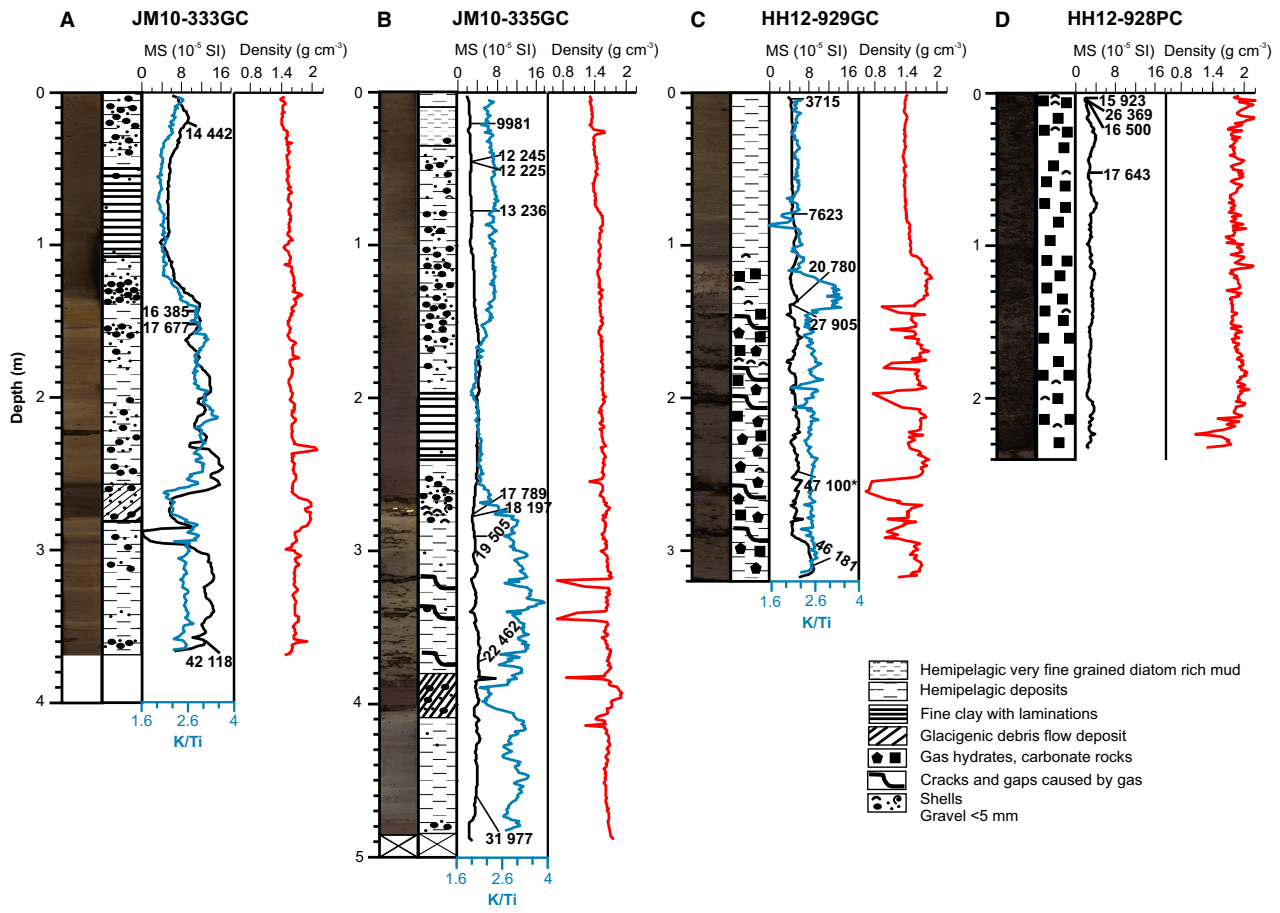

Fig. 4. Colour scan, lithological log, magnetic susceptibility (MS), K/Ti ratios, density and calibrated AMS ^{14}C dates of four cores from Vestnesa Ridge: control core JM10-333GC from outside the pockmark (A), cores from an active pockmark JM10-335GC (B), HH12-929GC (C) and HH12-928PC (D).

K/Ti ratios obtained from XRF-scanning essentially follow the pattern of MS. The four radiocarbon dates obtained for the core range from 14 442 to 42 118 cal. a BP (Table 2) with no age reversals.

Core JM10-335GC from the pockmark. – The upper part of the core contains very fine-grained, dark mud with a high abundance of large diatoms (>63 μm), followed by hemipelagic deposits with increasing amounts of IRD (Fig. 4B). An interval of laminated fine clay similar to the laminated layer in the control core is found between ~200 and 240 cm. A distinct layer of large bivalves of the family Vesicomyidae occurs at a depth of ~275 cm. The lower part of the core below the shell layer consists of light grey, silty clay. Similar to JM10-333GC, the core penetrated through coarse, unsorted sediments of very dark colour with numerous clasts. This interval is also characterized by higher density, reaching ~1.6 g cm^{-3}. The core is characterized by a strong H_2S odour between 0 and 400 cm down-core and numerous gas bubbles occur in the sediment between 280 and 370 cm down-core. The laminated layer, the horizon of bivalve shells and the coarse sediment layer are clearly visible on the X-ray photographs as shown in Fig. 4B. The MS values are low in the entire core. The K/Ti ratios are low in the laminated layer and the coarse-grained layer and high in the intervals dominated by hemipelagic deposits. A total of eight radiocarbon dates are in chronological order and range from 9009 to 31 900 cal. a BP (Table 2). Both planktonic and benthic $\delta^{18}O$ values are lowest in the upper 80 cm of the core (Fig. 5). The highest values occur in the lower part of the core, whereas intermediate values are observed between 275 and 80 cm. A prominent peak of low planktonic $\delta^{18}O$ values occurs at 280 cm depth. Benthic and planktonic $\delta^{13}C$ values are high and nearly constant throughout the record except for two excursions separated by over a metre of sediment at 85 and 225 cm.

Core HH12-929GC from the deepest part of the pockmark. – This core contains gas hydrates in the lower part (145 cm) to the bottom of the core (Fig. 4C). Except for the few nodules in the core catcher, most of

Table 2. AMS ^{14}C dates and calibrated ages of cores JM10-335GC, JM10-333GC and HH12-929GC. Correlation tie-points for Western Svalbard slope from Jessen *et al.* (2010) are shown in italics.

Core	Depth (cm)	Dated material	Laboratory code	Age (^{14}C a BP±1σ)	Calibrated age (cal. a BP±1σ)
Jessen *et al.* (2010) - TP2	10	Planktonic foraminifera	–	*9240±100*	*9840±200*
JM10-335GC	20	*N. pachyderma*	UBA-18137	9302±38	9981±111
Jessen *et al.* (2010) - TP3	35	Planktonic foraminifera	–	*9390±100*	*10 100±150*
JM10-335GC	56	*N. pachyderma*	UBA-23417	10 829±43	12 245±107
JM10-335GC	57	Mixed benthic foraminifera	UBA-23418	10 820±43	12 225±106
JM10-335GC	75	*N. pachyderma*	UBA-18138	11 830±44	13 236±69
Jessen *et al.* (2010) - TP5	198	Bivalve	–	*12 840±150*	*14 300±260*
Jessen *et al.* (2010) - TP6	240	Bivalve	–	*13 140±150*	*14 780±220*
JM10-335GC	278	*N. pachyderma*	UBA-23197	15 486±73	18 197±189
JM10-335GC	278	Bivalve	UBA-18142	15 283±56	17 789±182
JM10-335GC	290	*N. pachyderma*	UBA-18139	16 830±71	19 505±90
JM10-335GC	369	*N. pachyderma*	UBA-18140	19 327±77	22 462±95
Jessen *et al.* (2010) - TP7	380	*N. pachyderma*	–	*20 150±130*	*23 550±185*
Jessen *et al.* (2010) - TP8	405	*N. pachyderma*	–	*20 580±130*	*24 080±150*
JM10-335GC	460	*N. pachyderma*	UBA-18141	27 132±150	31 977±221
HH12-929GC	5	*N. pachyderma*	UBA-23198	3899±36	3715±56
HH12-929GC	80	*N. pachyderma*	UBA-23199	7219±38	7623±30
HH12-929GC	140	*N. pachyderma*	UBA-23200	18 011±101	20 780±152
HH12-929GC	141	Bivalve	UBA-23201	23 703±176	27 905±242
HH12-929GC	250	*N. pachyderma*	UBA-23202	44 047±2219	47 100[1]
HH12-929GC	311	*N. pachyderma*	UBA-23203	42 176±1709	46 181±2016
JM10-333GC	20	Mixed benthic foraminifera	Beta-4133010	12 920±40	14 442±119[2]
Jessen *et al.* (2010) - TP5	50	Bivalve	–	*12 840±150*	*14 300±260*
Jessen *et al.* (2010) - TP6	110	Bivalve	–	*13 140±150*	*14 780±220*
JM10-333GC	137	*N. pachyderma*	UBA-23419	14 475±61	16 385±142
JM10-333GC	147	*N. pachyderma*	UBA-23420	15 228±61	17 677±190
Jessen *et al.* (2010) - TP7	258	*N. pachyderma*	–	*20 150±130*	*23 550±185*
Jessen *et al.* (2010) - TP8	281	*N. pachyderma*	–	*20 580±130*	*24 080±150*
JM10-333GC	359	*N. pachyderma*	Beta-412869	37 420±340	42 118±339

[1]Calibrated with Calib 5.
[2]Unknown reservoir age. Calibrated age may be too old.

the hydrates consisted of small flakes evenly distributed in the sediments.

The upper ~100 cm of the core consists of dark hemipelagic, homogenous clayey silt without IRD. An interval of light grey clayey sediments of very high density with multiple authigenic carbonates occurs between 110 and 130 cm core depth. Dark grey clayey silt with numerous authigenic carbonates fills the core from 130 cm to the bottom. Five intervals with very low density are probably a result of cavities in the core sections. Several intervals of slightly higher density revealed both on X-ray photos and the density log correspond to horizons of high concentration of authigenic carbonates. Numerous bivalve shells (Vesicomyidae and Thyasira) were found at ~110–240 cm core depth. A strong H_2S odour occurs from 0 to 178 cm down-core. The MS signal is low throughout the core. The K/Ti ratios are low in the entire core except one interval at ~120–140 cm. The six calibrated radiocarbon dates range from 3700 to 47 100 cal. a BP (Table 2). They show an increasing trend down-core except for one sample at 250 cm. Low planktonic and benthic $\delta^{18}O$ values occur in the upper 95 cm of the core (Fig. 5). Below 100 cm $\delta^{18}O$ values are high (Fig. 5). The planktonic and benthic $\delta^{13}C$ values are high and nearly constant in the upper 95 cm. Below 95 cm, the values are very low, with a minimum at 115−130 cm (Fig. 5).

Table 3. AMS ^{14}C dates, calibrated ages and stable isotopes of bivalve shells from core HH12-928PC.

Identification no.	Depth (cm)	Material	$\delta^{13}C$	$\delta^{18}O$	Age (^{14}C a BP±1σ)	Calibrated age (cal. a BP±1σ)
1	Aragonitic	Bivalve shell	0.95	4.77	14 549±70	16 500±152
2	pavement from the top of the	Aragonite needles from inside a shell	−30.80	5.57	22 347±135	26 360±185
3	core (0–10 cm)	Bivalve shell	2.20	4.38	14 120±54	15 923±124
53	53	Bivalve shell	3.93	4.37	15 210±66	17 641±96

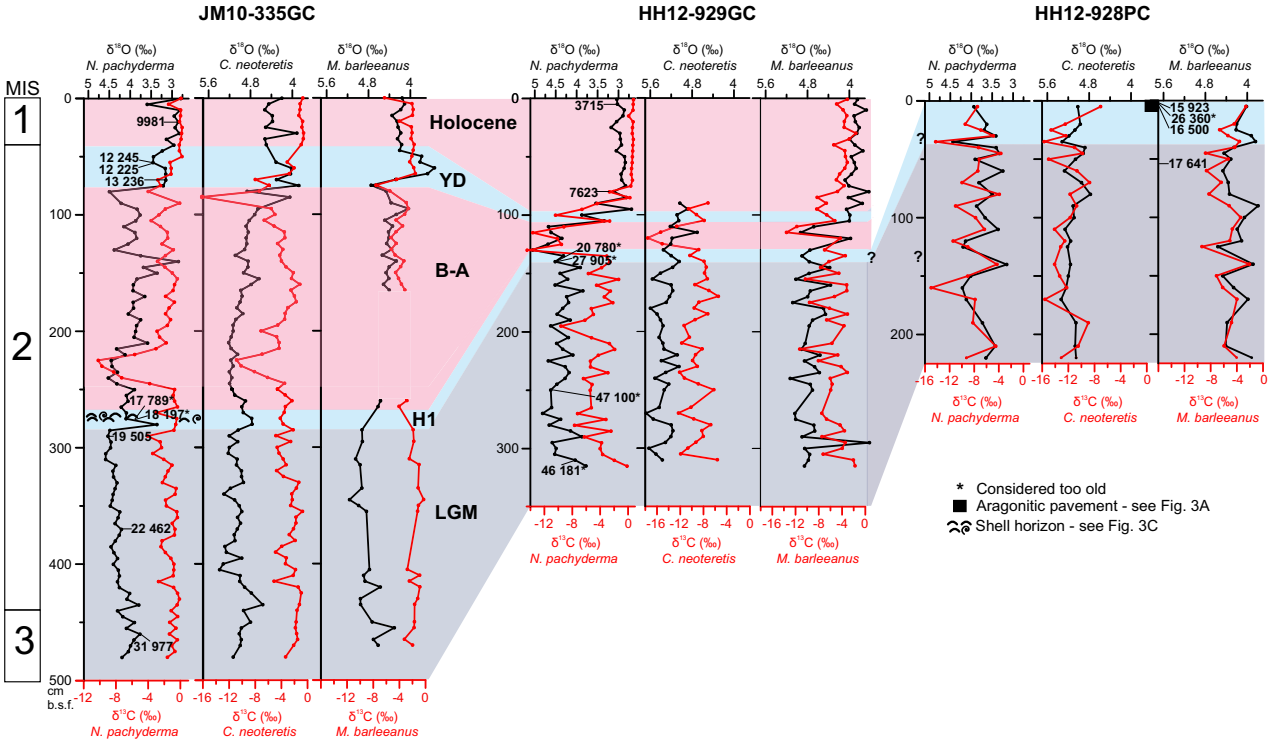

Fig. 5. Stable isotope records for pockmark cores: JM10-335GC, HH12-929GC and HH12-928PC plotted vs. depth in cm below sea floor (b.s.f.). Planktonic and benthic $\delta^{18}O$ values (black) were measured in *N. pachyderma*, *C. neoteretis* and *M. barleeanus*. $\delta^{13}C$ values (red) were measured in the same species. Calibrated AMS ^{14}C dates are shown. Coloured bars indicate correlation between cores based on stable isotopes, AMS ^{14}C dates and lithology. YD = Younger Dryas; B-A = Bølling-Allerød interstadials; H1 = Heinrich event H1; LGM = Last Glacial Maximum. ? = uncertainties in the age models.

Core HH12-928PC from the pockmark. – This core sampled dense carbonate crust and the density of the sediment is very high due to the presence of authigenic carbonates throughout the entire core (Fig. 4D). The top section of the core consists of aragonitic pavement (Fig. S1, Table S1) with numerous bivalve shells (Fig. 3B). Below the pavement, carbonate rocks and nodules of variable sizes, heavily encrusted bivalve shells and small amounts of very dark grey sediments fill the core liner. No recognizable lithology similar to the other records could be described. All core sections are characterized by very low MS values and strong H_2S odour. Three radiocarbon samples dated on bivalve shells drilled out from the carbonate crust range from 15 929 to 17 641 cal. a BP. One sample of aragonite needles precipitated inside a shell dates to 26 360 cal. a BP (Table 3). The planktonic and benthic $\delta^{18}O$ records from core HH12-928PC show very scattered values without any particular trend (Fig. 5). The $\delta^{13}C$ values are low in both planktonic and benthic specimens throughout the core (Fig. 5). One sample of stable isotopes measured on aragonite needles precipitated inside a vesicomyid shell stands out clearly with very low $\delta^{13}C$ values (−30.8‰) and with $\delta^{18}O$ values about 1‰ higher than average (5.57‰) (Table 3, Fig. 5). This sample dates about 10 000 years older than the other two samples from the same interval (Fig. 5).

Discussion

Biostratigraphy, correlation and construction of age models

In core JM10-335GC the calibrated AMS ^{14}C dates of 19 505–31 977 years together with the high $\delta^{18}O$ values show that the sediments below 280 cm correlate with the end of MIS 3 and MIS 2 including the LGM dating to 25 000–19 000 years BP (Martinson *et al.* 1987; Lisiecki & Raymo 2005). The interval below 145 cm in core HH12-929GC also most likely belongs to MIS 3 – MIS 2 given the high $\delta^{18}O$ values measured in *C. neoteretis* (Fig. 5). The interval 250–280 cm in core JM10-335GC recorded low values of both planktonic and benthic $\delta^{18}O$ typical of north Atlantic Heinrich event H1 (e.g. Bond *et al.* 1993). The two dates of 18 197 and 17 789 years are from the H1 interval, which dates to 19 000–15 600 years (e.g. Bond *et al.* 1993; Zahn *et al.* 1997; Fig. 5). The interval comprises the shell layer and very light grey, clayey sediments, the latter characteristic of H1 in Svalbard records and with similar dates (Rasmussen *et al.* 2007; Jessen *et al.*

Table 4. Stable isotopes of authigenic carbonates, cemented sediments and encrusted shells.

Core	Depth (cm)	Identification no.	$\delta^{13}C$	$\delta^{18}O$	Description
HH12-928 PC	0–5	1–1	−27.85	4.92	Grey, finely laminated hard crust
HH12-928 PC	0–5	1–2	−22.32	4.71	Grey, finely laminated hard crust
HH12-928 PC	0–5	1–3	−28.78	5.18	Needles from cavity
HH12-928 PC	0–5	1–4	−2.69	4.76	1.6-mm-thick shell
HH12-928 PC	0–5	1–5	−30.71	4.61	Spongy outer layer of concretion
HH12-928 PC	0–5	1–6	−18.45	4.15	Fragment of shell
HH12-928 PC	0–5	2	−28.86	4.92	Nodule
HH12-928 PC	0–5	3	−18.07	4.53	Layered massive lump
HH12-928 PC	0–5	4	0.86	3.49	Shell
JM10-335 GC	166		−38.80	5.90	Light grey crust

2010; see above and Figs 3C, 4). In core HH12-929GC, the interval 135–145 cm with low benthic and planktonic values most likely correlates with H1. Here, the sediments also consist of light grey clay with fragments of bivalve shells (Fig. 4). The low planktonic and benthic $\delta^{18}O$ values in the upper parts of the two cores together with the dates indicate that the upper 40 cm in core JM10-335GC and the upper 95 cm in core HH12-929GC belong to the Holocene (MIS 1). The low $\delta^{18}O$ values and dates of 12 245–13 236 years are typical of the Younger Dryas cold event of Svalbard (Rasmussen *et al.* 2007; Ślubowska-Woldengen *et al.* 2007; Jessen *et al.* 2010). The dark sediments at 250–75 cm in core JM10-335GC and 105–130 cm in HH12-929GC thus correlate with the Bølling-Allerød warm interstadials of the deglaciation, which comprises the laminated sediment layer dated to 14 700–14 380 cal. a BP (Jessen *et al.* 2010; Fig. 5).

High benthic $\delta^{18}O$ values from core HH12-928PC suggest that the record belongs to the glacial period of MIS 2. The lower $\delta^{18}O$ values in both planktonic and benthic species in the upper part of the record indicate that it belongs to the deglaciation (Fig. 5). However, the $\delta^{18}O$ values are very scattered without the typical pattern seen in the other records (Fig. 5). Based on the radiocarbon dates (excluding the one on aragonite needles with very low $\delta^{13}C$ values), we tentatively correlate the top of the core to Heinrich event H1 and the sediment below to the LGM (Fig. 5).

Lithostratigraphical units and MS patterns typical for the western Svalbard margin were described precisely by Jessen *et al.* (2010) based on 11 cores from the area. The records comprised mass transport deposits dated to ~24 000 cal. a BP, laminated fine-grained sediments deposited 14 780–14 300 cal. a BP and a diatom-rich, fine-grained layer dated 10 100–9840 cal. a BP (Jessen *et al.* 2010).

We excluded core HH12-928PC from the age model because of the difficulties in reconstructing the stratigraphy (see above). The age model is primarily based on core JM10-335GC from the pockmark with the fairly undisturbed lithology and the control core JM10-333GC from outside the pockmark. They were correlated with the well-dated MS stack records for the western Svalbard margin (Jessen *et al.* 2010) (Fig. 6). The characteristic lithological units were used as additional tie-points in the correlation and construction of the age model (Table 2; green ages in Fig. 6). Our own ^{14}C dates match well with the published dates of the lithological markers and were also used. In core JM10-335GC, a benthic foraminiferal assemblage containing species referred to as 'Atlantic species' is found. This assemblage has been shown to be characteristic for the H1 event as well as older Heinrich events (Rasmussen *et al.* 2007; Rasmussen *et al.* 2014). It has been dated to ~16 000 years in core JM03-373PC from Storfjorden Fan and in core JM02-460PC from Storfjorden Trough on the shelf (Rasmussen *et al.* 2007). A similar date of 16 446 years was obtained in the control core JM10-333GC (Table 2, Fig. 6). In core JM10-335GC, material from 2 cm above the assemblage has been dated to 17 789 years (bivalve shell) and 18 197 years (planktonic foraminifera) (Table 2, Fig. 6). The dated level is part of the shell horizon, containing mussels of the family Vesicomyidae (Figs 3C, 6). This family of species is known to live in sulphide-rich, reducing environments of cold seeps and hydrothermal vents (Boss & Turner 1980; Cosel & Salas 2001; Krylova & Sahling 2010). The relatively old ages for both bivalve shells and planktonic foraminifera together with the presence of the fossil chemosynthetic fauna suggest that the dated material could have been influenced by diagenesis (see also discussion below). Therefore, the two dates marked red in Fig. 6 were omitted from the construction of the age model of core JM10-335GC.

The age models for the cores JM10-335GC and JM10-333GC were constructed based on the linear interpolation between dates and tie-points (Fig. 6). Sedimentation rates were high during the deglaciation (131 cm ka^{-1}) and low during the beginning of the Holocene (15 cm ka^{-1}) and in the glacial period (9.5 cm ka^{-1}) (Fig. 7G).

Seeping of methane, $\delta^{13}C$ signals and authigenic carbonates

The benthic and planktonic foraminiferal $\delta^{13}C$ records of cores JM10-335GC and HH12-929GC show

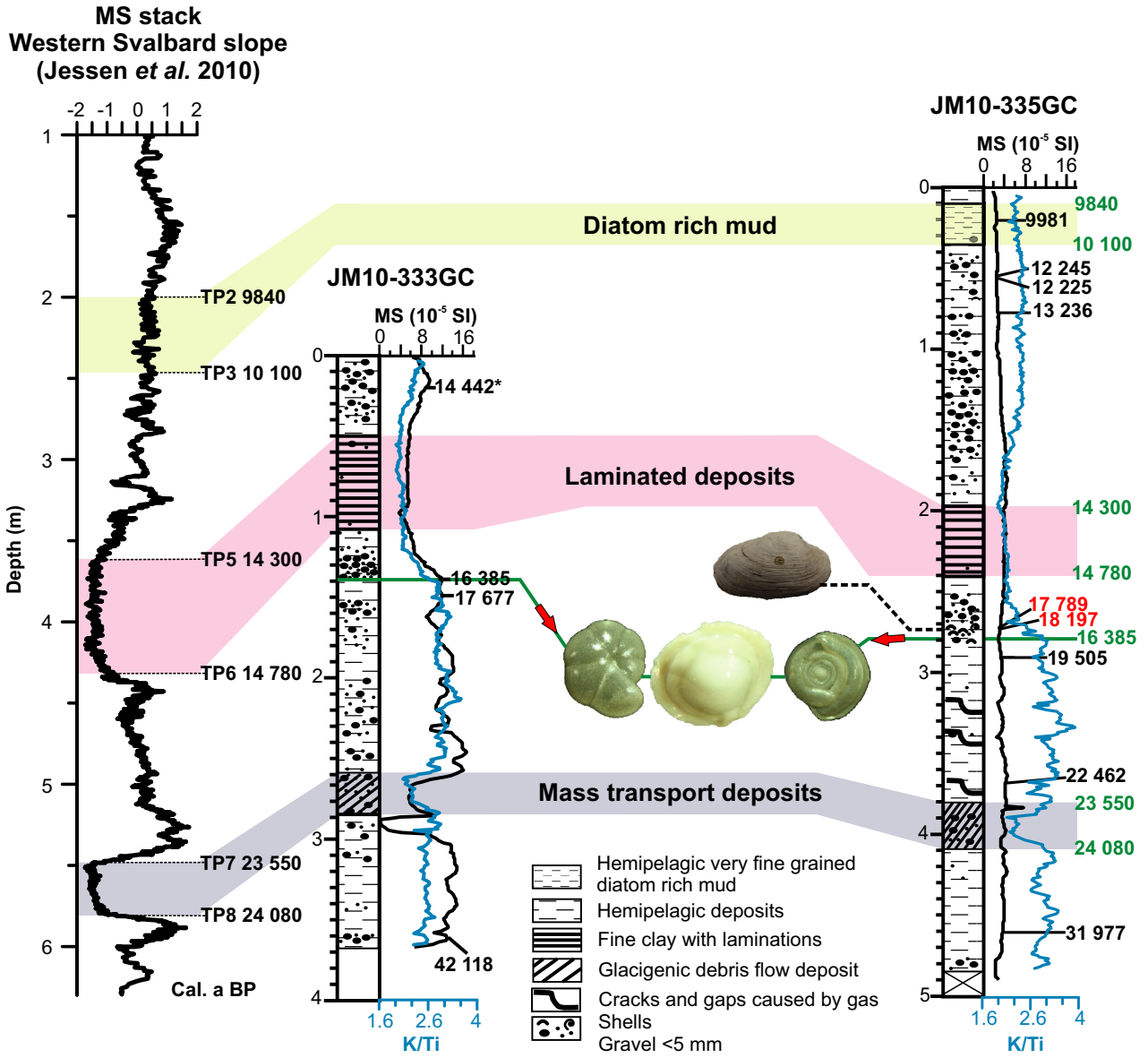

Fig. 6. Correlation between stacked magnetic susceptibility records from the western Svalbard slope (Jessen *et al.* 2010) and magnetic susceptibility, lithology and K/Ti ratio records in the control core from outside the pockmark JM10-333GC and pockmark core JM10-335GC. Three lithological stratigraphical marker horizons are shown with colour shading. Ages in green are based on correlation between the cores; ages in red are considered too old. Foraminiferal assemblages containing specimens of the 'Atlantic species group' and vesicomyids from the shell horizon in the core JM10-335GC are indicated.

significant negative excursions (−16 to −7.5‰) in the Bølling-Allerød interstadials 15 200–13 000 years BP (Figs 5, 7). In non-methane influenced sites, the $\delta^{13}C$ values are normally ~−0.3 to −1‰ for *C. neoteretis* (Wollenburg *et al.* 2001; Mackensen *et al.* 2006), ~−2‰ for *M. barleeanus* (McCorkle *et al.* 1990; Wollenburg *et al.* 2001) and between −0.5 and 0.5‰ for *N. pachyderma* (Knies & Stein 1998; Jessen *et al.* 2010; Zamelczyk *et al.* 2012, 2014).

Benthic foraminiferal species can incorporate the low $\delta^{13}C$ values of the DIC in the pore waters and thus record the presence of anaerobically oxidized methane in sediments during mineralization of their shells (Sen Gupta *et al.* 1997; Bernhard *et al.* 2001; Hill *et al.* 2012). It is impossible that planktonic foraminifera calcifying in the water column will be affected to the same extent as benthic foraminifera during calcification (Uchida *et al.* 2004; Cook *et al.* 2011; Consolaro *et al.* 2015). Therefore, the low $\delta^{13}C$ values observed in the planktonic foraminifera are most likely the result of diagenetic overgrowth by authigenic carbonates associated with the AOM at the SMTZ (Uchida *et al.* 2004; Cook *et al.* 2011). While the $\delta^{13}C$ signal in benthic foraminifera could be a combination of both primary

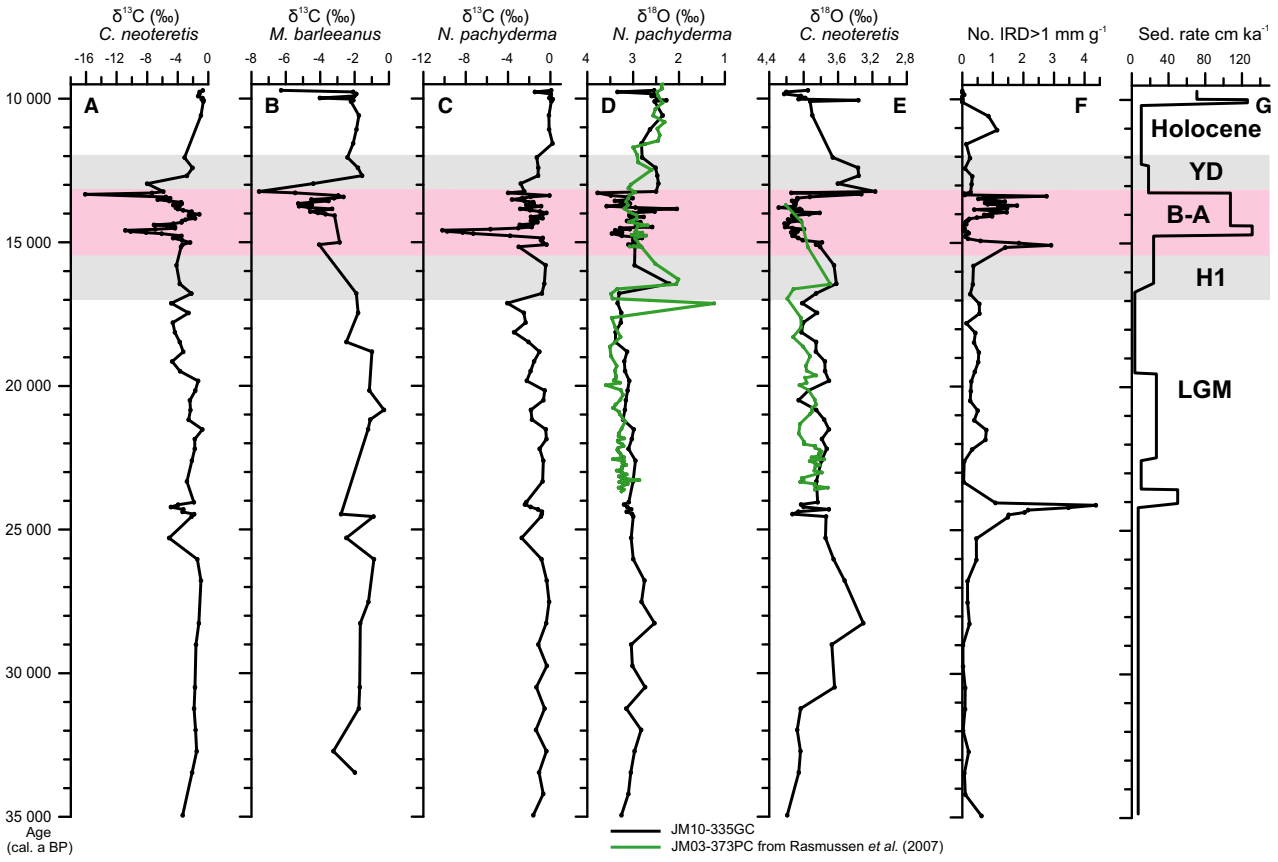

Fig. 7. Records for core JM10-335GC (black) plotted vs. age (cal. a BP). Data from core JM03-373PC (Rasmussen *et al.* 2007) are shown in green. Benthic $\delta^{13}C$ values measured in *C. neoteretis* (A), *M. barleeanus* (B), planktonic $\delta^{13}C$ values measured in *N. pachyderma* (C), planktonic $\delta^{18}O$ values corrected for ice-volume changes measured in *N. pachyderma* in core JM10-335GC and reference core JM03-373PC (D), benthic $\delta^{18}O$ values corrected for ice-volume changes measured on *C. neoteretis* in the core JM10-335GC and reference core JM03-373PC (E), number of IRD >1 mm per gram dry weight sediment (F), average sedimentation rates (G). YD = Younger Dryas; B-A = Bølling-Allerød interstadials; H1 = Heinrich event H1; LGM = Last Glacial Maximum.

and diagenetic calcite (Cook *et al.* 2011; Consolaro *et al.* 2015), the planktonic foraminifera can reach comparatively low $\delta^{13}C$ values due to their spiny and porous surfaces providing a larger surface area for authigenic carbonate growth than the smooth tests of benthic specimens (Cook *et al.* 2011; Kozdon *et al.* 2013). The effect of authigenic carbonates on the isotopic composition of foraminiferal shells has been identified previously (e.g. Torres *et al.* 2003; Martin *et al.* 2004; Uchida *et al.* 2008). However, authigenic overgrowth is not widely discussed and most studies from seep environments focus on benthic foraminifera without simultaneous measurements of the planktonic foraminifera, assuming that the entire depleted $\delta^{13}C$ signal is a result of calcification in pore water with DIC of very low $\delta^{13}C$ values (Hill *et al.* 2004; Martin *et al.* 2007, 2010; Panieri *et al.* 2009, 2012).

Alteration of the foraminiferal shells could have occurred soon after the foraminifera died or at any time during modern venting (Martin *et al.* 2004). As authigenic carbonates precipitate at the SMTZ it is important to establish the position of the zone in the sediment column. A deep SMTZ would result in authigenic carbonates forming in sediment much older than the actual event of enhanced methane flux (Ussler & Paull 2008). The position of the palaeo-SMTZ is unknown, making interpretation of the carbon isotopic signal as a proxy for methane seepage events problematical in all three records JM10-335GC, HH12-928PC and HH12-929GC. However, it is most likely that during events of intensified seeping, the SMTZ was at the sediment surface. In favour of our suggestions of increased activity in the Bølling and Allerød interstadials is the fact that four different isotope records from three different pockmarks from the Vestnesa Ridge located 35 km apart at the furthest distance (Fig. 1B) all show low $\delta^{13}C$ excursions with similar timing. The record of Consolaro *et al.* (2015) showed indications of higher methane flux in sediments belonging to the end of the Allerød interstadial in the western part of the Vestnesa Ridge, while Panieri *et al.* (2014) found the highest flux to occur in the lower Bølling interstadial as indicated by the distribution patterns and biostratigraphical correlation of the

benthic foraminiferal faunas. The events of low $\delta^{13}C$ values are located at different depths below the sediment surface in the various studied records, yet the timing of the event is similar: 390 cm in the core of Consolaro *et al.* (2015), 108–247 cm in the core of Panieri *et al.* (2014) (the SMTZ today is found 65 cm down-core), 85 and 225–230 cm in core JM10-335GC and 115–125 cm in core HH12-929GC (Fig. 5). The two excursions of low $\delta^{13}C$ in core JM10-335GC are separated by 145 cm of sediment, probably excluding the influence of the modern SMTZ.

In further support is the presence of chemosynthetic macrofauna just below the horizon with the lowest $\delta^{13}C$ values. In core JM10-335GC, high abundances of both whole and intact bivalve shells were observed (~30 specimens of family Vesicomyidae) at the point where the benthic $\delta^{13}C$ values start to decrease (Figs 3C, 5, 6). The bivalve shells are not present in the interval characterized by the lowest $\delta^{13}C$ excursions during the Bølling-Allerød interstadials as they occur in the upper part of H1 (Figs 5, 6). Vesicomyids are known to thrive in environments with medium to low methane flux generating an optimal sulphide flux (e.g. Sahling *et al.* 2002). We think that a potential enhanced methane flux during the Bølling-Allerød interstadials could have caused highly elevated concentrations of toxic hydrogen sulphide that may have been lethal for the bivalves.

We thus suggest that the increase in seepage began during the later phase of H1, and that it may have intensified during the Bølling-Allerød interstadials. However, as our evidence also shows the presence of highly complex and heterogeneous seep environments within the studied pockmark, the timing of seepage increase requires further investigations, including porewater studies of all the types of seep environments in the pockmark.

Oxygen isotopes

Postdepositional diagenesis can affect the oxygen isotope composition of foraminiferal shells (Killingley 1983; Kozdon *et al.* 2013). Coating of the foraminiferal shells by authigenic carbonates with high $\delta^{18}O$ values (~5–7‰) caused by ^{18}O-rich diagenetic fluids (Aloisi *et al.* 2002; Orphan *et al.* 2004) can increase $\delta^{18}O$ values. The $\delta^{18}O$ records of planktonic and benthic foraminifera from the Vestnesa cores JM10-335GC and HH12-929GC from the active pockmark are consistent with other $\delta^{18}O$ records from outside seep areas (e.g. Rasmussen *et al.* 2007; Jessen *et al.* 2010; Zamelczyk *et al.* 2012, 2014) showing very similar values through time (Figs 5, 7D, E). The reason for this, considering that the carbon isotope record was strongly influenced by diagenetic alteration, is most probably the very small difference between biogenic and authigenic oxygen isotope values (Table 4). The $\delta^{18}O$ values of the carbonate crust from core JM10-335GC was 5.9‰, while the variability of biogenic carbonate is between 5.6 and 2.8‰ (e.g. Rasmussen *et al.* 2007; Jessen *et al.* 2010; Zamelczyk *et al.* 2012, 2014; Fig. 5). Thus, in the specimens from the glacial period, the signal of the incorporation of authigenic carbonate would be negligible and give only slightly more positive values for the deglacial and Holocene specimens. The stratigraphical and palaeoceanographical signal in the $\delta^{18}O$ records are thus still fairly intact and useful for stratigraphy.

Magnetic susceptibility and K/Ti records

In general, the cores taken from inside the pockmark have very low MS values without the pattern seen in undisturbed records from the west Svalbard margin (Figs 4, 6). The most undisturbed core JM10-335GC of the pockmark cores had clear, easily recognizable and intact lithological features similar to other records from the Svalbard margin (e.g. Jessen *et al.* 2010; see Fig. 4 and Results). The common feature of all pockmark cores was the characteristic smell indicating the presence of hydrogen sulphide. Canfield & Berner (1987) observed that in anoxic sediments with high content of organic carbon the hydrogen sulphide produced during organoclastic sulphate reduction caused the dissolution of magnetite and formation of pyrite, which is a paramagnetic mineral giving magnetic susceptibility values of near-zero. This process is a major cause of the loss of magnetostratigraphical records in marine sediments (Karlin 1990; Passier *et al.* 1998; Riedinger *et al.* 2005). Given the low accumulation rates of organic matter in the Atlantic zone over the western Svalbard margin (Müller & Stein 2014; Sanchez-Vidal *et al.* 2015), the presence of hydrogen sulphide is most probably an indicator of ongoing AOM. Iron oxides after dissolution by hydrogen sulphide recombine to reduced forms of iron sulphides such as greigite and mackinawite that readily convert to the stable pyrite (Dewangan *et al.* 2013; Zhang *et al.* 2014). With sufficient amounts and long enough exposure to hydrogen sulphide, all iron is converted into pyrite, resulting in low MS values (Canfield & Berner 1987; Novosel *et al.* 2005; Dewangan *et al.* 2013; Usapkar *et al.* 2014; Zhang *et al.* 2014). The normal MS signal in the control core (JM10-333GC) as well as in other 'non-seep' records from the western Svalbard margin (e.g. Birgel & Hass 2004; Jessen *et al.* 2010; Müller & Stein 2014) indicate that the low MS signals in the pockmark cores are a local phenomenon connected with seeping of methane. Novosel *et al.* (2005) presented the potential of MS measurements as a reliable diagnostic tool of methane-induced sedimentological and mineralogical changes.

The K/Ti ratio reflects the sediment source and bottom current activity similarly to MS and has been

proposed as a stratigraphical tool resistant to diagenesis (Richter *et al.* 2006). During warm periods, enhanced inflow of Atlantic Waters brings eroded basaltic material derived from North Atlantic volcanic provinces, causing low K/Ti ratios, whereas during cold periods high K/Ti ratios indicate an increased importance of locally derived terrigenous material (Pirrung *et al.* 2002; Richter *et al.* 2006; Grützner & Higgins 2010). The K/Ti ratio follows the MS pattern in our control core JM10-333GC and shows the same pattern in the pockmark core JM10-335GC (Figs 4, 6). As titanium is not prone to diagenetic processes, this signal will be preserved as long as the sedimentary record is undisturbed. In core JM10-335GC, where diagenesis destroyed the MS signal (see above), the lithology was undisturbed and the K/Ti record intact. Core HH12-929GC lacks the chronostratigraphical signal seen in the undisturbed cores, which possibly could be related to the presence of the gas hydrates in the lower part (Fig. 4). It is not known if the K/Ti signal was destroyed after the core came on deck and the hydrates melted, or if it was already destroyed before core retrieval. The K/Ti ratio has the potential to be a reliable tool for chronostratigraphy and assessing the degree of disturbance of the lithology in methane seep environments, but this needs further investigations.

Radiocarbon dates

In methane-influenced environments, ^{14}C ages of ^{13}C-depleted foraminiferal tests are significantly older than those of foraminifera with normal $\delta^{13}C$ values from similar sediment horizons not affected by seeping (Uchida *et al.* 2008; Cook *et al.* 2011). According to Uchida *et al.* (2008), this indicates that ^{14}C-free carbon from methane is the main reason for the low $\delta^{13}C$ values. Our study confirms the impact of inorganic calcite precipitation on the radiocarbon ages, with the example from the H1 interval, where most probably the seeping of methane began to increase (slightly higher ages in core JM10-335GC; significantly higher ages in core HH12-929GC with presence of gas hydrates and of the ^{13}C-depleted shell fragment in core HH12-928PC; Table 3, Figs 4, 6). It is also likely that the two infinite ages in core HH12-929GC are caused by contamination from 'old' carbon.

Triggering mechanisms

The strongest methane release event, with extremely ^{13}C-depleted shells of planktonic and benthic foraminifera occurred during the Bølling-Allerød interstadial intervals (Figs 5, 7). The Bølling-Allerød interstadials were periods of warm climate, characterized on the Svalbard shelf and slope by high sedimentation rates and a periodic high flux of IRD (Birgel & Hass 2004; Ślubowska *et al.* 2005; Rasmussen *et al.* 2007; Jessen *et al.* 2010) (Fig. 7).

The increase in advective methane flux into surface sediments began towards the end of H1 (Figs 5, 7). Intermediate water began warming during H1 as indicated by lowering of benthic $\delta^{18}O$ values and rise in warm-water benthic foraminiferal species, the 'Atlantic species' (see e.g. Rasmussen *et al.* 2007). These are also present in low numbers at 1200 m water depth at the Vestnesa Ridge in core JM10-335GC (Fig. 6) and in core JM03-373PC from 1489 m water depth (Rasmussen *et al.* 2007). Mg/Ca measurements of benthic foraminifera from H1 in the SE Norwegian Sea indicated bottom-water temperatures (BWTs) there as high as 5–6 °C at 1179 m water depth (Ezat *et al.* 2014). The BWTs peaked right before the start of the Bølling interstadial. At the onset of the Bølling interstadial the BWT dropped very rapidly to <0–1 °C and remained low until the present. It might have been possible that the increase in BWT during H1 caused enhanced flux of methane increasing in intensity at the beginning of the Bølling-Allerød interstadials. Persistent bottom-water warming of 4–5 °C could provide enough heat propagation to result in a shallower depth of the base of the gas hydrate stability zone (BGHZ) and melting of gas hydrates. However, this remains speculative, as no record of the evolution of the BGHZ at Vestnesa Ridge exists so far.

Variations in gas emissions from the seabed have also been associated with seismic activity and changes in sedimentary regimes (Judd & Hovland 2007; Franek *et al.* 2014; Consolaro *et al.* 2015). The Vestnesa Ridge, because of its proximity to a mid-oceanic ridge system (the extension of the mid-Atlantic Ridge, the Knipovich Ridge) is located in a seismically active area (Mitchell *et al.* 1990; Vogt *et al.* 1999). Consolaro *et al.* (2015) suggested that increased seismic activity could have occurred as a response to the rapid melting of the nearby Svalbard-Barents Sea Ice Sheet during the Bølling interstadial.

The deglacial $\delta^{13}C$ excursions in our records have similar timings as those found in other records from the area (Fig. 1B), which we now can show occurred in the Bølling-Allerød interstadials, beginning during the late H1 event. Methane release could be caused by climatic events with concomitant bottom-water warming, sea-level change or increase in seismic activity after the rapid retreat of the former large ice sheets or by other climate-related factors.

Conclusions

This study aimed to reconstruct the timing of events of increase in methane emission during the past 35 000 years and to evaluate the effects of the varying degrees of disturbance by methane release on the

sediments and palaeo-proxies in three sedimentary records from methane-influenced environments. A record from outside the methane-affected areas was studied for comparison and stratigraphy. The interpretation of the palaeo-proxy records led to the following conclusions.

- Low $\delta^{13}C$ values in both benthic and planktonic foraminiferal tests during the Bølling-Allerød interstadials are mainly a result of authigenic carbonate overgrowth of the shells. Even though this is not a primary signal recorded during calcification, we argue that it is evidence of increased flux of methane at that time. A layer of vesicomyid bivalve shells marks the time of increase in methane seepage, correlating with the end of the H1 event.
- Additionally, in records influenced by a weak degree of methane seepage, even a thin coating of authigenic carbonates precipitated on foraminiferal shells can apparently result in significantly older ages from AMS ^{14}C dating. This was demonstrated via correlation of stable isotope and lithological records from well-dated and undisturbed records from outside of seep areas.
- The influence of authigenic overgrowth on the $\delta^{18}O$ records is minor and the $\delta^{18}O$ values recorded here are close to values within the normal range of foraminiferal calcite. Therefore, $\delta^{18}O$ records remain a valid stratigraphical tool in methane seep sites when the influence of authigenic carbonate overgrowth is low. The oxygen isotope record is probably not reliable in the case of heavily encrusted samples, such as in core HH12-928PC.
- In environments of methane release, magnetic susceptibility records are no longer reliable stratigraphical tools. The reductive conditions dissolve magnetite grains responsible for signal variations on the Svalbard margin. However, because of this process the magnetic susceptibility can be used as a diagnostic tool for methane-affected palaeo-reductive environments.
- The stratigraphy was reconstructed by detailed investigation of the lithology and biostratigraphy, which allowed us to construct a reliable age model for the pockmark based on core JM10-335GC, but not for core sections where the lithology has been severely disturbed by carbonate encrustations, presence of gas hydrates and/or gas under high pressure (cores HH12-928PC and HH12-929GC).
- It is difficult to pinpoint the dominant factor that triggered the seepage events. However, it appears that the timing of our recorded methane events coincides with the timing of events from other pockmarks of Vestnesa Ridge, suggesting that the methane emission events affected a larger part of the hydrate reservoir area of Vestnesa Ridge than the area investigated here.

Acknowledgements. – We thank the captain and crew of RV 'Helmer Hanssen' for their assistance in retrieving the sediment cores. The research was supported by UiT, Arctic University of Norway, and the Mohn Foundation via the Paleo-CIRCUS project and by the Research Council of Norway through its Centre of Excellence funding scheme for CAGE, project number 223259. The study was also supported by ResClim. We thank E. Thomsen and O. B. Nielsen for the XRD analyses, M. Forwick for XRF scanning and N.-M. Hanken for help with handling carbonates. U. Ninnemann and R. Søraas, University of Bergen, supervised the isotope measurements. S. Vadakkepuliyambatta and T. Grytå helped to prepare Fig. 2. J. Mienert and S. Bünz are sincerely thanked for their comments on the earlier versions of the manuscript. The editor J. A. Piotrowski and an anonymous reviewer are sincerely thanked for their very constructive and helpful reviews of the manuscript.

References

Aagaard, K., Foldvik, A. & Hillman, S. R. 1987: The west Spitsbergen current: disposition and water mass transformation. *Journal of Geophysical Research 92*, 3778–3784.

Aagaard, K., Swift, J. H. & Carmack, E. C. 1985: Thermohaline circulation in the Arctic Mediterranean Seas. *Journal of Geophysical Research 90*, 4833–4846.

Aloisi, G., Pierre, C., Rouchy, J.-M. & Faugeres, J.-C. 2002: Isotopic evidence of methane-related diagenesis in the mud volcanic sediments of the Barbados Accretionary Prism. *Continental Shelf Research 22*, 2355–2372.

Barry, J. P., Greene, H. G., Orange, D. L., Baxter, C. H., Robison, B. H., Kochevar, R. E., Nybakken, J. W., Donald, L. R. & McHugh, C. M. 1996: Biologic and geologic characteristics of cold seeps in Monterey Bay, California. *Deep Sea Research, Part I: Oceanographic Research Papers 43*, 1739–1762.

Bernhard, J. M., Buck, K. R. & Barry, J. P. 2001: Monterey Bay cold-seep biota: assemblages, abundance, and ultrastructure of living foraminifera. *Deep Sea Research, Part I: 48*, 2233–2249.

Beszczynska-Möller, A., Fahrbach, E., Schauer, U. & Hansen, E. 2012: Variability in Atlantic water temperature and transport at the entrance to the Arctic Ocean, 1997–2010. *ICES Journal of Marine Science 69*, 852–863.

Bhatnagar, G., Chatterjee, S., Chapman, W. G., Dugan, B., Dickens, G. R. & Hirasaki, G. J. 2011: Analytical theory relating the depth of the sulfate-methane transition to gas hydrate distribution and saturation. *Geochemistry, Geophysics, Geosystems 12*, Q03003, doi:10.1029/2010GC003397.

Birgel, D. & Hass, H. C. 2004: Ocean and atmospheric variations during the last deglaciation in the Fram Strait (Arctic Ocean): a coupled high-resolution organic-geochemical and sedimentological study. *Quaternary Science Reviews 23*, 29–47.

Boetius, A., Ravenschlag, K., Schubert, C. J., Rickert, D., Widdel, F., Gieseke, A., Amann, R., Jorgensen, B. B., Witte, U. & Pfannkuche, O. 2000: A marine microbial consortium apparently mediating anaerobic oxidation of methane. *Nature 407*, 623–626.

Bond, G., Broecker, W., Johnsen, S., McManus, J., Labeyrie, L., Jouzel, J. & Bonani, G. 1993: Correlations between climate records from North Atlantic sediments and Greenland ice. *Nature 365*, 143–147.

Borowski, W. S., Paull, C. K. & Ussler, W. 1996: Marine pore-water sulfate profiles indicate *in situ* methane flux from underlying gas hydrate. *Geology 24*, 655–658.

Boss, K. & Turner, R. 1980: The giant white clam from the Galapagos Rift, Calyptogena magnifica species novum. *Malacologia 20*, 161–194.

Bünz, S., Polyanov, S., Vadakkepuliyambatta, S., Consolaro, C. & Mienert, J. 2012: Active gas venting trough hydrate-bearing sediments on the Vestnesa Ridge, offshore W-Svalbard. *Marine Geology 332–334*, 189–197.

Canfield, D. E. & Berner, R. A. 1987: Dissolution and pyritization of magnetite in anoxic marine sediments. *Geochimica et Cosmochimica Acta 51*, 645–659.

Chatterjee, S., Dickens, G. R., Bhatnagar, G., Chapman, W. G., Dugan, B., Snyder, G. T. & Hirasaki, G. J. 2011: Pore water sulfate, alkalinity, and carbon isotope profiles in shallow sediment above marine gas hydrate systems: a numerical modeling perspective. *Journal of Geophysical Research 116*, B09103, doi:10.1029/2011JB008290.

Chen, Y., Ussler, W., Haflidason, H., Lepland, A., Rise, L., Hovland, M. & Hjelstuen, B. O. 2010: Sources of methane inferred from pore-water $\delta^{13}C$ of dissolved inorganic carbon in Pockmark G11, offshore Mid-Norway. *Chemical Geology 275*, 127–138.

Consolaro, C., Rasmussen, T. L., Panieri, G., Mienert, J., Bünz, S. & Sztybor, K. 2015: Carbon isotope ($\delta^{13}C$) excursions suggest times of major methane release during the last 14kyr in Fram Strait, the deep-water gateway to the Arctic. *Climate of the Past 11*, 669–685.

Cook, M. S., Keigwin, L. D., Birgel, D. & Hinrichs, K.-U. 2011: Repeated pulses of vertical methane flux recorded in glacial sediments from the southeast Bering Sea. *Paleoceanography 26*, PA2210, doi:10.1029/2010PA001993.

Cosel, R. V. & Salas, C. 2001: Vesicomyidae (Mollusca: Bivalvia) of the genera *Vesicomya*, *Waisiuconcha*, *Isorropodon* and *Callogonia* in the eastern Atlantic and the Mediterranean. *Sarsia 86*, 333–366.

Dewangan, P., Basavaiah, N., Badesab, F. K., Usapkar, A., Mazumdar, A., Joshi, R. & Ramprasad, T. 2013: Diagenesis of magnetic minerals in a gas hydrate/cold seep environment off the Krishna-Godavari basin, Bay of Bengal. *Marine Geology 340*, 57–70.

Dickens, G. R. 2003: Rethinking the global carbon cycle with large, dynamic and microbially mediated gas hydrate capacitor. *Earth and Planetary Science Letters 213*, 169–183.

Eiken, O. & Hinz, K. 1993: Contourites in the Fram Strait. *Sedimentary Geology 82*, 15–32.

Engen, Ø., Faleide, J. I. & Dyreng, T. K. 2008: Opening of the Fram Strait gateway: a review of plate tectonic constrains. *Tectonophysics 450*, 51–69.

Ezat, M. M., Rasmussen, T. L. & Groeneveld, J. 2014: Persistent intermediate water warming during cold stadials in the southeastern Nordic seas during the past 65 k.y. *Geology 42*, 663–666.

Fairbanks, R. G. 1989: A 17 000-year glacio-eustatic sea level record: influence of glacial melting rates on the Younger Dryas event and deep-ocean circulation. *Nature 342*, 637–742.

Fairbanks, R. G., Mortlock, R. A., Chiu, T.-C., Cao, L., Kaplan, A., Guilderson, T. P., Fairbanks, T. W., Bloom, A. L., Grootes, P. M. & Nadeau, M. J. 2005: Radiocarbon curve spanning 0 to 50,000 years BP based on paired $^{230}TH/^{234}U/^{238}U$ and ^{14}C dates on pristine corals. *Quaternary Science Reviews 24*, 1781–1796.

Franek, P., Mienert, J., Buenz, S. & Géli, L. 2014: Character of seismic motion at a location of a gas hydrate-bearing mud volcano on the SW Barents Sea margin. *Journal of Geophysical Research, Solid Earth 119*, 6159–6177.

Grützner, J. & Higgins, S. M. 2010: Threshold behavior of millennial scale variability in deep water hydrography inferred from a 1.1 Ma long record of sediment provenance at the southern Gardar Drift. *Paleoceanography 25*, PA4204, doi:10.1029/2009PA001873.

Hensen, C., Nuzzo, M., Hornibrook, E., Pinheiro, L. M., Bock, B., Magalhães, V. H. & Brückmann, W. 2007: Sources of mud volcano fluids in the Gulf of Cadiz—indications for hydrothermally altered fluids. *Geochimica et Cosmochimica Acta 71*, 1232–1248.

Hill, T. M., Kennett, J. P. & Valentine, D. L. 2004: Isotopic evidence for the incorporation of methane-derived carbon into foraminifera from modern methane seeps, Hydrate Ridge, Northeast Pacific. *Geochimica et Cosmochimica Acta 68*, 4619–4627.

Hill, T. M., Paull, C. K. & Crister, R. B. 2012: Glacial and deglacial seafloor methane emissions from pockmarks on the northern flank of the Storegga Slide complex. *Geo-Marine Letters 32*, 73–84.

Hinrichs, K-U., Hayes, J. M., Sylva, S. P., Brewer, P. G. & DeLong, E. F. 1999: Methane-consuming archaebacterial in marine sediments. *Nature 398*, 802–805.

Hinrichs, K.-U., Hmelo, L. R. & Sylva, S. P. 2003: Molecular fossil record of elevated methane levels in Late Pleistocene coastal waters. *Science 299*, 1214–1217.

Hovland, M. & Judd, A. 1988: *Seabed Pockmarks and Seepages: Impact on Geology, Biology and the Marine Environment*. 293 pp. Graham & Trotman Ltd., London.

Hovland, M. & Thomsen, E. 1989: Hydrocarbon-based communities in the North Sea? *Sarsia 74*, 29–42.

Howe, J. A., Shimmield, T. M. & Harland, R. 2008: Late Quaternary contourites and glaciomarine sedimentation in the Fram Strait. *Sedimentology 55*, 179–200.

Hustoft, S., Bünz, S., Mienert, J. & Chand, S. 2009: Gas hydrate reservoir and active methane-venting province in sediments on <20 Ma young oceanic crust in the Fram Strait, offshore NW-Svalbard. *Earth and Planetary Science Letters 284*, 12–24.

Jakobsson, M., Cherkis, N., Woodward, J., Macnab, J. & Coakley, B. 2000: A new grid of Arctic bathymetry: a significant resource for scientists and mapmakers. *EOS, Transactions American Geophysical Union 81*, 89–96.

Jessen, S. P., Rasmussen, T. L., Nielsen, T. & Solheim, A. 2010: A new Late Weichselian and Holocene marine chronology for the western Svalbard slope 30,000–0 cal years BP. *Quaternary Science Reviews 29*, 1301–1312.

Jørgensen, N. O. 1992: Methane-derived carbonate cementation of marine sediments from the Kattegat, Denmark: geochemical and geological evidence. *Marine Geology 103*, 1–13.

Judd, A. G. & Hovland, M. 2007: *Seabed Fluid Flow: The Impact on Geology, Biology, and the Marine Environment*. 475 pp. Cambridge University Press, Cambridge.

Judd, A. G., Hovland, M., Dimitrov, L. I., Gil, S. G. & Jukes, V. 2002: The geological methane budget at continental margins and its influence on climate change. *Geofluids 2*, 109–126.

Karlin, R. 1990: Magnetite diagenesis in marine sediments from the Oregon continental margin. *Journal of Geophysical Research 95*, 4405–4419.

Killingley, J. S. 1983: Effects of diagenetic recrystallization on $^{18}O/^{16}O$ values of deep-sea sediments. *Nature 301*, 594–597.

Knies, J. & Stein, R. 1998: New aspects of organic carbon deposition and its paleoceanographic implications along the northern Barents Sea margin during the last 30,000 years. *Paleoceanography 13*, 384–394.

Kozdon, R., Kelly, D. C., Kitajima, K., Strickland, A., Fournelle, J. H. & Valley, J. W. 2013: *In situ* $\delta^{18}O$ and Mg/Ca analyses of diagenetic and planktic foraminiferal calcite preserved in a deep-sea record of the Paleocene-Eocene thermal maximum. *Paleoceanography 28*, 517–528.

Krylova, E. M. & Sahling, H. 2010: Vesicomyidae (Bivalvia): current taxonomy and distribution. *PLoS ONE 5*, e9957, doi:10.1371/journal.pone.0009957.

Kvenvolden, K. A. 1988: Methane hydrate – a major reservoir of carbon in the shallow geosphere? *Chemical Geology 71*, 41–51.

Kvenvolden, K. A. 2002: Methane hydrate in the global organic carbon cycle. *Terra Nova 14*, 302–306.

Kvenvolden, K. A., Ginsburg, G. D. & Soloviev, V. A. 1993: Worldwide distribution of subaquatic gas hydrates. *Geo-Marine Letters 13*, 32–40.

Levin, L. 2005: Ecology of cold seep sediments: interactions of fauna with flow, chemistry and microbes. *Oceanography and Marine Biology: An Annual Review 43*, 1–46.

Lisiecki, L. E. & Raymo, M. E. 2005: A Pliocene-Pleistocene stack of 57 globally distributed benthic $\delta^{18}O$ records. *Paleoceanography 20*, PA1003, doi:10.1029/2004PA001071.

Luff, R. & Wallmann, K. 2003: Fluid flow, methane fluxes, carbonate precipitation and biogeochemical turnover in gas hydrate-bearing sediments at Hydrate Ridge, Cascadia Margin: numerical modeling and mass balances. *Geochimica et Cosmochimica Acta 67*, 3403–3421.

MacDonald, I. R., Guinasso, N. L. Jr, Reilly, J. F., Brooks, J. M., Callender, W. R. & Gabrielle, S. G. 1990: Gulf of Mexico hydrocarbon seep communities: VI. Patterns in community structure and habitat. *Geo-Marine Letters 10*, 244–252.

Mackensen, A., Wollenburg, J. & Licari, L. 2006: Low $\delta^{13}C$ in tests of live epibenthic and endobenthic foraminifera at a site of active methane seepage. *Paleoceanography 12*, PA2022, doi:10.1029/2005PA001196.

Magalhães, V. H., Pinheiro, L. M., Ivanov, M. K., Kozlova, E., Blinova, V., Kolganova, J., Vasconcelos, C., McKenzie, J. A., Bernasconi, S. M., Kopf, A. J., Diaz-del-Rio, V., Gonzalez, F. J. &

Samoza, L. 2012: Formation processes of methane-derived authigenic carbonates from the Gulf of Cadiz. *Sedimentary Geology 243–244*, 155–168.

Mangerud, J. & Gulliksen, S. 1975: Apparent radiocarbon ages of recent marine shells from Norway, Spitsbergen, and Arctic Canada. *Quaternary Research 5*, 263–273.

Martin, J. B., Day, S. A., Rathburn, A. E., Perez, M. E., Mahn, C. & Gieskes, J. 2004: Relationships between the stable isotopic signatures of living and fossil foraminifera in Monterey Bay, California. *Geochemistry, Geophysics, Geosystems 5*, Q04004, doi:10.1029/2003GC000629.

Martin, R. A., Nesbitt, E. A. & Campbell, K. A. 2007: Carbon stable isotopic composition of benthic foraminifera from Pliocene cold methane seeps, Cascadia accretionary margin. *Palaeogeography, Palaeoclimatology, Palaeoecology 246*, 260–277.

Martin, R. A., Nesbitt, E. A. & Campbell, K. A. 2010: The effects of anaerobic methane oxidation on benthic foraminiferal assemblages and stable isotopes on the Hikurangi Margin of eastern New Zealand. *Marine Geology 272*, 270–284.

Martinson, D. G., Pisias, N. G., Hays, J. D., Imbrie, J., Moore, T. C. Jr & Shackleton, N. J. 1987: Age dating and the orbital theory of the ice ages: development of a high-resolution 0 to 300,000-year chronostratigraphy. *Quaternary Research 27*, 1–29.

McCorkle, D. C., Keigwin, L. D., Corliss, B. H. & Emerson, S. R. 1990: The influence of microhabitats on the carbon isotopic composition of deep-sea benthic foraminifera. *Paleoceanography 5*, 161–185.

Milkov, A. V. 2004: Global estimates of hydrate-bound gas in marine sediments: how much is really out there? *Earth-Science Reviews 66*, 183–197.

Mitchell, B. J., Bungum, H., Chan, W. W. & Mitchell, P. B. 1990: Seismicity and present-day tectonics of Svalbard. *Geophysical Journal International 102*, 139–149.

Müller, J. & Stein, R. 2014: High-resolution record of late glacial and deglacial sea ice changes in Fram Strait corroborates ice-ocean interactions during abrupt climate shifts. *Earth and Planetary Science Letters 403*, 446–455.

Naehr, T. H., Eichhubl, P., Orphan, V. J., Hovland, M., Paull, C. K., Ussler, W. III, Lorenson, T. D. & Greene, H. G. 2007: Authigenic carbonate formation at hydrocarbon seeps in continental margin sediments: a comparative study. *Deep-Sea Research, Part II 54*, 1268–1291.

Niemann, H., Losekann, T., de Beer, D., Elvert, M., Nadalig, T., Knittel, K., Amann, R., Sauter, E. J., Schluter, M., Klages, M., Foucher, J. P. & Boetius, A. 2006: Novel microbial communities of the Haakon Mosby mud volcano and their role as a methane sink. *Nature 443*, 854–858.

Nöthen, K. & Kasten, S. 2011: Reconstructing changes in seep activity by means of pore water and solid phase Sr/Ca and Mg/Ca ratios in pockmark sediments of the Northern Congo Fan. *Marine Geology 287*, 1–13.

Novosel, I., Spence, G. D. & Hyndman, R. D. 2005: Reduced magnetization produced by increased methane flux at a gas hydrate vent. *Marine Geology 216*, 265–274.

Orcutt, B. N., Boetius, A., Lugo, S. K., MacDonald, I. R., Samarkin, V. A. & Joye, S. B. 2004: Life at the edge of methane ice: microbial cycling of carbon and sulfur in Gulf of Mexico gas hydrates. *Chemical Geology 205*, 239–251.

Orphan, V. J., Ussler, W. III, Naehr, T. H., House, C. H., Hinrichs, K.-U. & Paull, C. K. 2004: Geological, geochemical, and microbiological heterogeneity of the seafloor around methane vents in the Eel River Basin, offshore California. *Chemical Geology 205*, 265–289.

Panieri, G., Camerlenghi, A., Cacho, I., Sanchez Cervera, C., Canals, M., Lafuerza, S. & Herrera, G. 2012: Tracing seafloor methane emissions with benthic foraminifera: results from the Ana submarine landslide (Eivissa Channel, Western Mediterranean Sea). *Marine Geology 291–294*, 97–112.

Panieri, G., Camerlenghi, A., Conti, S., Pini, G. A. & Cacho, I. 2009: Methane seepages recorded in benthic foraminifera from Miocene seep carbonates, Northern Apennines (Italy). *Palaeogeography, Palaeoclimatology, Palaeoecology 284*, 271–282.

Panieri, G., James, R. H., Camerlenghi, A., Westbrook, G. K., Consolaro, C., Cacho, I., Cesari, V. & Cervera, C. S. 2014: Record of methane emissions from the West Svalbard continental margin during the last 23.500 yrs revealed by $\delta^{13}C$ of benthic foraminifera. *Global and Planetary Change 122*, 151–160.

Passier, H. F., Dekkers, M. J. & de Lange, G. J. 1998: Sediment chemistry and magnetic properties in anomalously reducing core from the eastern Mediterranean Sea. *Chemical Geology 152*, 287–306.

Paull, C. K., Chanton, J. P., Neumann, A. C., Coston, J. A., Martens, C. S. & Showers, W. 1992: Indicators of methane-derived carbonates and chemosynthetic organic carbon deposits: examples from the Florida Escarpment. *Palaios 7*, 361–375.

Paull, C. K., Hecker, B., Commeau, R., Freeman-Lynde, R. P., Neumann, C., Corso, W. P., Golubic, S., Hook, J. E., Sikes, E. & Curray, J. 1984: Biological communities at the Florida escarpment resemble hydrothermal vent taxa. *Science 226*, 965–967.

Paull, C. K., Ussler, W. III, Borowski, W. S. & Spiess, F. N. 1995: Methane-rich plumes on the Carolina continental rise: associations with gas hydrates. *Geology 23*, 89–92.

Petersen, C. J., Bünz, S., Hustoft, S., Mienert, J. & Klaeschen, D. 2010: High-resolution P-Cable 3D seismic imaging of gas chimney structures in gas hydrated sediments of an Arctic sediment drift. *Marine and Petroleum Geology 27*, 1981–1994.

Pirrung, M., Fütterer, D., Grobe, H., Matthiessen, J. & Niessen, F. 2002: Magnetic susceptibility and ice-rafted debris in surface sediments of the Nordic Seas: implications for Isotope Stage 3 oscillations. *Geo-Marine Letters 22*, 1–11.

Plaza-Faverola, A., Bünz, S., Johnson, J. E., Chand, S., Knies, J., Mienert, J. & Franek, P. 2015: Role of tectonic stress in seepage evolution along the gas hydrate-charged Vestnesa Ridge, Fram Strait. *Geophysical Research Letters 42*, 733–742.

Pohlman, J. W., Bauer, J. E., Canuel, E. A., Grabowski, K. S., Knies, D. L., Mitchell, C. S., Whiticar, M. J. & Coffin, R. B. 2009: Methane sources in gas hydrate-bearing cold seeps: evidence from radiocarbon and stable isotopes. *Marine Chemistry 115*, 102–109.

Rasmussen, T. L., Thomsen, E. & Nielsen, T. 2014: Water mass exchange between the Nordic seas and the Arctic Ocean on millennial timescale during MIS 4-MIS 2. *Geochemistry, Geophysics, Geosystems 15*, 530–544.

Rasmussen, T. L., Thomsen, E., Ślubowska, M. A., Jessen, S., Solheim, A. & Koç, N. 2007: Paleoceanographic evolution of the SW Svalbard margin (76°N) since 20,000 ^{14}C yr BP. *Quaternary Research 67*, 100–114.

Rasmussen, T. L., Thomsen, E., van Weering, T. C. E. & Labeyrie, L. 1996: Rapid changes in surface and deep water conditions at the Faroe margin during the last 58,000 years. *Paleoceanography 11*, 757–771.

Reeburgh, W. S. 1976: Methane consumption in Cariaco Trench waters and sediments. *Earth and Planetary Science Letters 28*, 337–344.

Richter, T. O., van der Gaast, S., Koster, B., Vaars, A., Gieles, R., de Stiger, H. C., de Haas, H. & van Weering, T. C. E. 2006: The Avaatech XRF core scanner: technical description and applications to NE Atlantic sediments. *Geological Society of London Special Publications 267*, 39–50.

Riedinger, N., Pfeifer, K., Kasten, S., Garming, J. F. L., Vogt, C. & Hensen, C. 2005: Diagenetic alteration of magnetic signals by anaerobic oxidation of methane related to a change in sedimentation rate. *Geochimica et Cosmochimica Acta 69*, 4117–4126.

Ritzmann, O., Jokat, W., Czuba, W., Guterch, A., Mjelde, R. & Nishimura, Y. 2004: A deep seismic transect from Hovgård Ridge to northwestern Svalbard across the continental-ocean transition: a sheared margin study. *Geophysical Journal International 157*, 683–702.

Roberts, H. H. 2001: Fluid and gas expulsion on the northern Gulf of Mexico continental slope: mud-prone to mineral-prone responses. *In* Paull, C. K. & Dillon, W. P. (eds.): *Natural Gas Hydrates: Occurrence, Distribution, and Detection*, 145–161. *Geophysical Monograph Series 124*. American Geophysical Union.

Sahling, H., Rickert, D., Lee, R. W., Linke, P. & Suess, E. 2002: Macrofaunal community structure and sulfide flux at the gas hydrate deposits from the Cascadia convergent margin, NE Pacific. *Marine Ecology Progress Series 231*, 121–138.

Sanchez-Vidal, A., Llorca, M., Farré, M., Canals, M., Barceló, D., Puig, P. & Calafat, A. 2015: Delivery of unprecedented amounts of perfluoroalkyl substances towards the deep-sea. *Science of the Total Environment 526*, 41–48.

Schauer, U., Fahrbach, E., Osterhus, S. & Rohardt, G. 2004: Arctic warming through the Fram Strait: oceanic heat transport from 3 years of measurements. *Journal of Geophysical Research 109*, C06026, doi:10.1029/2003JC001823.

Sen Gupta, B. K., Platon, E., Bernhard, J. M. & Aharon, P. 1997: Foraminiferal colonization of hydrocarbon-seep bacterial mats and underlying sediment, Gulf of Mexico slope. *Journal of Foraminiferal Research 27*, 292–300.

Sibuet, M. & Olu, K. 1998: Biogeography, biodiversity and fluid dependence of deep-sea cold-seep communities at active and passive margins. *Deep Sea Research, Part II 45*, 517–567.

Ślubowska, M. A., Koç, N., Rasmussen, T. L. & Klitgaard-Kristensen, D. 2005: Changes in the flow of Atlantic water into the Arctic Ocean since the last deglaciation: evidence from the northern Svalbard continental margin, 80°N. *Paleoceanography 20*, PA4014, doi:10.1029/2005PA001141.

Ślubowska-Woldengen, M., Rasmussen, T. L., Koç, N., Klitgaard-Kristensen, D., Nilsen, F. & Solheim, A. 2007: Advection of Atlantic Water to the western and northern Svalbard shelf since 17,500 cal yr BP. *Quaternary Science Reviews 26*, 463–478.

Snyder, G. T., Hiruta, A., Matsumoto, R., Dickens, G. R., Tomaru, H., Takeuchi, R., Komatsubara, J., Ishida, Y. & Yu, H. 2007: Pore water profiles and authigenic mineralization in shallow marine sediments above the methane-charged system on Umitaka Spur, Japan Sea. *Deep-Sea Research, Part II 54*, 1216–1239.

Suess, E., Torres, M. E., Bohrmann, G., Collier, R. W., Greinert, J., Linke, P., Rehder, G., Trehu, A., Wallmann, K., Winckler, G. & Zuleger, E. 1999: Gas hydrate destabilization: enhanced dewatering, benthic material turnover and large methane plumes at the Cascadia convergent margin. *Earth and Planetary Science Letters 170*, 1–15.

Torres, M. E., Mix, A. C., Kinports, K., Haley, B., Klinkhammer, G. P., McManus, J. & de Angelis, M. A. 2003: Is methane venting at the seafloor recorded by $\delta^{13}C$ of benthic foraminifera shells? *Paleoceanography 18*, 1062, doi:10.1029/2002PA000824.

Treude, T., Boetius, A., Knittel, K., Wallmann, K. & Jørgensen, B. B. 2003: Anaerobic oxidation of methane above gas hydrates at Hydrate Ridge, NE Pacific Ocean. *Marine Ecology Progress Series 264*, 1–14.

Treude, T., Niggemann, J., Kallmeyer, J., Wintersteller, P., Schubert, C. J., Boetius, A. & Jørgensen, B. B. 2005: Anaerobic oxidation of methane and sulfate reduction along the Chilean continental margin. *Geochimica et Cosmochimica Acta 69*, 2767–2779.

Uchida, M., Ohkushi, K., Kimoto, K., Inagaki, F., Ishimura, T., Tsunogai, U., TuZino, T. & Shibata, Y. 2008: Radiocarbon-based carbon source quantification of anomalous isotopic foraminifera in last glacial sediments in the western North Pacific. *Geochemistry, Geophysics, Geosystems 9*, Q04N14, doi:10.1029/2006GC001558.

Uchida, M., Shibata, Y., Ohkushi, K., Ahagon, N. & Hoshiba, M. 2004: Episodic methane release events from Last Glacial marginal sediments in the western North Pacific. *Geochemistry, Geophysics, Geosystems 5*, Q08005, doi:10.1029/2004GC000699.

Usapkar, A., Dewangan, P., Kocherla, M., Ramprasad, T., Mazumdar, A. & Ramana, M. V. 2014: Enhanced methane flux event and sediment dispersal pattern in the Krishna-Godavari offshore basin: evidences from rock magnetic techniques. *Marine and Petroleum Geology 58*, 461–475.

Ussler, W. III & Paull, C. K. 2008: Rates of anaerobic oxidation of methane and authigenic carbonate mineralization in methane-rich deep-sea sediments inferred from models and geochemical profiles. *Earth and Planetary Science Letters 266*, 271–287.

Vanneste, M., Guidard, S. & Mienert, J. 2005: Bottom-simulating reflections and geothermal gradients across the western Svalbard margin. *Terra Nova 17*, 510–516.

Vogt, P. R., Crane, K., Sundvor, E., Max, M. D. & Pfirman, S. L. 1994: Methane-generated (?) pockmarks on young, thickly sedimented oceanic crust in the Arctic: Vestnesa ridge, Fram strait. *Geology 22*, 255–258.

Vogt, P. R., Gardner, J., Crane, K., Sundvor, E., Bowles, F. & Cherkashev, G. 1999: Ground-truthing 11- to 12-kHz side-scan sonar imagery in the Norwegian-Greenland Sea: part I: pockmarks on the Vestnesa Ridge and Storegga slide margin. *Geo-Marine Letters 19*, 97–110.

Vorren, T. O. & Laberg, J. S. 1997: Trough mouth fans - palaeoclimate and ice-sheet monitors. *Quaternary Science Reviews 16*, 865–881.

Walczowski, W., Piechura, J., Osinski, R. & Wieczorek, P. 2005: The West Spitsbergen Current volume and heat transport from synoptic observations in summer. *Deep-Sea Research, Part I 52*, 1374–1391.

Whiticar, M. J. 1999: Carbon and hydrogen isotope systematics of bacterial formation and oxidation of methane. *Chemical Geology 161*, 291–314.

Wollenburg, J. E., Kuhnt, W. & Mackensen, A. 2001: Changes in Arctic Ocean paleoproductivity and hydrography during the last 145 kyr: the benthic foraminiferal record. *Paleoceanography 16*, 65–77.

Zahn, R., Schönfeld, J., Kudrass, H.-R., Park, M.-H., Erlenkeuser, H. & Grootes, P. 1997: Thermohaline instability in the North Atlantic during meltwater events: stable isotope and ice-rafted detritus records from Core SO75-26KL, Portuguese Margin. *Paleoceanography 12*, 696–710.

Zamelczyk, K., Rasmussen, T. L., Husum, K., Godtliebsen, F. & Hald, M. 2014: Surface water conditions and calcium carbonate preservation in the Fram Strait during marine isotope stage 2, 28.8–15.4 kyr. *Paleoceanography 29*, 1–12, doi:10.1002/2012PA002448.

Zamelczyk, K., Rasmussen, T. L., Husum, K., Haflidason, H., de Vernal, A., Ravna, E. K., Hald, M. & Hillaire-Marcel, C. 2012: Between two oceanic fronts: paleoceanographic changes and calcium carbonate dissolution in the central Fram Strait during the last 20,000 years. *Quaternary Research 78*, 405–416.

Zhang, M., Konishi, H., Xu, H., Sun, X., Lu, H., Wu, D. & Wu, N. 2014: Morphology and formation mechanism of pyrite induced by the anaerobic oxidation of methane from the continental slope of the NE South China Sea. *Journal of Asian Earth Sciences 92*, 293–301.

Supporting Information

Additional Supporting Information may be found in the online version of this article at http://www.boreas.dk.

Fig. S1. X-ray diffractograms of two untreated bulk samples from core HH12-929PC showing distribution of main minerals with dominance of aragonite and quartz. (a) Sample 12ET0888. (b) Sample 12ET0889. The calculated percentages of the minerals are shown in Table S1.

Table S1. Bulk mineralogy in percentages from XRD-analysis of two samples from core HH12-928PC.

Supporting Information

Methods for XRD analysis

The XRD analyses were performed on a Panalytical X'pert PRO MPD PW3040/x0 diffractometer) at the Department of Geoscience, University of Aarhus, Denmark. The bulk sample material was grinded and pressed into a sample holder. The following X-ray setup was used: Goniometer theta/2theta scan from 2-65 degrees. The anode material was Cu with generator settings at 40mA and 45 kV during measurements. The program used a scan step time of approximately 20 seconds per step (stepsize 0.0170).

The results of the XRD-analyses are shown in Figure S1 and Table S1.

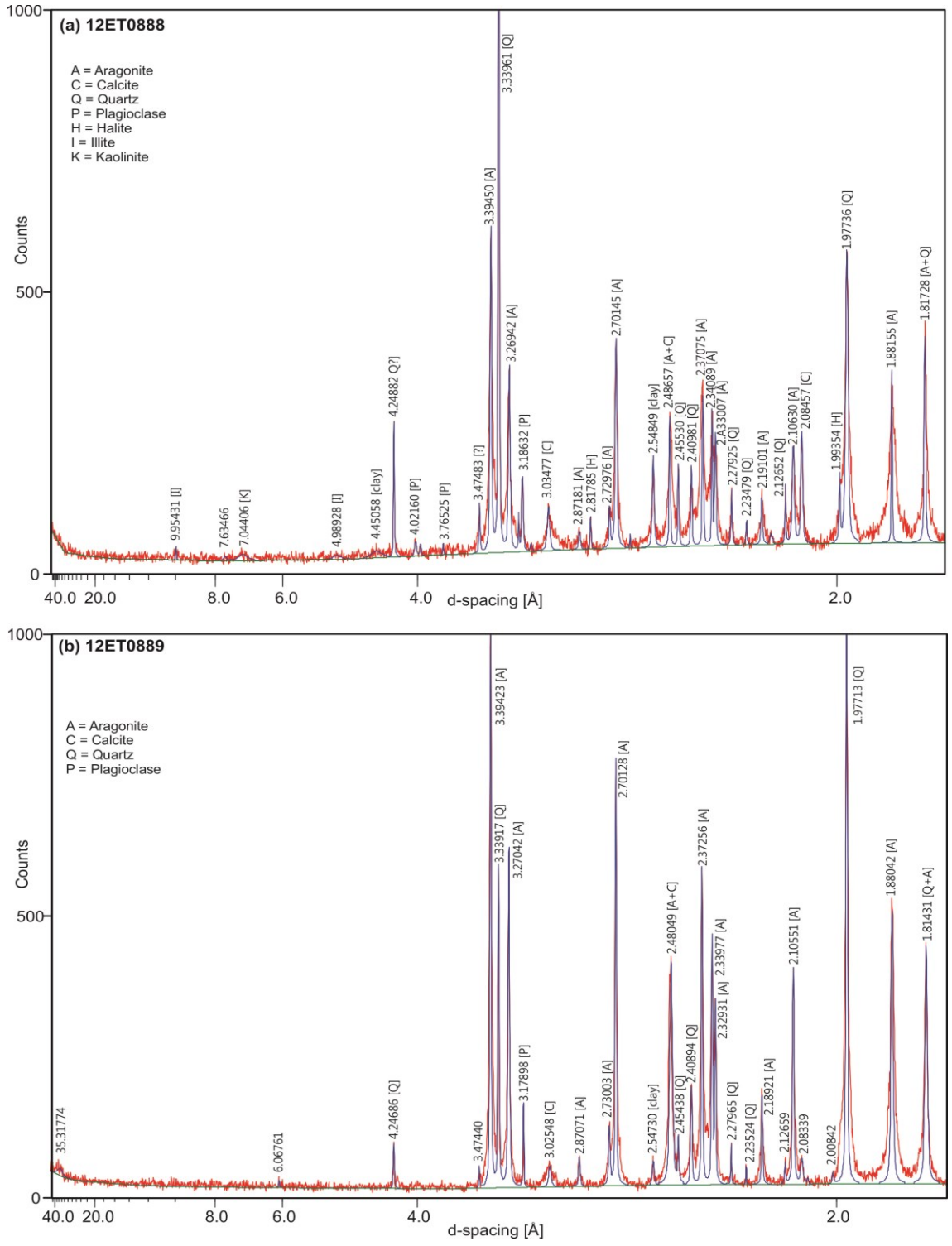

Figure S1. X-ray diffractograms of two untreated bulk samples from core HH12-929PC showing main minerals with dominance of aragonite and quartz. (a) Sample 12ET0888, (b) sample 12ET0889. The calculated proportions of the minerals are shown in Table S1.

Table S1. Bulk mineralogy in percentage from XRD-analysis of two samples from core HH12-928PC.

Sample id	Quartz	Plagioclase	Aragonite	Calcite	Halite	Clay minerals
12ET0888	11.32	6.39	55.37	3.60	6.98	16.35
12ET0889	5.54	4.96	87.62	1.89	0.00	0.00

Paper 2

Late glacial and deglacial paleoceanographic and environmental changes at Vestnesa Ridge, Fram Strait.

Kamila Sztybor and Tine Lander Rasmussen

In review in Palaeogeography, Palaeoclimatology, Palaeoecology

Late glacial and deglacial paleoceanographic and environmental changes at Vestnesa Ridge, Fram Strait.

Kamila Sztybor[1]*, Tine L. Rasmussen[1]

[1] ***CAGE*** *- Centre for Arctic Gas Hydrate, Environment and Climate, Department of Geology, UiT The Arctic University of Norway, Dramsveien 201, N-9037 Tromsø, Norway,*

**Corresponding author. Email: kamila.sztybor@uit.no*

Abstract:

Two cores from 1200 m water depth from Vestnesa Ridge on the western Svalbard margin have been studied. Vestnesa Ridge is known for presence of numerous pockmarks, where methane gas is bubbling out from the seafloor. One core was taken from a pockmark with active seepage of methane, while the second core was taken just outside the seepage area for comparison. Together, the two cores have been analyzed for the distribution of benthic and planktonic foraminiferal assemblages and stable isotopes, geochemical and sedimentological data including magnetic susceptibility, total organic carbon (TOC) and $CaCO_3$ content of the sediment. The purpose of the study is twofold: 1) to reconstruct the paleoceanography of the area and 2) to investigate if seepage of methane have had any impact on the distribution patterns of benthic foraminiferal faunas and the sedimentary environments through time. The results indicate almost continuous presence of warm Atlantic water throughout the last 43,000 years. During the transition from the glacial maximum to the deglaciation and during the deglaciation the Atlantic water shifted abruptly its position in the water column. During the Heinrich H1 interval 17,000-15,300 cal years BP it flowed subsurface along the bottom and the period stands out with the highest bottom water temperatures of the last 43,000 years. The warmer bottom water conditions allowed

settlement of a community of chemo-synthesizing bivalves. However, the distribution patterns of foraminiferal species were the same in both records, indicating that seepage of methane had no influence on the species composition of the foraminiferal faunas.

1. Introduction

Vestnesa Ridge is a south-east to north-west stretching ridge off northwestern Svalbard in the Fram Strait (Fig. 1a). Methane is released from numerous pockmarks located at the southeastern part of the ridge (Bünz et al., 2012; Pimenov et al., 2000). Pockmark arrangement, gas migration pathways and gas hydrate distribution in the area have been extensively studied (Bünz et al., 2012; Eiken and Hinz, 1993; Hustoft et al., 2009; Petersen et al., 2010; Plaza-Faverola et al., 2015; Smith et al., 2014; Vogt et al., 1994). Geophysical studies of the deposits allowed to constrain the major stratigraphic sequences (Eiken and Hinz, 1993) and correlate the seismic reflectors with the results of ODP sites from the Yermak Plateau (910C, 911A and 912A) (Knies et al., 2009; Knies et al., 2002; Mattingsdal et al., 2014; Myhre, 1995) to provide a wide chronostratigraphic framework (Ma scale) (Plaza-Faverola et al., 2015). Investigation of a sediment core with late Quaternary sediments from the Vestnesa Ridge at 1226 m water depth shows that the ridge is characterized by generally high sedimentation rates, with predominantly contourite deposits punctuated by episodic deposition of turbidites (Eiken and Hinz, 1993; Howe et al., 2008; Vogt et al., 1994). The high sedimentation rates allow us to study the activity of release of methane in high-resolution and at the same time detailed reconstructions of the paleoceanography. The location of Vestnesa Ridge in the eastern Fram Strait, the only deep-water connection between North Atlantic and Arctic Ocean, and the proximity to the Svalbard margin makes the area a perfect place to study the changes in advection of Atlantic Water in relation to climate and ice sheet dynamics in the past. Paleoceanographic changes on the western

Svalbard slope were mainly controlled by the inflow of Atlantic Water into the Arctic Ocean that regulated sea-ice cover, bottom current activity and evolution of the Svalbard-Barents Sea Ice Sheet (SBIS) (e.g., Elverhøi et al., 1995).

In order to time and reconstruct the warm water transport into the high northern latitudes many of the previous works focused on reconstructing the surface water conditions in the eastern Fram Strait (e.g., Aagaard-Sørensen et al., 2014a; Müller and Stein, 2014; Nørgaard-Pedersen et al., 2003; Werner et al., 2013; Zamelczyk et al., 2014). Recent discovery of cold methane seeps at the Vestnesa Ridge (Pimenov et al., 2000; Vinogradov, 1999) made this area of special interest in reconstructing past changes affecting the bottom environment.

Methane seeps, because of their unique setting, often host rich chemosynthetic benthic communities and are subjected to a wide variety of diagenetic processes, which have been intensively studied over the last three decades (Hovland and Thomsen, 1989; Orphan et al., 2004; Paull et al., 1984; Sibuet and Olu, 1998). The most interesting feature of cold seeps in the deep-sea is the change of the geometry of the carbon cycle. The energy needed for existence of benthic communities is not depending only of the surface productivity and rain of phytodetritus to the seafloor as the basis of the food chain. In the seep environments the energy can be obtained from anaerobic methane oxidation (AOM). A microbial consortium of archaea and bacteria is mediating the process of AOM, including methane oxidation and sulfate reduction (Boetius et al., 2000). One of the products, hydrogen sulfide, is actively oxidized by filamentous sulfur bacteria, tubeworms and bivalves hosting chemoautotrophic bacteria in their own tissues (Levin, 2005; MacDonald et al., 1989). These microbial processes at seep sites serve as the base of the food chain and can lead to increased benthic productivity compared to areas of no influence of methane release (Brooks et al., 1987; MacDonald et al., 1989; Paull et al., 1984; Paull et al., 1985; Sahling et al., 2002). Hence,

benthic foraminifera, during times of high methane supply/AOM rates should be able to thrive even in times of low surface productivity.

In the present study, we focus on the distribution patterns of planktonic and benthic foraminiferal species assemblages and the geochemistry of the sediment in two cores from Vestnesa Ridge. The purpose is to reconstruct the paleoceanography of the area and to find out if release of methane-rich fluids had any influence on the composition, structure and paleoproductivity of benthic foraminiferal faunas. Benthic and planktonic foraminiferal faunas from Vestnesa Ridge have not been investigated before, as previous studies have mainly focused on isotopic (e.g., Consolaro et al., 2015) or geophysical (Bünz et al., 2012; Hustoft et al., 2009; Plaza-Faverola et al., 2015) studies.

The study is based on two cores that have been investigated previously for stable isotopes of benthic and planktonic foraminifera, authigenic carbonates, magnetic susceptibility, lithology and the distribution of IRD with the purpose of reconstructing the degree of methane release in the past in relation to climate changes (Sztybor and Rasmussen, submitted manuscript). The results on $\delta^{13}C$ in benthic and planktonic foraminifera showed evidence for increased activity during the Bølling-Allerød interstadials 15,300–13,000 cal years BP, beginning at the H1 event ca. 16,385 years marked by presence of chemoautotrophy-dependent bivalves of family Vesicomyidae (Sztybor et al., 2013; Sztybor and Rasmussen, submitted manuscript). The two cores from the previous investigation selected for this study consist of one core with undisturbed lithology from a pockmark of very active site of methane release and a control core from outside the pockmark for comparison (Sztybor and Rasmussen, submitted manuscript).

2. Oceanographic setting

Vestnesa Ridge is located in eastern Fram Strait, at the western continental slope of Svalbard (Fig.1a) at 1200 to >1300 m water depth. The northernmost extension of the Norwegian Atlantic Current - the West Spitsbergen Current (WSC), which is steered by topography, flows along the western coast of Svalbard through eastern Fram Strait into the Arctic Ocean (Fig 1a). The WSC reaches maximum current speed on the upper slope down to 800 m water depth (Beszczynska-Möller et al., 2012; Walczowski et al., 2005). The WSC transports heat and salt into the Arctic Ocean and maintains ice-free conditions in the eastern Fram Strait throughout most of the year (Aagaard et al., 1987; Schauer, 2004; Walczowski et al., 2005). North of Svalbard the WSC continues as subsurface current and splits into the Yermak Slope Current and the Svalbard Branch (Aagaard et al., 1987; Manley, 1995) (Fig. 1a). In the western Fram Strait, cold, low-salinity water is transported by the East Greenland Current along the East Greenland margin into the North Atlantic Ocean (Aagaard et al., 1987; Beszczynska-Möller et al., 2012). In the central Fram Strait warm Atlantic Water mix with cold Polar Water and generate Arctic water masses (Hop et al., 2006). The CTD record taken at the core sites in June 2010 shows a relatively thin surface layer influenced by summer melt-water (10–30 m) above the Atlantic Water extending down to c. 500 m (Fig. 1b). The Atlantic layer overlies the cold Greenland Sea Intermediate Water (c. -0.9 ºC, Fig 1b) generated by convection in the Greenland Sea (Aagaard et al., 1985).

3. Material and methods

The two gravity cores JM10-335GC and JM10-333GC were taken at Vestnesa Ridge in June 2010 during a cruise with *RV Jan Mayen* (now *RV Helmer Hanssen).* Core JM10-335GC was taken from an active pockmark from the base of a gas flare recorded on the echo sounder during coring (Sztybor and Rasmussen, submitted manuscript). Core JM10-333GC

was taken 1.4 km from core JM10-335GC outside the pockmark field as a control site (Fig. 1c). Both cores were collected from a water depth of c. 1200 m within the cold Greenland Sea Intermediate Water and beneath the warmer Atlantic Water (Figs. 1b, c).

Details of core handling was described previously (Sztybor and Rasmussen, submitted manuscript). For this study samples at 5 cm intervals were used in both records. Benthic and planktonic foraminifera were counted in the size fraction larger than 0.100 mm. A total number of >300 benthic and >300 planktonic specimens of foraminifera were picked and identified to species level. Some samples contained less than 300 specimens and samples containing less than 100 specimens were regarded as non-representative and excluded from the faunal analysis. In core JM10-333GC two samples were barren and 26 samples contained very low numbers of foraminifera (22–100 specimens per sample). In these intervals an additional thirteen samples were sampled (one cm above or below) in an attempt to fill the gap in the data. In core JM10-335GC four samples were excluded from faunal analysis, because of very low number of foraminifera (41–100 specimens per sample). Foraminifera were identified to species level (if possible) by using the systematics of Feyling-Hanssen et al. (1971), and Loeblich and Tappan (1988). *Nonionella* species (mainly *N. stella*, *N. turgida*, *N. iridea* and *Nonionellina labradorica*) and 'Atlantic species' consisting of species with an affinity for bottom water with a temperature >2°C (*Pullenia bulloides, P. quinqueloba, Eggerella bradyi, Sigmoilopsis schlumbergeri, Bulimina marginata, Gyroidina sp., Gavelinopsis praegeri, Pyrgo serrata, Spirophtalmidium acutimargo*) (Rasmussen et al., 1996, 2003; Wollenburg et al., 2001, 2004) were grouped together and are presented as *Nonionella* spp. and 'Atlantic species', respectively.

Species richness was defined as the total number of species in a sample. Diversity indices were calculated with PAST software (Hammer et al., 2001) to describe diversities and distribution in all samples except barren intervals. The species diversity was measured using

the Fisher α index (Fisher et al., 1943) and the evenness using the Pielou index (J) (Pielou, 1966).

Concentration of planktonic and benthic foraminifera were calculated as number per gram dry weight sediment. The foraminiferal accumulation rates (in number/cm^2/ka) were calculated using the formula:

number/g x Mass Accumulation Rate (MAR)

where MAR=Linear Sedimentation Rate (LSR) (cm/ka) x Dry Bulk Density (DBD) (g/cm^3).

Total carbon (TC) and total organic carbon (TOC) were measured in bulk samples from the same depth-intervals as the foraminiferal samples using a Leco CS-200 induction furnace instrument. The weight percentage (wt.%) of TC and TOC was calculated. For calculating the content of $CaCO_3$ the following equation was used: $CaCO_3=(TC-TOC)\times 8.33$.

AMS-^{14}C dates and calibrated ages are presented in Sztybor and Rasmussen (submitted manuscript) and shown in Figs. 2–5. Stable isotopes were measured in several benthic foraminiferal species and one planktonic species. Here we present the published stable isotope values measured in the benthic foraminiferal species *Cassidulina neoteretis* and the planktonic species *Neogloboquadrina pachyderma*.

4. Results

Age models

The age models are based on four (JM10-333GC) and nine (JM10-335GC) AMS ^{14}C dates, oxygen isotopes, lithology and correlation with the western Svalbard slope MS stack as presented in Fig. 2. Detailed description of stratigraphy, lithology and construction of the age models was published previously by Sztybor and Rasmussen (submitted manuscript). The cores contain hemi-pelagic silty clay comprising early Holocene and glacial intervals, fine clay with laminations in the Bølling-Allerød interval and a layer of coarse sediments

interpreted as glacigenic debris flow deposits in the glacial interval (Sztybor and Rasmussen, submitted manuscript) (Fig. 2). The fine clay with laminations and the coarse layer were found in other cores from the western Svalbard margin (Jessen et al., 2010; Müller et al., 2009; Müller and Stein, 2014; Rasmussen et al., 2007) and are interpreted as deposited from deglacial turbid meltwater plumes and downslope mass transport deposits, respectively. The age of these conspicuous horizons plus the ages of a diatom layer in the lower Holocene sediments were used as tie-points in the construction of the age model (see Sztybor and Rasmussen, submitted manuscript) (Fig. 2). The age models were calculated assuming linear sedimentation rates between dates and tie-points from Jessen et al. (2010) (Sztybor and Rasmussen, submitted manuscript) (Fig. 2). All ages presented in the following text will be in calendar years.

Together the two cores cover the time interval 43,000 to 9500 years. Core JM10-335GC from the pockmark dates 35,000 years at the bottom and contain 40 cm thick sediments from the lower Holocene at the top, while core JM10-333GC dates 43,000 years at the bottom and has no Holocene sediments at the top. According to the age model the youngest sediments dates c. 13,955 years at the core top (Fig. 2).

Based on the previously established age models, and published stable isotopes, lithofacies, content of IRD, MS, grain size with the addition of the foraminiferal assemblage data and geochemical analyses obtained in this study (Figs. 3–6), the records have been subdivided into the following intervals: Late glacial (~43,000–23,500 years), Last Glacial Maximum (LGM) (23,500–19,000 years), LGM-H1 transition (19,000–17,000 years), Heinrich event H1 (17,000–15,300 years), Bølling-Allerød interstadials (15,300–13,000 years), Younger Dryas (13,000–11,900 years) and early Holocene (11,900– ~9500 years).

Foraminifera and geochemistry

Benthic foraminiferal diversity and accumulation rates (AR)

The benthic foraminiferal fauna comprises 40 species in core JM10-333GC (from now referred to as 333GC) and 44 species in core JM10-335GC (from now referred to as 335GC). The assemblages in both cores consist mainly of calcareous species. Agglutinated species are absent except for a few single specimens in the core top samples and they were excluded from the diversity estimates. The number of species per sample (excluding barren samples) varies between 3 and 20 in core 335GC and between 2 and 21 in core 333GC giving an average of 11 and 8.6 species per sample, respectively (Fig. 3). Number of species and the Fisher α diversity index show similar fluctuations reaching lowest values during the Bølling-Allerød interstadials and highest during Heinrich event H1, Younger Dryas and top most sections of both cores (Fig. 3). The evenness (J) in both cores has the same pattern showing highest values during the Bølling-Allerød interstadials where specimens are nearly equally distributed (only few species present) (Fig. 3), while lowest values occurred during the LGM and the late glacial, which are caused by strong dominance of the assemblages by one species (*C. neoteretis*).

The benthic foraminiferal accumulation rates (AR) are also similar in both cores (Fig. 3). The lowest AR – below 2000 specimens per cm^2\ka occurred during the glacial period. From ca 25,000 years the AR shows an increasing trend and reach highest values exceeding 12,000 specimens cm^2\ka during the Bølling-Allerød interstadials. The fluctuations in the AR are highly correlated with the changes in sedimentation rate (Fig. 3).

Major trends in distribution patterns of species

The glacial and deglacial intervals in both cores are strongly dominated by *Cassidulina neoteretis*, which exceeds 70% in the majority of the samples (Fig. 4). Other common species in both records are *Cassidulina reniforme* and *Melonis barleeanus*. They can

reach above 60% and dominate the assemblages in the intervals of lower abundance of *C. neoteretis* (Fig. 4). *Nonionella* spp. and *Stainfortia loeblichi* shows peaks of about 25–20% during the Younger Dryas and late glacial that appear asynchronous. *Cibicidoides wuellerstorfi* occurs only in the Holocene section of core 335GC. *Oridorsalis umbonatus* shows sporadic peaks during the glacial period and at the beginning of the Holocene. *Elphidium excavatum* has a peak in both cores at ca 30,000 years and shows a decreasing trend in relative abundance towards the deglaciation (Fig. 4). The Atlantic species has only one peak in both cores during Heinrich event H1 reaching 3–6% of the assemblage (Fig. 4).

Planktonic foraminiferal assemblages and fluxes

Planktonic foraminifera were only examined in core 335GC. The assemblages are basically dominated by two species *N. pachyderma* and *Turborotalita quinqueloba* together constituting an average of 97.6% of the assemblages (Fig. 5). Other identified species are *N. incompta*, *Globigerinita uvula, G. glutinata* and *Globigerina bulloides*. The glacial part of the record is strongly dominated by *N. pachyderma*, while the early Holocene shows higher relative abundance of *T. quinqueloba* (Fig. 5). The planktonic foraminiferal fluxes and the planktonic\benthic ratio has the same pattern and shows apparently random peaks in the interval 31,000–26,000 years, a strong peak at ca 16,500 years and reach the highest values in the early Holocene (Fig. 5).

Geochemistry

The TOC content is nearly identical in both cores (Fig. 5). It has low and stable values of about 0.7% on average in the glacial period with one exception in the interval 23,500–24,500 years where the TOC content reaches 1.5–2% (Fig. 5). The TOC content increases in the Bølling-Allerød interstadials to ca 1.3% and remains quite high (0.9%) until the early

Holocene, where it increase slightly (1.2%). Higher content of TOC correlates with higher sedimentation rates (Fig. 5). The TC and $CaCO_3$ content in both cores show the same pattern, but reaches slightly higher values in the seep core 335GC (Fig. 5). Both TC and $CaCO_3$ have lower values during the Younger Dryas and early Holocene.

Methane seep site versus non-seep site

The benthic foraminiferal fauna shows the same patterns of relative abundance in both cores with overall similar timing (Fig.4). There is a slight asynchrony in the abundance peaks in the oldest part of both records, where the age control is based on extrapolation and is tentative. The diversity patterns are very similar and minor differences in species numbers concern mainly single specimens of accessory species (Figs. 3, 4). The content of TOC is also nearly identical in both records. For the time interval present in both records (ca 35,000–14,000 years), the average values of TC are slightly higher in the seep core 335GC (~1.75 %) than in the control core 333GC (~1.55 %). This is the result of a higher content of $CaCO_3$ in core 335GC (Fig. 4). Because of lack of significant differences between the foraminiferal faunas and geochemical data of the two records, we first discuss paleoceanographic changes and then inspect the potential influence of methane.

5. Discussion

Interpretation of faunas and geochemistry in terms of paleoceanography

Time interval ~43,000–23,500 years (Late glacial)

The time interval 43,000 to 35,000 years is only represented in core 333GC, the control core. The benthic assemblage of the oldest part of the interval is dominated by *M. barleeanus* together with *C. neoteretis* and *O. umbonatus* (Fig. 4). This indicates relatively

stable food supply and seasonally ice-free conditions (Hald and Steinsund, 1992; Korsun and Hald, 1998; Wollenburg and Mackensen, 1998). At ca 38,000 years *C. reniforme*, *S. loeblichi*, *E. excavatum* and *Cibicides lobatulus* increase in relative abundance (Fig. 4) indicating more polar conditions with extended sea-ice cover (Hald and Korsun, 1997; Wollenburg et al., 2001). The general interpretation of this part of the record (43,000–35,000) is tentative because of the very low resolution - only four data points (Fig. 4).

The interval from 35,000 years is represented by both cores 335GC and 333GC. The oldest part of core 335GC consists of dense hemi-pelagic sediments characterized by high $\delta^{18}O$ values for both planktonic and benthic foraminifera (Fig. 3). Such high $\delta^{18}O$ values are typical for the end of MIS 3 and MIS 2, including the LGM (Lisiecki and Raymo, 2005). The planktonic foraminiferal fauna are strongly dominated by *N. pachyderma* (>90%), an indicator of cold, polar surface water masses (Bauch et al., 2001; Carstens and Wefer, 1992; Zamelczyk et al., 2014). From ca 31,000 years both the planktonic and benthic $\delta^{18}O$ values start to decrease reaching the lowest values at 29,000 years. The values remains low until ca 26,000 years (Fig. 3). The interval of lower $\delta^{18}O$ values contains three peaks of high concentration of planktonic foraminifera and high planktonic foraminiferal flux (Fig. 3). The highest flux of planktonic foraminifera at ca 27,000 years is consistent with findings of Dokken and Hald (1996) and Zamelczyk et al. (2014). The increased flux in planktonic foraminifera are interpreted as enhanced paleoproductivity and called high productivity zones considered typical for the western Svalbard margin (Hald et al., 2001). The increased productivity was due to inflow of Atlantic Water (Dokken and Hald, 1996; Hebbeln et al., 1994; Hebbeln and Wefer, 1997).

The benthic foraminiferal assemblages in cores 333GC and 335GC are characterized by relatively high and variable diversity (Fisher α index) (Fig 3). Both records shows high diversity and number of species around 30,000 years (Fig. 4). The assemblages consist mainly

of *C. neoteretis, C. reniforme, S. loeblichi* and *E. excavatum* (Fig. 4), which are characteristic species for cold glacial stadials at intermediate water depth (Rasmussen et al., 2007, 2014; Wollenburg et al., 2001). A small peak in relative abundance of *C. lobatulus* spanning ca 32,000–29,000 years most likely indicate moderate bottom current activity (Hald and Korsun, 1997; Sejrup et al., 1981). At ca 31,000 and 29,000 years increase in relative abundance of *Islandiella norcrossi, S. loeblichi, E. excavatum* and *C. reniforme* correlates with decrease in diversity and number of species (Figs. 3-4). Increased percentages of *I. norcrossi* and *S. loeblichi* indicate enhanced seasonal paleoproductivity and food supply (Wollenburg et al., 2001), while *E. excavatum* and *C. reniforme* are associated with cold polar water and unstable conditions (Hald and Korsun, 1997; Hald and Vorren, 1987; Polyak et al., 2002). Enrichment in phytodetritus species (*I. norcrossi, S. loeblichi)* in the foraminiferal assemblages together with lowered $\delta^{18}O$ values of planktonic and benthic foraminifera suggest enhanced heat advection and meltwater events.

Between 43,000 (35,000; 335GC) –25,000 years the TOC content is quite low in both records (Fig. 5). In both cores, TOC and TC increase rapidly at ca 24,000 years, while the content of $CaCO_3$ decreases (Fig. 5). A similar event of high TOC and low $CaCO_3$ and of similar timing was also found by Zamelczyk et al. (2014) just south of Vestnesa at 1500 m water depth. The interval is characterized by high sedimentation rate of coarse material and high IRD supply (Fig. 5) and was interpreted as mass transport deposits from glacigenic debris flow and turbidity flow events that occurred at the western Svalbard margin, when the SBIS reached the shelf edge (e.g., Jessen et al., 2010 and references therein). As a result, high amounts of organic matter (TOC) of terrestrial origin have been deposited (Elverhøi et al., 1995; Hebbeln et al., 1994; Knies and Stein, 1998; Müller and Stein, 2014).

Time interval 23,500–19,000 years (Last Glacial Maximum (LGM))

Both planktonic and benthic $\delta^{18}O$ values are high (Fig. 3). The planktonic fauna is dominated by *N. pachyderma*, but the subpolar species *T. quinqueloba* reaches up to 40% in this interval indicating high productivity and seasonal open water and inflow of Atlantic Water in accordance with numerous studies from the Svalbard margin (e.g., Dokken and Hald, 1996; Hebbeln et al., 1994; Rasmussen et al., 2007; Zamelczyk et al., 2014) (Fig. 5). Fluctuations in the planktonic foraminiferal flux and species (Fig. 5) probably correlate with advances and retreats of the sea-ice cover in the study area caused by perturbations in the advection of warm Atlantic water (Hebbeln et al., 1994; Müller and Stein, 2014).

The benthic foraminiferal faunas at both sites are strongly dominated by *C. neoteretis* with low species richness, diversity and evenness (Fig. 4). The *C. neoteretis* assemblage is associated with seasonally ice-free conditions and moderate to high seasonal productivity (Jennings and Weiner, 1996; Jennings et al., 2004; Osterman et al., 1999; Wollenburg and Mackensen, 1998). Benthic foraminiferal fluxes of this low diversity fauna shows multiple fluctuations, but generally increase in both cores from ca 24,000–19,000 years (Fig.3).

The content of TOC is low in both records (~0,8%) while the $CaCO_3$ content reach its highest values (Fig. 5). This is related to the generally enhanced preservation of $CaCO_3$ during the LGM (e.g., Zamelczyk et al., 2014 and references therein).

Time interval 19,000–17,000 years (LGM-H1 transition)

High planktonic $\delta^{18}O$ values (Fig. 3) indicate low surface temperatures and decreased advection of Atlantic water. The planktonic fauna is almost completely dominated by *N. pachyderma* (>90%), while the flux of planktonic and AR of benthic foraminifera decrease (Figs. 3, 5). A possible explanation is increase in sea-ice cover to perennial or near-perennial that caused decrease in productivity. In a study from the Fram Strait, Zamelczyk et al. (2014) observed a similar decrease in planktonic foraminiferal flux and connected it with cooling of

the surface water. Müller and Stein (2014) measured extremely low values of algae biomarkers, which they attributed to the presence of permanent sea-ice cover. Low relative abundance of *C. lobatulus* suggests weakened bottom current activity (Fig. 4).

Time interval 17,000–15,300 years (Heinrich event H1)

A spike of very low planktonic $\delta^{18}O$ values correlating with Heinrich event H1 (Fig. 3) have been observed in many records from the North Atlantic and the western Svalbard margin (Birgel and Hass, 2004; Dokken and Hald, 1996; Jones and Keigwin, 1988; Myrvang, 2015; Nørgaard-Pedersen et al., 1998; Rasmussen et al., 2007; Sarnthein et al., 1995; Zamelczyk et al., 2014). The event has been interpreted to indicate presence of meltwater at the surface. Benthic $\delta^{18}O$ values also tend to decrease towards the end of H1, but with smaller magnitude (Fig. 3). This has also been found in other records from the Nordic seas and the Svalbard margin (Rasmussen et al., 2007; Sarnthein et al., 1994) and in two records from Vestnesa Ridge (Myrvang, 2015). Increasing concentration of IRD indicate enhanced calving of icebergs (cf. Bond et al., 1993) (Fig. 3). The high amount of melt water provided inorganic nutrients for phytoplankton (Müller and Stein, 2014). This probably intensified the planktonic productivity as seen in the peak in planktonic foraminiferal flux (Fig. 5). Benthic foraminifera are characterized by moderate AR and prominent changes in the assemblage structure. A rapid increase in biodiversity (Fischer α) in both records is caused by decrease in dominance of *C. neoteretis* (Figs. 3, 4) and occurrence of a more diverse assemblage of species with a southern affinity referred to 'Atlantic species' (see methods). The 'Atlantic species' are known to be associated with Atlantic water and elevated bottom water temperatures (Rasmussen et al., 1996; Wollenburg et al., 2001, 2004, 2007). The group of 'Atlantic species' reach up to 3.5–6% of the assemblage. Rasmussen et al. (2007) in a study from southwestern slope of Storfjorden at ca 1500 m water depth noted enrichment in 'Atlantic

species' of 4–7% that together with a 0.5 ‰ decrease in the benthic $\delta^{18}O$ values gave an estimated bottom temperature rise of at least 2 ºC. In our study the recorded 0.4 ‰ decrease in the benthic $\delta^{18}O$ would correspond to a temperature rise in the bottom water of at least 1.6 ºC (e.g., Duplessy et al., 2001).

The TOC content in both records is low (~0.4 %) and shows increasing trend towards the end of the interval (~1.2 %) (Fig. 5). Peaks of higher % $CaCO_3$ occur in both records (Fig. 5). The increase in % $CaCO_3$ in core 335GC correlate with the peak in planktonic foraminiferal concentration and flux (Fig. 5) probably caused by both enhanced planktonic productivity (Müller and Stein, 2014) and improved preservation of calcium carbonate in the warmer bottom water (Barker et al., 2004; Rasmussen et al., 2007; Zamelczyk et al., 2014).

In the seep core 335GC the upper part of the Heinrich H1 interval contains a shell horizon with about thirty well-preserved valves of various sizes of mussels from the family Vesicomyidae (Sztybor and Rasmussen, submitted manuscript). Vesicomyids are associated with sulphide-rich, reducing environments of cold seeps and hydrothermal vents (Boss and Turner, 1980; Krylova and Sahling, 2010; von Cosel et al., 2001). Presence of Vesicomyids shells indicates that hydrogen sulfide, a product of anaerobic oxidation of methane, was available in the near-surface sediments at that time (Sztybor et al., 2013; Sztybor and Rasmussen, submitted manuscript). The shell layer is absent from cores from outside the pockmarks (Myrvang, 2015; Sztybor and Rasmussen, submitted manuscript).

Time interval 15,300–13,000 years (Bølling-Allerød interstadials)

The planktonic and benthic $\delta^{18}O$ values rapidly increase and reveal high variability (Fig. 3) indicating enhanced inflow of Atlantic water and relatively unstable conditions (Aagaard-Sørensen et al., 2014a; Birgel and Hass, 2004; Ebbesen et al., 2007). The composition of the planktonic assemblages varies in the same pace as the oxygen isotope

values with >90% of *N. pachyderma* associated with cold polar waters dropping several times to 75–60%, which indicates episodic advection of Atlantic water. The sedimentation rate was extremely high in both records consisting of fine clays in the Bølling interstadial, with an increasing trend in the IRD content reaching very high values towards the end of the Allerød interstadial (Fig. 3). The fine sediments deposited in the lower part of the Bølling interstadial are laminated and deposited rapidly from turbid meltwater plumes released from the melting of the Svalbard-Barents sea ice sheet (e.g., Ebbesen et al., 2007; Jessen et al., 2010; Knies and Stein, 1998). It is possible that the pulsed inflow of Atlantic water caused the release of these meltwater plumes. The flux of planktonic foraminifera were low (Fig. 5), probably caused by the high turbidity from the high sedimentation rates (Birgel and Hass, 2004; Howe et al., 2008; Rasmussen et al., 2007). Similar low planktonic flux was also found in a record off southwestern Svalbard (Rasmussen et al., 2007), continental margin off western Svalbard (Ebbesen et al., 2007), Fram Strait (Aagaard-Sørensen et al., 2014a; Nørgaard-Pedersen et al., 2003) and Yermak Plateau (Chauhan et al., 2014; Nørgaard-Pedersen et al., 2003). The $\delta^{13}C$ values of benthic and planktonic foraminifera in the seep core shows very low values (Fig. 3) from coating by authigenic carbonates probably as a result of enhanced AOM (Sztybor and Rasmussen, submitted manuscript).

The benthic foraminiferal assemblages are characterized by the lowest biodiversity of both cores (Fig. 4). The assemblage is dominated by *C. neoteretis* with increasing relative abundance of *C. reniforme* at ca 14,500 years and *M. barleeanus* at ca 13,500 years (Fig. 4). The increase of *C. reniforme* and *M. barleeanus* caused more even distribution of the species as observed by the maximum values in the Pielou index (J) (Fig. 3). The increase of *C. reniforme* may indicate unstable conditions with high turbidity as the species is common in glaciomarine environments (Hald and Korsun, 1997; Korsun and Hald, 1998). The increase of *M. barleeanus* and *C. lobatulus* at ca 13,500 years (Fig. 4) can be referred to a more stable

food supply and higher bottom current activity during the Allerød interstadial (Korsun and Hald, 1998; Mackensen et al., 1985; Rasmussen and Thomsen, 2015; Rasmussen et al., 2007; Ślubowska-Woldengen et al., 2007). The concentration of benthic foraminifera per g of dry weight sediment was quite low, but gave relatively high AR as a result of the extremely high sediment accumulation rates (Fig. 3).

The TOC content in both cores is high (~1.2 %) (Fig. 5). Similar high concentrations of TOC during Bølling-Allerød interstadials were observed in records from western Svalbard and northwestern Barents Shelf (Elverhøi et al., 1995; Knies and Stein, 1998; Müller and Stein, 2014). The organic carbon is of mixed marine and terrigenous origin and was deposited due to high mineral flux in the meltwater plumes that enhanced organic carbon preservation (Knies and Stein, 1998 and references therein). The $CaCO_3$ content is low and reach lowest values in both cores (Fig. 5) indicating polar conditions probably caused probably by high influence of meltwater (Aagaard-Sørensen et al., 2014a; Ebbesen et al., 2007).

Time interval 13,000–11,900 years (Younger Dryas)

The interval is presented only by the seep core 335GC (Figs. 2–5). A decrease in planktonic and benthic $\delta^{18}O$ values at the beginning of the Younger Dryas (ca 13,000–12,400 years) (Fig.3) indicate cold conditions with polar surface water (Aagaard-Sørensen et al., 2014a) most likely caused reduced salinity (Rasmussen et al., 2007). The planktonic assemblage is dominated by *N. pachyderma* except for a short-lasting increase in relative abundance of *T. quinqueloba* (<40%) at 12,600 years (Fig. 3). Towards the end of the interval (ca 12,400–11,900 years) planktonic and benthic $\delta^{18}O$ values increase together with stronger dominance of the polar planktonic foraminiferal species *N. pachyderma* (Fig. 3), which imply cold conditions. Numerous large diatoms *Coscinodiscus* spp. became abundant in the sample in the size-fraction 63–100 μm, which can be interpreted as increase in primary

productivity associated with the passage of an oceanic front (Karpuz and Jansen, 1992; Rasmussen et al., 1996; Stabell, 1986). Our results correlate with the findings of Müller and Stein (2014), who measured high productivity of sea-ice diatoms followed by increase in phytoplankton productivity at the beginning of the Younger Dryas. Despite the enhanced primary productivity the planktonic foraminifera concentration and flux are very low (Fig.5). The reduced production of planktonic fauna was also observed in a study from southwestern Svalbard slope (Rasmussen et al., 2007), western Svalbard margin (Ebbesen et al., 2007) and eastern Fram Strait (Aagaard-Sørensen et al., 2014a) and was explained by expanded sea-ice cover. The observed very low IRD concentrations support the interpretation of increased sea-ice cover (Fig. 3).

Major shifts occurred in the benthic foraminiferal assemblages (Figs. 4). The abundance of *C. neoteretis* decreased rapidly and the assemblage became dominated by *Nonionella* spp. (mainly *Nonionella stella*), *S. loeblichi* and *C. reniforme* (Fig. 4). *Nonionella* species are known as opportunistic species often associated with seasonally elevated organic carbon flux and periodic low oxygen conditions (Bernhard et al., 1997; Corliss, 1991; Fontanier et al., 2014a; Jorissen et al., 1992; Korsun and Hald, 1998; Rasmussen et al., 2012). Reduced relative abundances of *C. neoteretis* and *C. lobatulus* (Fig. 4) indicate weaker influence of Atlantic water and weak bottom current activity (Jennings et al., 2004; Wollenburg et al., 2001), slightly resembling conditions during Heinrich event H1. Benthic foraminiferal AR were low (Fig.3). High abundance of *S. loeblichi* may be connected with increasing sea-ice cover (Polyak et al., 2002; Ślubowska et al., 2005). Increased percentages of *C. reniforme* in the benthic assemblages and extremely low benthic AR (Figs. 3, 4) also point to presence of cold water masses and unstable environmental conditions.

The TOC content is lower than during the Bølling-Allerød interstadials, but higher than during the glacial period (Fig. 5). This is most likely a result of high primary productivity

(Müller and Stein, 2014) and low sedimentation rates (Fig. 5) (see discussion in Knies and Stein, 1998). The low $CaCO_3$ content is a consequence of low planktonic faunal productivity and poor carbonate preservation (Aagaard-Sørensen et al., 2014a; Ebbesen et al., 2007; Rasmussen et al., 2007) (Fig. 5).

Time interval 11,900–~9500 years (early Holocene)

This interval is also only present in the seep core 335GC (Figs. 2–5). The beginning of the period is characterized by increasing concentrations of IRD, which points to increase in meltwater and iceberg supply (Fig. 3). According to the study of Aagaard-Sørensen et al. (2014a) from the eastern Fram Strait cold surface water conditions continued until ca. 10,500 years. Gradual surface warming and\or increasing amounts of fresh water supply is inferred from decreasing planktonic $\delta^{18}O$ values and increasing relative abundance of *T. quinqueloba* (Fig. 5). At ca 10,100 years *T. quinqueloba* dominate the planktonic assemblages (>90%), which indicates strong inflow of Atlantic water, high productivity and warmer surface conditions. High surface productivity is reflected in the very high planktonic foraminiferal flux (Fig. 5). Numerous diatoms (*Coscinodiscus* spp.) were abundant in the size-fraction 63–100 µm (Fig.2) and are linked to the northward movement of the Polar front (Jessen et al., 2010 and references therein). Benthic $\delta^{18}O$ values increase and *M. barleeanus*, *O. umbonatus* and *C. reniforme* dominate the benthic foraminiferal assemblages indicating stronger inflow of Atlantic water and a stable food supply (Hald and Steinsund, 1992). Higher abundance of *C. lobatulus* and occurrence of *C. wuellerstorfi* indicate increase of bottom current activity (Jennings et al., 2004; Mackensen et al., 1985; Sejrup et al., 1981).

The TOC content increase from the end of Younger Dryas and reach ~1.2 % in the early Holocene (Fig. 5). The $CaCO_3$ is very low ~4% and drops to 2.5 % at the beginning of the interval to reach ~6 % at the end of the studied interval (Fig. 5). The initially low content

of $CaCO_3$ is most likely caused by post-depositional dissolution, while the increase in $CaCO_3$ after ca ~10,000 years indicate enhanced carbonate preservation (Aagaard-Sørensen et al., 2014b).

Seeping of methane and benthic foraminiferal assemblages

The species composition of foraminiferal assemblages depends mostly on food availability and quality, oxygen, substrate, bottom water temperature and salinity (Corliss and Emerson, 1990; Hald and Korsun, 1997; Jernas et al., 2013; Jorissen et al., 1992). The importance of carbon flux and primary productivity in the Arctic Ocean recently came into focus (Loubere and Rayray, 2016; Osterman et al., 1999; Wollenburg and Kuhnt, 2000; Wollenburg et al., 2001; Wollenburg and Mackensen, 1998). Wollenburg and Mackensen (1998) suggested that benthic foraminiferal distribution in high Arctic is controlled mainly by food supply. A more detailed study of Wollenburg and Kuhnt (2000) confirmed that the majority of the benthic foraminiferal species in the central Arctic Ocean and western Svalbard are attracted by the availability of fresh organic material. Anaerobic oxidation of methane releases hydrogen sulfide that provides a source of energy for chemosynthetic benthic communities (Brooks et al., 1987; Levin, 2005; Paull et al., 1985). In the oligotrophic deep-sea environment this process is expected to enrich benthic communities and affect the species composition and accumulation rates of benthic foraminiferal faunas (Hovland and Thomsen, 1989 and references therein; Levin, 2005). In addition, from studies of modern methane seeps it is known that the methane release may influence benthic foraminiferal assemblages by favoring opportunistic species tolerant of low oxygen (e.g., Bernhard et al., 2001; Sen Gupta et al., 1997; Wefer et al., 1994). The dominant species are infaunal, otherwise typically found in organic-rich oxygen poor environments (Rathburn et al., 2000; Sen Gupta and Aharon,

1994; Sen Gupta and Machain-Castillo, 1993; Wiedicke and Weiss, 2006). Some occur at deeper infaunal habitats than normally found (Rathburn et al., 2000; Rathburn et al., 2003). A number of the species occurring most frequently at the seep sites were recognized to host endosymbionts that most likely facilitates survival in the unfavorable, low-oxygen conditions (Bernhard et al., 2000; Bernhard et al., 2001). Epifaunal species have been observed to colonize tubeworms above the seafloor to escape from hypoxia and sulfide toxicity (Lobegeier and Sen Gupta, 2008; Sen Gupta et al., 2007; Wollenburg and Mackensen, 2009). The concentration of benthic foraminifera at the seep sites may display complex patterns depending on the severity of the environments. It is sometimes comparable to the non-seep site (Fontanier et al., 2014b; Martin et al., 2010), it can be lowered (Bernhard et al., 2001) or fluctuate from elevated concentrations at the margin of the seep site to become nearly barren in the center (Wollenburg and Mackensen, 2009). The diversity patterns in relation to methane release are also complex. Modern benthic foraminiferal faunas at many seep sites can in some cases be characterized by lower diversity than at the control sites outside the seep areas (Martin et al., 2010; Wollenburg and Mackensen, 2009) or it may also show no differences (Fontanier et al., 2014b).

Fossil records apparently reflect this complexity and can show either no difference between seep and non-seep assemblages (Barbieri and Panieri, 2004), or clear differences with strong dominance of opportunistic\organic carbon related taxa (Bhaumik and Gupta, 2007; Wefer et al., 1994). Fossilized episodes of increased seep activity may also be inferred from slightly elevated concentrations of opportunistic benthic foraminiferal species in comparison to the control site (Wiedicke and Weiss, 2006).

In the two records from Vestnesa Ridge no significant changes in concentrations of benthic foraminifera, diversity or assemblage structure in comparison to the control site were observed (Figs. 3, 4). In the Bølling-Allerød interstadials characterized by extremely low $\delta^{13}C$

excursions (Sztybor and Rasmussen, submitted manuscript), we also saw no differences in the composition of the benthic foraminiferal assemblages between the two records (Figs. 3, 4). In Heinrich event H1, when a large population of Vesicomyids clams colonized the seafloor, being a sign of sulfide rich fluids being available close to the seafloor (Sztybor et al., 2013; Sztybor and Rasmussen, submitted manuscript), the benthic fauna was similar to faunas found in other studies from the Svalbard margin (Rasmussen et al., 2007, 2014) and from areas far away from Vestnesa (e.g., Rasmussen and Thomsen, 2004; Wollenburg et al., 2004).

The observed minor differences in benthic foraminiferal absolute and relative abundances and accumulation rates between the cores are within the normal variability and patchiness of the marine seafloor environment. The lack of real differences preserved in the fossil record could be caused by time-averaging of the assemblages, short lasting methane events or species richness elevation by post-mortem mixing of foraminiferal tests as described previously (Barbieri and Panieri, 2004; Lobegeier and Sen Gupta, 2008). We suggest that another explanation for the lack of differences in the foraminiferal faunas can be actual lack of influence by seepage on foraminifera caused by a too deep sulfate-methane transition zone. The present day SMTZ is located ca 1 m downcore at the position of 335GC (Hong et al., 2016), therefore living foraminifera at the sediment surface today are unlikely to register any effects of the seeping. In the past, when seepage was stronger such as during H1 and the Bølling-Allerød interstadials, the SMTZ may have been shallower, but still too deep. The overall dominant species *C. neoteretis* lives close to the actual surface of the sediment (shallow infaunal) (e.g., Wollenburg and Mackensen, 2009), while Vesicomyids clams dig deeper into the sediments in search of hydrogen sulfide (Sahling et al., 2002). Highly depleted $\delta^{13}C$ values in both planktonic and benthic foraminifera from core 335GC confirms diagenetic alteration of empty shells in the shallow subsurface sediments (Sztybor and Rasmussen,

submitted manuscript), that may have been the only influence the seeping of methane has had on the foraminifera in the area.

A notable difference between the studied cores is the age of the core-top sediments. The topmost sediments of pockmark core 335GC consist of an early Holocene section, while the core top of the control core dates from the Bølling-Allerød interval (Fig. 2). It is known that Holocene sediments are usually not present in the cores from western Svalbard slope at water depths above ~1200 m due to strong Holocene bottom currents (Jessen et al., 2010; Rasmussen et al., 2014). Pockmarks at Vestnesa work as 'sediment traps' and have enabled the deposition of Holocene sediments (see also Sztybor and Rasmussen, submitted manuscript).

Seeping of methane vs oceanography

Our result show that during the last glacial several episodes of higher productivity occurred. Increased surface productivity cause temporal increase in organic carbon and anoxic conditions that favor opportunistic species like *Nonionella* spp. and *S. loeblichi* (Fig. 4). The assemblage structure changed, but the accumulation rates of benthic foraminifera remained the same. The episodes were driven by enhanced inflow of Atlantic water that caused temporal retreat in the sea ice (Müller and Stein, 2014). It is in agreement with previous studies (e.g., Hebbeln et al., 1994) that postulated increased advection of Atlantic water as a moisture source for the growing SBIS. No changes in the foraminiferal assemblage or accumulation of TOC were recorded during episodes of increased methane seepage.

Sztybor et al. (2013) reported the first discovery of Vesicomyid clams at Vestnesa Ridge. A thick layer of well-preserved shells mark the horizon dated to Heinrich event H1 (Sztybor et al., 2013, 2014; Sztybor and Rasmussen, submitted manuscript). Ambrose et al. (2015) collected a core at the same location as core 335GC and confirmed the occurrence of

Vesicomyid shells exclusively in the H1 interval. Suitable rates of sulfate reduction are currently present at Vestnesa Ridge to sustain a community of chemosymbiotic bivalves (Hong et al., 2016; Pimenov et al., 2000), however despite a recent submersible survey (Vinogradov, 1999) and extensive bottom sampling in the area during recent years, no living Vesicomyids have been found so far. Heinrich event H1 on the western Svalbard margin was characterized by elevated bottom water temperatures (Rasmussen et al., 2007, see discussion) the highest recorded in the entire examined records of 333GC and 335GC (Fig. 4). We claim that the factor restricting the occurrence of bivalves to this specific interval was the elevated bottom water temperature (~1ºC). Current bottom water temperature at Vestnesa is ~-1ºC, most likely too cold to sustain the bivalve community. This emphasizes the importance of familiarity with paleoceanographic conditions for the correct reconstruction of paleo-seepage.

6. Conclusions

- No seep influence on diversity, density or assemblage structure of the benthic foraminifera communities for the last 43,000–9000 years were found
- The lack of difference in the diversity and community structure of the seep core compared to the non-seep core suggests that the low $\delta^{13}C$ values of foraminiferal tests are a result of diagenesis of the dead assemblages at the depth of the SMTZ.
- There was a clear control of ocean circulation on the assemblage structure and density.
- Significantly higher bottom water temperature during glacial time than in the Holocene with a possible maximum during Heinrich event H1
- There was probably a paleoceanographic (temperature) control on the occurrence of the chemosynthetic bivalve community

Acknowledgments

The research was supported by UiT, Arctic University of Norway and the Mohn Foundation to the Paleo-CIRCUS project and by the Research Council of Norway through its Centre of Excellence funding scheme for CAGE, project number 223259. We thank E. Thomsen, S. Vadakkepuliyambatta and T. Grytå for help with preparing Fig. 1a and Fig. 1c.

Table captions:

Table 1. AMS ^{14}C dates and calibrated ages of cores JM10-333GC and JM10-335GC. Correlation tie points for Western Svalbard slope from Jessen et al. (2010) are shown in italics.

Figures captions:

Figure 1. (a) Map of the Nordic seas and the Barents Sea with major surface currents. Red box shows location of Vestnesa Ridge. (b) CTD (conductivity-temperature-depth) data of temperature and salinity from the coring site JM10-335GC taken in June 2010. (c) Detailed bathymetric map of the pockmark on the southern part of Vestnesa Ridge with location of the two studied gravity cores (JM10-335GC inside the pockmark and JM10-333GC outside the pockmark). The map is based on data from Bünz et al. (2012).

Figure 2. Correlation between the control core JM10-333GC and pockmark core JM10-335GC and the stacked magnetic susceptibility record for the western Svalbard slope (Jessen et al., 2010), lithological log, calibrated AMS^{14} dates, and grain size. Three lithological stratigraphic markers are indicated with color shading. Ages in green are based on correlation between the cores, ages in red are considered too old (see Sztybor and Rasmussen, submitted manuscript).

Figure 3. Records for core JM10-333GC (grey) and JM10-335GC (black) plotted versus age (cal yr BP). (a) number of species, (b) Fischer α index, (c) Pielou index (J), (d) benthic foraminifera per gram dry weight sediment, (e) benthic foraminiferal accumulation rate, (f) average sedimentation rates, (g) number of IRD >1mm per gram dry weight sediment. (h) Planktonic (*N. pachyderma,* red) and benthic (*C. neoteretis,* black) $\delta^{18}O$ values corrected for ice volume measured in core JM10-335GC. (i) Planktonic (*N. pachyderma,* red) and benthic (*C. neoteretis,* black) $\delta^{13}C$ values measured in core JM10-335GC. Abbreviations: YD, Younger Dryas; B-A, Bølling-Allerød interstadials; H1, Heinrich event H1; LGM, last glacial maximum.

Figure. 4. (a) Benthic $\delta^{18}O$ (black) and $\delta^{13}C$ (red) values measured on *C. neoteretis* in core JM10-335GC. (b–k) Records of relative abundance of benthic foraminiferal species in percentages of total benthic fauna for core JM10-333GC (grey) and JM10-335GC (black) plotted versus age (cal yr BP), (b) *Cassidulina neoteretis*, (c) *Cassidulina reniforme*, (d) *Melonis barleeanus*, (e) *Nonionella* spp, (f) *Stainfortia loeblichi*, (g) *Islandiella norcrossi*, (h) 'Atlantic species' group, (i) *Oridorsalis umbonatus*, (j) *Elphidium excavatum*, (k) *Cibicides lobatulus\ Cibicidoides wuellerstorfi*. Abbreviations: YD, Younger Dryas; B-A, Bølling-Allerød interstadials; H1, Heinrich event H1; LGM, last glacial maximum.

Figure 5. (a) Planktonic $\delta^{18}O$ (black) and $\delta^{13}C$ (red) values measured on *N. pachyderma,* in core JM10-335GC. (b–e) Records for core JM10-333GC (grey) and JM10-335GC (black) plotted versus age (cal yr BP), (b) % TOC, (c) % TC, (d) % $CaCO_3$, (e) sedimentation rates. (f-i) Planktonic records from core JM10-225GC. (f) Relative abundance of planktonic foraminifera species in percentages of total planktonic fauna, *N. pachyderma* (black) and *T. quinqueloba* (red, inverse scale), (g) planktonic foraminifera per gram dry weight sediment,

(h) flux of planktonic foraminifera, (i) planktonic\benthic foraminifera ratio. Abbreviations: YD, Younger Dryas; B-A, Bølling-Allerød interstadials; H1, Heinrich event H1; LGM, last glacial maximum.

References

Aagaard-Sørensen, S., Husum, K., Werner, K., Spielhagen, R.F., Hald, M., Marchitto, T.M., 2014a. A Late Glacial–Early Holocene multiproxy record from the eastern Fram Strait, Polar North Atlantic. Marine Geology 355, 15-26.

Aagaard-Sørensen, S., Husum, K., Hald, M., Marchitto, T.M., Godtliebsen, F., 2014b. Sub sea surface temperatures in the Polar North Atlantic during the Holocene: Planktic foraminiferal Mg/Ca temperature reconstructions. The Holocene 24, 93-103.

Aagaard, K., Foldvik, A., Hillman, S.R., 1987. The West Spitsbergen Current: Disposition and water mass transformation. Journal of Geophysical Research 92, 3778.

Aagaard, K., Swift, J.H., Carmack, E.C., 1985. Thermohaline circulation in the Arctic Mediterranean Seas. Journal of Geophysical Research: Oceans 90, 4833-4846.

Ambrose, W.G., Panieri, G., Schneider, A., Plaza-Faverola, A., Carroll, M.L., Åström, E.K.L., Locke, W.L., Carroll, J., 2015. Bivalve shell horizons in seafloor pockmarks of the last glacial-interglacial transition: a thousand years of methane emissions in the Arctic Ocean. Geochemistry, Geophysics, Geosystems 16, 4108-4129.

Barbieri, R., Panieri, G., 2004. How are benthic foraminiferal faunas influenced by cold seeps? Evidence from the Miocene of Italy. Palaeogeography, Palaeoclimatology, Palaeoecology 204, 257-275.

Barker, S., Kiefer, T., Elderfield, H., 2004. Temporal changes in North Atlantic circulation constrained by planktonic foraminiferal shell weights. Paleoceanography 19, PA3008.

Bauch, H.A., Erlenkeuser, H., Spielhagen, R.F., Struck, U., Matthiessen, J., Thiede, J., Heinemeier, J., 2001. A multiproxy reconstruction of the evolution of deep and surface waters in the subarctic Nordic seas over the last 30,000 yr. Quaternary Science Reviews 20, 659-678.

Bernhard, J.M., Buck, K.R., Barry, J.P., 2001. Monterey Bay cold-seep biota: Assemblages, abundance, and ultrastructure of living foraminifera. Deep Sea Research Part I: Oceanographic Research Papers 48, 2233-2249.

Bernhard, J.M., Buck, K.R., Farmer, M.A., Bowser, S.S., 2000. The Santa Barbara Basin is a symbiosis oasis. Nature 403, 77-80.

Bernhard, J.M., Sen Gupta, B.K., Borne, P.F., 1997. Benthic foraminiferal proxy to estimate dysoxic bottom-water oxygen concentrations; Santa Barbara Basin, U.S. Pacific continental margin. The Journal of Foraminiferal Research 27, 301-310.

Beszczynska-Möller, A., Fahrbach, E., Schauer, U., Hansen, E., 2012. Variability in Atlantic water temperature and transport at the entrance to the Arctic Ocean, 1997-2010. ICES Journal of Marine Science 69, 852-863.

Bhaumik, A.K., Gupta, A.K., 2007. Evidence of methane release from Blake Ridge ODP Hole 997A during the Plio-Pleistocene: Benthic foraminifer fauna and total organic carbon. Current Science 92, 192-199.

Birgel, D., Hass, H., 2004. Oceanic and atmospheric variations during the last deglaciation in the Fram Strait (Arctic Ocean): a coupled high-resolution organic-geochemical and sedimentological study. Quaternary Science Reviews 23, 29-47.

Boetius, A., Ravenschlag, K., Schubert, C.J., Rickert, D., Widdel, F., Gieseke, A., Amann, R., Jorgensen, B.B., Witte, U., Pfannkuche, O., 2000. A marine microbial consortium apparently mediating anaerobic oxidation of methane. Nature 407, 623-626.

Bond, G., Broecker, W., Johnsen, S., McManus, J., Labeyrie, L., Jouzel, J., Bonani, G., 1993. Correlations between climate records from North Atlantic sediments and Greenland ice. Nature 365, 143-147.

Boss, K., Turner, R., 1980. The Giant White Clam From The Galapagos Rift, Calyptogena-Magnifica Species Novum. Malacologia 20, 161-194.

Brooks, J.M., Kennicutt, M.C., Fisher, C.R., Macko, S.A., Cole, K., Childress, J.J., Bidigare, R.R., Vetter, R.D., 1987. Deep-Sea Hydrocarbon Seep Communities: Evidence for Energy and Nutritional Carbon Sources. Science 238, 1138-1142.

Bünz, S., Polyanov, S., Vadakkepuliyambatta, S., Consolaro, C., Mienert, J., 2012. Active gas venting through hydrate-bearing sediments on the Vestnesa Ridge, offshore W-Svalbard. Marine Geology 332-334, 189-197.

Carstens, J., Wefer, G., 1992. Recent distribution of planktonic foraminifera in the Nansen Basin, Arctic Ocean. Deep Sea Research Part A. Oceanographic Research Papers 39, S507-S524.

Chauhan, T., Rasmussen, T.L., Noormets, R., Jakobsson, M., Hogan, K.A., 2014. Glacial history and paleoceanography of the southern Yermak Plateau since 132 ka BP. Quaternary Science Reviews 92, 155-169.

Consolaro, C., Rasmussen, T.L., Panieri, G., Mienert, J., Bünz, S., Sztybor, K., 2015. Carbon isotope (δ13C) excursions suggest times of major methane release during the last 14 kyr in Fram Strait, the deep-water gateway to the Arctic. Climate of the Past 11, 669-685.

Corliss, B.H., 1991. Morphology and microhabitat preferences of benthic foraminifera from the northwest Atlantic Ocean. Marine Micropaleontology 17, 195-236.

Corliss, B.H., Emerson, S., 1990. Distribution of rose bengal stained deep-sea benthic foraminifera from the Nova Scotian continental margin and Gulf of Maine. Deep Sea Research Part A. Oceanographic Research Papers 37, 381-400.

Dokken, T.M., Hald, M., 1996. Rapid climatic shifts during isotope stages 2–4 in the Polar North Atlantic. Geology 24, 599-602.

Duplessy, J.-C., Ivanova, E., Murdmaa, I., Paterne, M., Labeyrie, L., 2001. Holocene paleoceanography of the northern Barents Sea and variations of the northward heat transport by the Atlantic Ocean. Boreas 30, 2-16.

Ebbesen, H., Hald, M., Eplet, T.H., 2007. Lateglacial and early Holocene climatic oscillations on the western Svalbard margin, European Arctic. Quaternary Science Reviews 26, 1999-2011.

Eiken, O., Hinz, K., 1993. Contourites in the Fram Strait. Sedimentary Geology 82, 15-32.

Elverhøi, A., Andersen, E.S., Dokken, T., Hebbeln, D., Spielhagen, R., Svendsen, J.I., Sørflaten, M., Rørnes, A., Hald, M., Forsberg, C.F., 1995. The Growth and Decay of the Late Weichselian Ice Sheet in Western Svalbard and Adjacent Areas Based on Provenance Studies of Marine Sediments. Quaternary Research 44, 303-316.

Feyling-Hanssen, R.W., Jørgensen, J.A., Knudsen, K.L., Lykke-Andersen, A.-L., 1971. Late Quaternary Foraminifera from Vendsyssel, Denmark and Sandnes, Norway. Geological Society of Denmark.

Fisher, R.A., Corbet, A.S., Williams, C.B., 1943. The Relation Between the Number of Species and the Number of Individuals in a Random Sample of an Animal Population. Journal of Animal Ecology 12, 42-58.

Fontanier, C., Duros, P., Toyofuku, T., Oguri, K., Koho, K.A., Buscail, R., Grémare, A., Radakovitch, O., Deflandre, B., De Nooijer, L.J., Bichon, S., Goubet, S., Ivanovsky, A., Chabaud, G., Menniti, C., Reichart, G.-J., Kitazato, H., 2014a. LIVING (STAINED) DEEP-SEA FORAMINIFERA OFF HACHINOHE (NE JAPAN, WESTERN PACIFIC): ENVIRONMENTAL INTERPLAY IN OXYGEN-DEPLETED ECOSYSTEMS. The Journal of Foraminiferal Research 44, 281-299.

Fontanier, C., Koho, K.A., Goñi-Urriza, M.S., Deflandre, B., Galaup, S., Ivanovsky, A., Gayet, N., Dennielou, B., Grémare, A., Bichon, S., Gassie, C., Anschutz, P., Duran, R., Reichart, G.J., 2014b. Benthic foraminifera from the deep-water Niger delta (Gulf of Guinea): Assessing present-day and past activity of hydrate pockmarks. Deep Sea Research Part I: Oceanographic Research Papers 94, 87-106.

Hald, M., Dokken, T., Mikalsen, G., 2001. Abrupt climatic change during the last interglacial–glacial cycle in the polar North Atlantic. Marine Geology 176, 121-137.

Hald, M., Korsun, S., 1997. Distribution of modern benthic foraminifera from fjords of Svalbard, European Arctic. The Journal of Foraminiferal Research 27, 101-122.

Hald, M., Steinsund, P.I., 1992. Distribution of surface sediment benthic Foraminifera in the southwestern Barents Sea. The Journal of Foraminiferal Research 22, 347-362.

Hald, M., Vorren, T.O., 1987. Foraminiferal stratigraphy and environment of Late Weichselian deposits on the continental shelf off Troms, northern Norway. Marine Micropaleontology 12, 129-160.

Hammer, Ø., Harper, D.A.T., Ryan, P.D., 2001. PAST: Paleontological Statistics Software Package for Education and Data Analysis, 3.12 ed, Palaeontologia Electronica.

Hebbeln, D., Dokken, T., Andersen, E.S., Hald, M., Elverhoi, A., 1994. Moisture supply for northern ice-sheet growth during the Last Glacial Maximum. Nature 370, 357-360.

Hebbeln, D., Wefer, G., 1997. Late Quaternary paleoceanography in the Fram Strait. Paleoceanography 12, 65-78.

Hong, W.-L., Sauer, S., Panieri, G., Ambrose, W.G., James, R.H., Plaza-Faverola, A., Schneider, A., 2016. Removal of methane through hydrological, microbial, and geochemical processes in the shallow sediments of pockmarks along eastern Vestnesa Ridge (Svalbard). Limnology and Oceanography, n/a-n/a.

Hop, H., Falk-Petersen, S., Svendsen, H., Kwasniewski, S., Pavlov, V., Pavlova, O., Søreide, J.E., 2006. Physical and biological characteristics of the pelagic system across Fram Strait to Kongsfjorden. Progress in Oceanography 71, 182-231.

Hovland, M., Thomsen, E., 1989. Hydrocarbon-based communities in the North Sea? Sarsia 74, 29-42.

Howe, J.A., Shimmield, T.M., Harland, R.E.X., Eyles, N., 2008. Late Quaternary contourites and glaciomarine sedimentation in the Fram Strait. Sedimentology 55, 179-200.

Hustoft, S., Bünz, S., Mienert, J., Chand, S., 2009. Gas hydrate reservoir and active methane-venting province in sediments on <20 Ma young oceanic crust in the Fram Strait, offshore NW-Svalbard. Earth and Planetary Science Letters 284, 12-24.

Jennings, A.E., Weiner, N.J., 1996. Environmental change in eastern Greenland during the last 1300 years: evidence from foraminifera and lithofacies in Nansen Fjord, 68°N. The Holocene 6, 179-191.

Jennings, A.E., Weiner, N.J., Helgadottir, G., Andrews, J.T., 2004. MODERN FORAMINIFERAL FAUNAS OF THE SOUTHWESTERN TO NORTHERN ICELAND SHELF: OCEANOGRAPHIC AND ENVIRONMENTAL CONTROLS. The Journal of Foraminiferal Research 34, 180-207.

Jernas, P., Klitgaard Kristensen, D., Husum, K., Wilson, L., Koç, N., 2013. Palaeoenvironmental changes of the last two millennia on the western and northern Svalbard shelf. Boreas 42, 236-255.

Jessen, S.P., Rasmussen, T.L., Nielsen, T., Solheim, A., 2010. A new Late Weichselian and Holocene marine chronology for the western Svalbard slope 30,000–0 cal years BP. Quaternary Science Reviews 29, 1301-1312.

Jones, G.A., Keigwin, L.D., 1988. Evidence from Fram Strait (78[deg] N) for early deglaciation. Nature 336, 56-59.

Jorissen, F.J., Barmawidjaja, D.M., Puskaric, S., van der Zwaan, G.J., 1992. Approaches to Paleoproductivity ReconstructionsVertical distribution of benthic foraminifera in the northern Adriatic Sea: The relation with the organic flux. Marine Micropaleontology 19, 131-146.

Karpuz, N.K., Jansen, E., 1992. A high-resolution diatom record of the last deglaciation from the SE Norwegian Sea: Documentation of rapid climatic changes. Paleoceanography 7, 499-520.

Knies, J., Matthiessen, J., Vogt, C., Laberg, J.S., Hjelstuen, B.O., Smelror, M., Larsen, E., Andreassen, K., Eidvin, T., Vorren, T.O., 2009. The Plio-Pleistocene glaciation of the Barents Sea–Svalbard region: a new model based on revised chronostratigraphy. Quaternary Science Reviews 28, 812-829.

Knies, J., Matthiessen, J., Vogt, C., Stein, R., 2002. Evidence of 'Mid-Pliocene (˜3 Ma) global warmth' in the eastern Arctic Ocean and implications for the Svalbard/Barents Sea ice sheet during the late Pliocene and early Pleistocene (˜3 – 1.7 Ma). Boreas 31, 82-93.

Knies, J., Stein, R., 1998. New aspects of organic carbon deposition and its paleoceanographic implications along the Northern Barents Sea Margin during the last 30,000 years. Paleoceanography 13, 384-394.

Korsun, S., Hald, M., 1998. Modern Benthic Foraminifera off Novaya Zemlya Tidewater Glaciers, Russian Arctic. Arctic and Alpine Research 30, 61-77.

Krylova, E.M., Sahling, H., 2010. Vesicomyidae (Bivalvia): current taxonomy and distribution. PLoS One 5, e9957.

Levin, L.A., 2005. Ecology of cold seep sediments: Interactions of fauna with flow, chemistry and microbes, in: Gibson, R.N., Atkinson, R.J.A., Gordon, J.D.M. (Eds.), Oceanography and Marine Biology - an Annual Review, Vol. 43. Crc Press-Taylor & Francis Group, Boca Raton, pp. 1-46.

Lisiecki, L.E., Raymo, M.E., 2005. A Pliocene-Pleistocene stack of 57 globally distributed benthic $\delta^{18}O$ records. Paleoceanography 20, PA1003.

Lobegeier, M.K., Sen Gupta, B.K., 2008. FORAMINIFERA OF HYDROCARBON SEEPS, GULF OF MEXICO. The Journal of Foraminiferal Research 38, 93-116.

Loeblich, A.R., Tappan, H.N., 1988. Foraminiferal genera and their classification. Van Nostrand Reinhold Co.

Loubere, P., Rayray, S., 2016. Benthic foraminiferal assemblage formation: Theory and observation for the European Arctic Margin. Deep Sea Research Part I: Oceanographic Research Papers 113, 107-118.

MacDonald, I.R., Boland, G.S., Baker, J.S., Brooks, J.M., Kennicutt, M.C., Bidigare, R.R., 1989. Gulf of Mexico hydrocarbon seep communities. Marine Biology 101, 235-247.

Mackensen, A., Sejrup, H.P., Jansen, E., 1985. The distribution of living benthic foraminifera on the continental slope and rise off southwest Norway. Marine Micropaleontology 9, 275-306.

Manley, T.O., 1995. Branching of Atlantic Water within the Greenland-Spitsbergen Passage: An estimate of recirculation. Journal of Geophysical Research: Oceans 100, 20627-20634.

Martin, R.A., Nesbitt, E.A., Campbell, K.A., 2010. The effects of anaerobic methane oxidation on benthic foraminiferal assemblages and stable isotopes on the Hikurangi Margin of eastern New Zealand. Marine Geology 272, 270-284.

Martinson, D.G., Pisias, N.G., Hays, J.D., Imbrie, J., Moore, T.C., Shackleton, N.J., 1987. Age dating and the orbital theory of the ice ages: Development of a high-resolution 0 to 300,000-year chronostratigraphy. Quaternary Research 27, 1-29.

Mattingsdal, R., Knies, J., Andreassen, K., Fabian, K., Husum, K., Grøsfjeld, K., De Schepper, S., 2014. A new 6 Myr stratigraphic framework for the Atlantic–Arctic Gateway. Quaternary Science Reviews 92, 170-178.

Myhre, A.M., Thiede, J., Firth, J.V., et al.,, 1995. Proceedings of the Ocean Drilling Program. Initial Reports, Leg 151, Ocean Drilling Program. College Station, Texas.

Müller, J., Masse, G., Stein, R., Belt, S.T., 2009. Variability of sea-ice conditions in the Fram Strait over the past 30,000 years. Nature Geosci 2, 772-776.

Müller, J., Stein, R., 2014. High-resolution record of late glacial and deglacial sea ice changes in Fram Strait corroborates ice–ocean interactions during abrupt climate shifts. Earth and Planetary Science Letters 403, 446-455.

Myrvang, K., 2015. Correlation between changes in paleoceanography, paleoclimate and methane seepage on Vestnesa Ridge, eastern Fram Strait. The Arctic University of Norway, Tromsø, p. 178.

Nørgaard-Pedersen, N., Spielhagen, R.F., Erlenkeuser, H., Grootes, P.M., Heinemeier, J., Knies, J., 2003. Arctic Ocean during the Last Glacial Maximum: Atlantic and polar domains of surface water mass distribution and ice cover. Paleoceanography 18, n/a-n/a.

Nørgaard-Pedersen, N., Spielhagen, R.F., Thiede, J., Kassens, H., 1998. Central Arctic surface ocean environment during the past 80,000 years. Paleoceanography 13, 193-204.

Orphan, V.J., Ussler, W., Naehr, T.H., House, C.H., Hinrichs, K.U., Paull, C.K., 2004. Geological, geochemical, and microbiological heterogeneity of the seafloor around methane vents in the Eel River Basin, offshore California. Chemical Geology 205, 265-289.

Osterman, L.E., Poore, R.Z., Foley, K.M., 1999. Distribution of benthic foraminifers (> 125 μm) in the surface sediments of the Arctic Ocean. US Government Printing Office.

Paull, C.K., Hecker, B., Commeau, R., Freeman-Lynde, R.P., Neumann, C., Corso, W.P., Golubic, S., E., H.J., Sikes, E., Curray, J., 1984. Biological Communities at the Florida Escarpment Resemble Hydrothermal Vent Taxa. Science 226, 965-967.

Paull, C.K., Jull, A.J.T., Toolin, L.J., Linick, T., 1985. Stable isotope evidence for chemosynthesis in an abyssal seep community. Nature 317, 709-711.

Petersen, C.J., Bünz, S., Hustoft, S., Mienert, J., Klaeschen, D., 2010. High-resolution P-Cable 3D seismic imaging of gas chimney structures in gas hydrated sediments of an Arctic sediment drift. Marine and Petroleum Geology 27, 1981-1994.

Pielou, E.C., 1966. The measurement of diversity in different types of biological collections. Journal of Theoretical Biology 13, 131-144.

Pimenov, N., Savvichev, A., Rusanov, I., Lein, A., Ivanov, M.V., 2000. Microbiological Processes of the Carbon and Sulfur Cycles at Cold Methane Seeps of the North Atlantic. Microbiology 69, 831-843.

Plaza-Faverola, A., Bünz, S., Johnson, J.E., Chand, S., Knies, J., Mienert, J., Franek, P., 2015. Role of tectonic stress in seepage evolution along the gas hydrate-charged Vestnesa Ridge, Fram Strait. Geophysical Research Letters 42, 733-742.

Polyak, L., Levitan, M., Khusid, T., Merklin, L., Mukhina, V., 2002. Variations in the influence of riverine discharge on the Kara Sea during the last deglaciation and the Holocene. Global and Planetary Change 32, 291-309.

Rasmussen, T.L., Forwick, M., Mackensen, A., 2012. Reconstruction of inflow of Atlantic Water to Isfjorden, Svalbard during the Holocene: Correlation to climate and seasonality. Marine Micropaleontology 94-95, 80-90.

Rasmussen, T.L., Thomsen, E., 2004. The role of the North Atlantic Drift in the millennial timescale glacial climate fluctuations. Palaeogeography, Palaeoclimatology, Palaeoecology 210, 101-116.

Rasmussen, T.L., Thomsen, E., 2015. Palaeoceanographic development in Storfjorden, Svalbard, during the deglaciation and Holocene: evidence from benthic foraminiferal records. Boreas 44, 24-44.

Rasmussen, T.L., Thomsen, E., Labeyrie, L., van Weering, T.C.E., 1996. Circulation changes in the Faeroe-Shetland Channel correlating with cold events during the last glacial period (58–10 ka). Geology 24, 937.

Rasmussen, T.L., Thomsen, E., Nielsen, T., 2014. Water mass exchange between the Nordic seas and the Arctic Ocean on millennial timescale during MIS 4-MIS 2. Geochemistry, Geophysics, Geosystems 15, 530-544.

Rasmussen, T.L., Thomsen, E., Ślubowska, M.A., Jessen, S., Solheim, A., Koç, N., 2007. Paleoceanographic evolution of the SW Svalbard margin (76°N) since 20,000 14C yr BP. Quaternary Research 67, 100-114.

Rasmussen, T.L., Thomsen, E., Troelstra, S.R., Kuijpers, A., Prins, M.A., 2003. Millennial-scale glacial variability versus Holocene stability: changes in planktic and benthic foraminifera faunas and ocean circulation in the North Atlantic during the last 60 000 years. Marine Micropaleontology 47, 143-176.

Rasmussen, T.L., van Weering, T.C.E., Labeyrie, L., 1996. High resolution stratigraphy of the Faeroe-Shetland Channel and its relation to North Atlantic paleoceanography: the last 87 kyr. Marine Geology 131, 75-88.

Rathburn, A.E., Levin, L.A., Held, Z., Lohmann, K.C., 2000. Benthic foraminifera associated with cold methane seeps on the northern California margin: Ecology and stable isotopic composition. Marine Micropaleontology 38, 247-266.

Rathburn, A.E., Pérez, M.E., Martin, J.B., Day, S.A., Mahn, C., Gieskes, J., Ziebis, W., Williams, D., Bahls, A., 2003. Relationships between the distribution and stable isotopic composition of living benthic foraminifera and cold methane seep biogeochemistry in Monterey Bay, California. Geochemistry, Geophysics, Geosystems 4, 1106.

Sahling, H., Rickert, D., Lee, R.W., Linke, P., Suess, E., 2002. Macrofaunal community structure and sulfide flux at gas hydrate deposits from the Cascadia convergent margin, NE Pacific. Marine Ecology Progress Series 231, 121-138.

Sarnthein, M., Jansen, E., Weinelt, M., Arnold, M., Duplessy, J.C., Erlenkeuser, H., Flatøy, A., Johannessen, G., Johannessen, T., Jung, S., Koc, N., Labeyrie, L., Maslin, M., Pflaumann, U., Schulz, H., 1995. Variations in Atlantic surface ocean paleoceanography, 50°-80°N: A time-slice record of the last 30,000 years. Paleoceanography 10, 1063-1094.

Sarnthein, M., Winn, K., Jung, S.J.A., Duplessy, J.-C., Labeyrie, L., Erlenkeuser, H., Ganssen, G., 1994. Changes in East Atlantic Deepwater Circulation over the last 30,000 years: Eight time slice reconstructions. Paleoceanography 9, 209-267.

Schauer, U., 2004. Arctic warming through the Fram Strait: Oceanic heat transport from 3 years of measurements. Journal of Geophysical Research 109.

Sejrup, H.-P., Fjaeran, T., Hald, M., Beck, L., Hagen, J., Miljeteig, I., Morvik, I., Norvik, O., 1981. Benthonic foraminifera in surface samples from the Norwegian continental margin between 62 degrees N and 65 degrees N. The Journal of Foraminiferal Research 11, 277-295.

Sen Gupta, B.K., Aharon, P., 1994. Benthic foraminifera of bathyal hydrocarbon vents of the Gulf of Mexico: Initial report on communities and stable isotopes. Geo-Marine Letters 14, 88-96.

Sen Gupta, B.K., Machain-Castillo, M.L., 1993. Benthic foraminifera in oxygen-poor habitats. Marine Micropaleontology 20, 183-201.

Sen Gupta, B.K., Platon, E., Bernhard, J.M., Aharon, P., 1997. Foraminiferal colonization of hydrocarbon-seep bacterial mats and underlying sediment, Gulf of Mexico slope. The Journal of Foraminiferal Research 27, 292-300.

Sen Gupta, B.K., Smith, L.E., Lobegeier, M.K., 2007. Attachment of Foraminifera to vestimentiferan tubeworms at cold seeps: Refuge from seafloor hypoxia and sulfide toxicity. Marine Micropaleontology 62, 1-6.

Sibuet, M., Olu, K., 1998. Biogeography, biodiversity and fluid dependence of deep-sea cold-seep communities at active and passive margins. Deep Sea Research Part II: Topical Studies in Oceanography 45, 517-567.

Ślubowska-Woldengen, M., Rasmussen, T.L., Koç, N., Klitgaard-Kristensen, D., Nilsen, F., Solheim, A., 2007. Advection of Atlantic Water to the western and northern Svalbard shelf since 17,500calyr BP. Quaternary Science Reviews 26, 463-478.

Ślubowska, M.A., Koç, N., Rasmussen, T.L., Klitgaard-Kristensen, D., 2005. Changes in the flow of Atlantic water into the Arctic Ocean since the last deglaciation: Evidence from the northern Svalbard continental margin, 80°N. Paleoceanography 20, n/a-n/a.

Smith, A.J., Mienert, J., Bünz, S., Greinert, J., 2014. Thermogenic methane injection via bubble transport into the upper Arctic Ocean from the hydrate-charged Vestnesa Ridge, Svalbard. Geochemistry, Geophysics, Geosystems 15, 1945-1959.

Stabell, B., 1986. A diatom maximum horizon in upper quaternary deposits. Geologische Rundschau 75, 175-184.

Sztybor, K., Rasmussen, T.L., submitted manuscript. Marine sedimentary records from methane influenced environments at Vestnesa Ridge, Fram Strait: Response to disturbances from variations in seep intensity during the last 35,000 years, Submitted to Boreas.

Sztybor, K., Rasmussen, T.L., Mienert, J., Bünz, S., Consolaro, C., 2013. Climate reconstruction from a methane influenced environment, AGU Fall Meeting 2013. AGU, San Francosco.

Sztybor, K., Rasmussen, T.L., Mienert, J., Bünz, S., Consolaro, C., 2014. Methane release from the seabed and reliability of the paleo-record, 12th International Conference on Gas in Marine Sediments, Taipei, Taiwan.

Vinogradov, G.M., 1999. Deep-sea near-bottom swarms of pelagic amphipods Themisto: observations from submersibles. Sarsia 84, 465-467.

Vogt, P.R., Crane, K., Sundvor, E., Max, M.D., Pfirman, S.L., 1994. Methane-generated(?) pockmarks on young, thickly sedimented oceanic crust in the Arctic: Vestnesa ridge, Fram strait. Geology 22, 255-258.

von Cosel, R., Salas, C., Høisæter, T., 2001. Vesicomyidae (Mollusca: Bivalvia) of the genera Vesicomya, Waisiuconcha, Isorropodon and Callogonia in the eastern Atlantic and the Mediterranean. Sarsia 86, 333-366.

Walczowski, W., Piechura, J., Osinski, R., Wieczorek, P., 2005. The West Spitsbergen Current volume and heat transport from synoptic observations in summer. Deep Sea Research Part I: Oceanographic Research Papers 52, 1374-1391.

Wefer, G., Heinze, P.M., Berger, W.H., 1994. Clues to ancient methane release. Nature 369, 282-282.

Werner, K., Spielhagen, R.F., Bauch, D., Hass, H.C., Kandiano, E., 2013. Atlantic Water advection versus sea-ice advances in the eastern Fram Strait during the last 9 ka: Multiproxy evidence for a two-phase Holocene. Paleoceanography 28, 283-295.

Wiedicke, M., Weiss, W., 2006. Stable carbon isotope records of carbonates tracing fossil seep activity off Indonesia. Geochemistry, Geophysics, Geosystems 7, Q11009.

Wollenburg, J.E., Knies, J., Mackensen, A., 2004. High-resolution paleoproductivity fluctuations during the past 24 kyr as indicated by benthic foraminifera in the marginal Arctic Ocean. Palaeogeography, Palaeoclimatology, Palaeoecology 204, 209-238.

Wollenburg, J.E., Kuhnt, W., 2000. The response of benthic foraminifers to carbon flux and primary production in the Arctic Ocean. Marine Micropaleontology 40, 189-231.

Wollenburg, J.E., Kuhnt, W., Mackensen, A., 2001. Changes in Arctic Ocean paleoproductivity and hydrography during the last 145 kyr: The benthic foraminiferal record. Paleoceanography 16, 65-77.

Wollenburg, J.E., Mackensen, A., 1998. Living benthic foraminifers from the central Arctic Ocean: faunal composition, standing stock and diversity. Marine Micropaleontology 34, 153-185.

Wollenburg, J.E., Mackensen, A., 2009. The ecology and distribution of benthic foraminifera at the Håkon Mosby mud volcano (SW Barents Sea slope). Deep Sea Research Part I: Oceanographic Research Papers 56, 1336-1370.

Wollenburg, J.E., Mackensen, A., Kuhnt, W., 2007. Benthic foraminiferal biodiversity response to a changing Arctic palaeoclimate in the last 24.000 years. Palaeogeography, Palaeoclimatology, Palaeoecology 255, 195-222.

Zamelczyk, K., Rasmussen, T.L., Husum, K., Godtliebsen, F., Hald, M., 2014. Surface water conditions and calcium carbonate preservation in the Fram Strait during marine isotope stage 2, 28.8-15.4 kyr. Paleoceanography 29, 1-12.

Table 1. AMS ^{14}C dates and calibrated ages of cores JM10-333GC and JM10-335GC. Correlation tie points for Western Svalbard slope from Jessen et al. (2010) are shown in italics.

Core	Depth (cm)	Dated material	Laboratory code	Age ($^{14}C \pm 1\sigma$)	Calibrated age ± 1σ
JM10-333GC	20	mixed benthic foraminifera	Beta-4133010	12920 ± 40	14442 ± 119**
Jessen et al., 2010-TP5	50	bivalve	–	12840 ± 150	14300 ± 260
Jessen et al., 2010-TP6	110	bivalve	–	13140 ± 150	14780 ± 220
JM10-333GC	137	*N. pachyderma* sin	UBA-23419	14475 ± 61	16385 ± 142
JM10-333GC	147	*N. pachyderma* sin	UBA-23420	15228 ± 61	17677 ± 190
Jessen et al., 2010-TP7	258	*N. pachyderma* sin	–	20150 ± 130	23550 ± 185
Jessen et al., 2010-TP8	281	*N. pachyderma* sin	–	20580 ± 130	24080 ± 150
JM10-333GC	359	*N. pachyderma* sin	Beta-412869	37420 ± 340	42118 ± 339
Jessen et al., 2010-TP2	10	planktonic foraminifera	–	9240 ± 100	9840 ± 200
JM10-335GC	20	*N. pachyderma* sin	UBA-18137	9302 ± 38	9981 ± 111
Jessen et al., 2010-TP3	35	planktonic foraminifera	–	9390 ± 100	10100 ± 150
JM10-335GC	56	*N. pachyderma* sin	UBA-23417	10829 ± 43	12245 ± 107
JM10-335GC	57	mixed benthic foraminifera	UBA-23418	10820 ± 43	12225 ± 106
JM10-335GC	75	*N. pachyderma* sin	UBA-18138	11830 ± 44	13236 ± 69
Jessen et al., 2010-TP5	198	bivalve	–	12840 ± 150	14300 ± 260
Jessen et al., 2010-TP6	240	bivalve	–	13140 ± 150	14780 ± 220
JM10-335GC	278	*N. pachyderma* sin	UBA-23197	15486 ± 73	18197 ± 189
JM10-335GC	278	bivalve	UBA-18142	15283 ± 56	17789 ± 182
JM10-335GC	290	*N. pachyderma* sin	UBA-18139	16830 ± 71	19505 ± 90
JM10-335GC	369	*N. pachyderma* sin	UBA-18140	19327 ± 77	22462 ± 95
Jessen et al., 2010-TP7	380	*N. pachyderma* sin	–	20150 ± 130	23550 ± 185
Jessen et al., 2010-TP8	405	*N. pachyderma* sin	–	20580 ± 130	24080 ± 150
JM10-335GC	460	*N. pachyderma* sin	UBA-18141	27132 ± 150	31977 ± 221
**Unknown reservoir age. Calibrated age may be too old.					

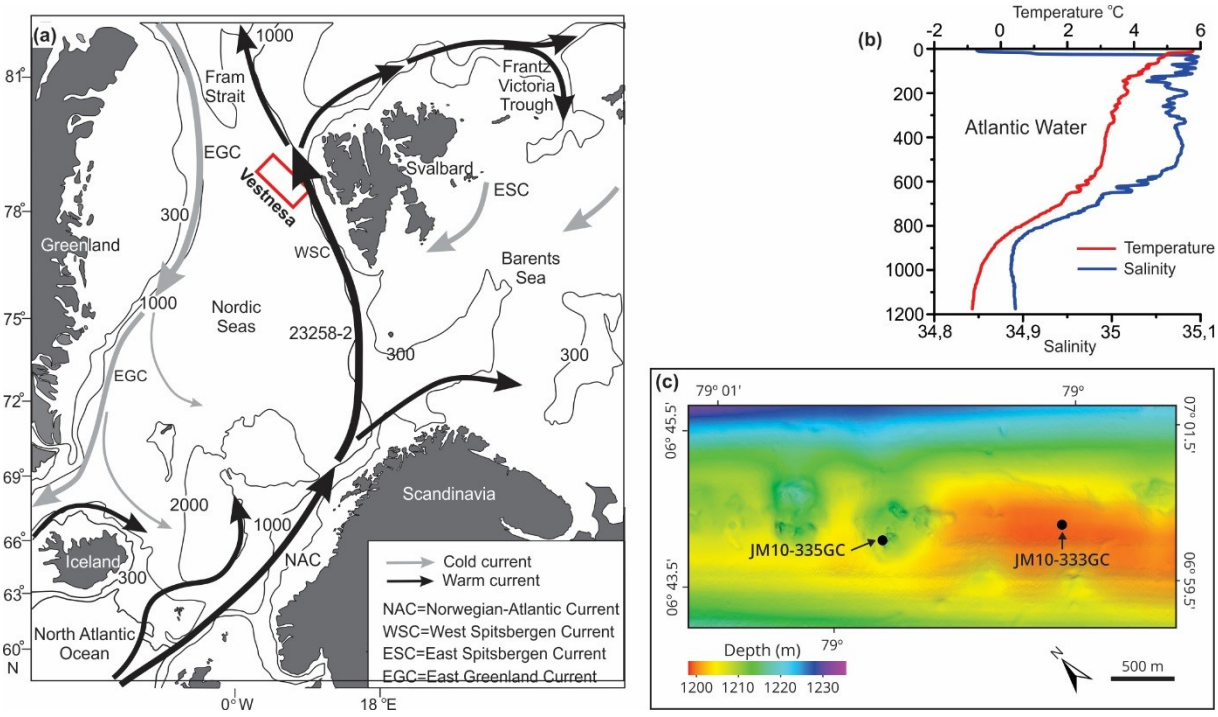

Figure 1. (a) Map of the Nordic seas and the Barents Sea with major surface currents. Red box shows location of Vestnesa Ridge. (b) CTD (conductivity-temperature-depth) data of temperature and salinity from the coring site JM10-335GC taken in June 2010. (c) Detailed bathymetric map of the pockmark on the southern part of Vestnesa Ridge with location of the two studied gravity cores (JM10-335GC inside the pockmark and JM10-333GC outside the pockmark). The map is based on data from Bünz et al. (2012).

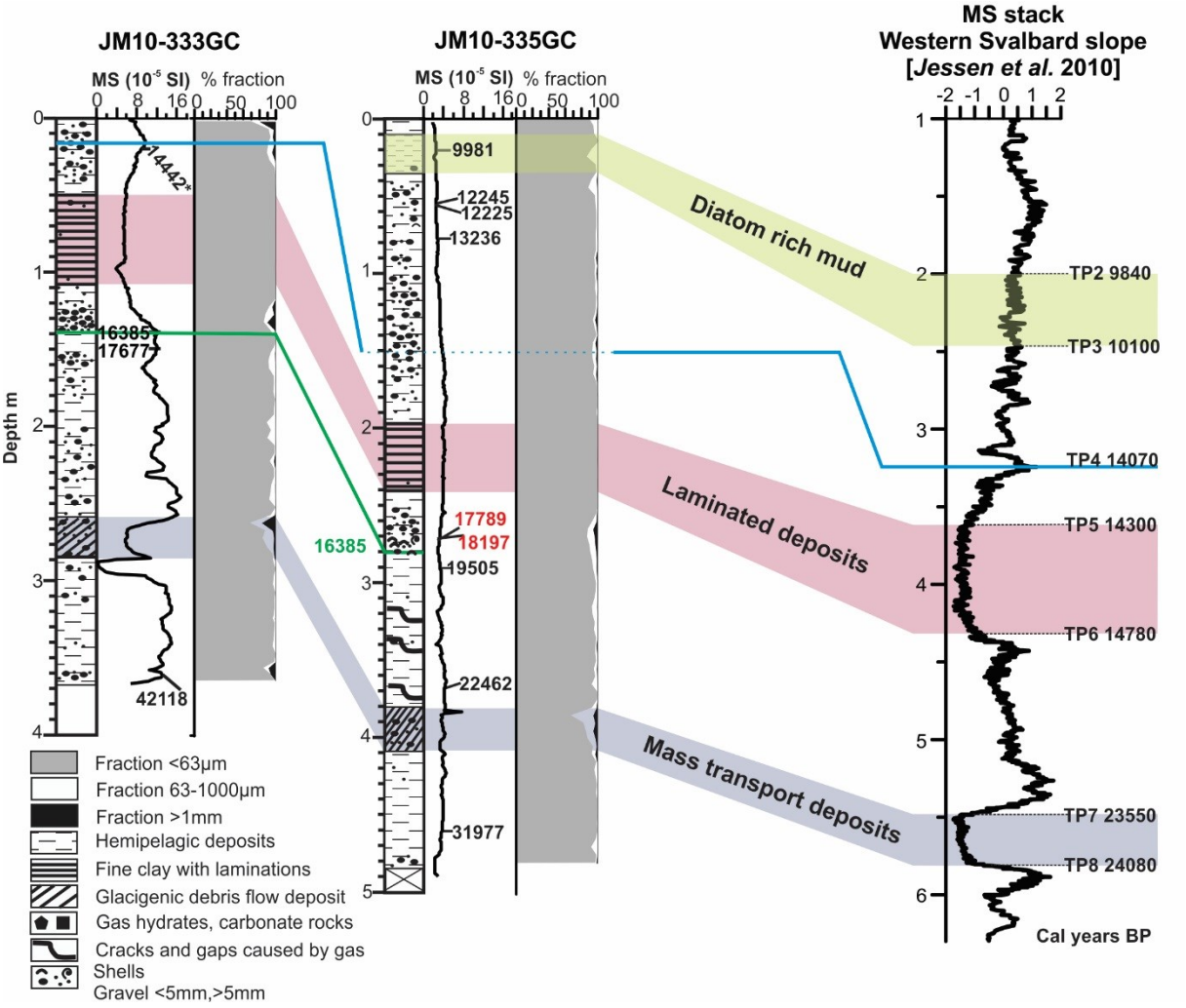

Figure 2. Correlation between the control core JM10-333GC and pockmark core JM10-335GC and the stacked magnetic susceptibility record for the western Svalbard slope (Jessen et al., 2010), lithological log, calibrated AMS^{14} dates, and grain size. Three lithological stratigraphic markers are indicated with color shading. Ages in green are based on correlation between the cores, ages in red are considered too old (see Sztybor and Rasmussen, submitted manuscript).

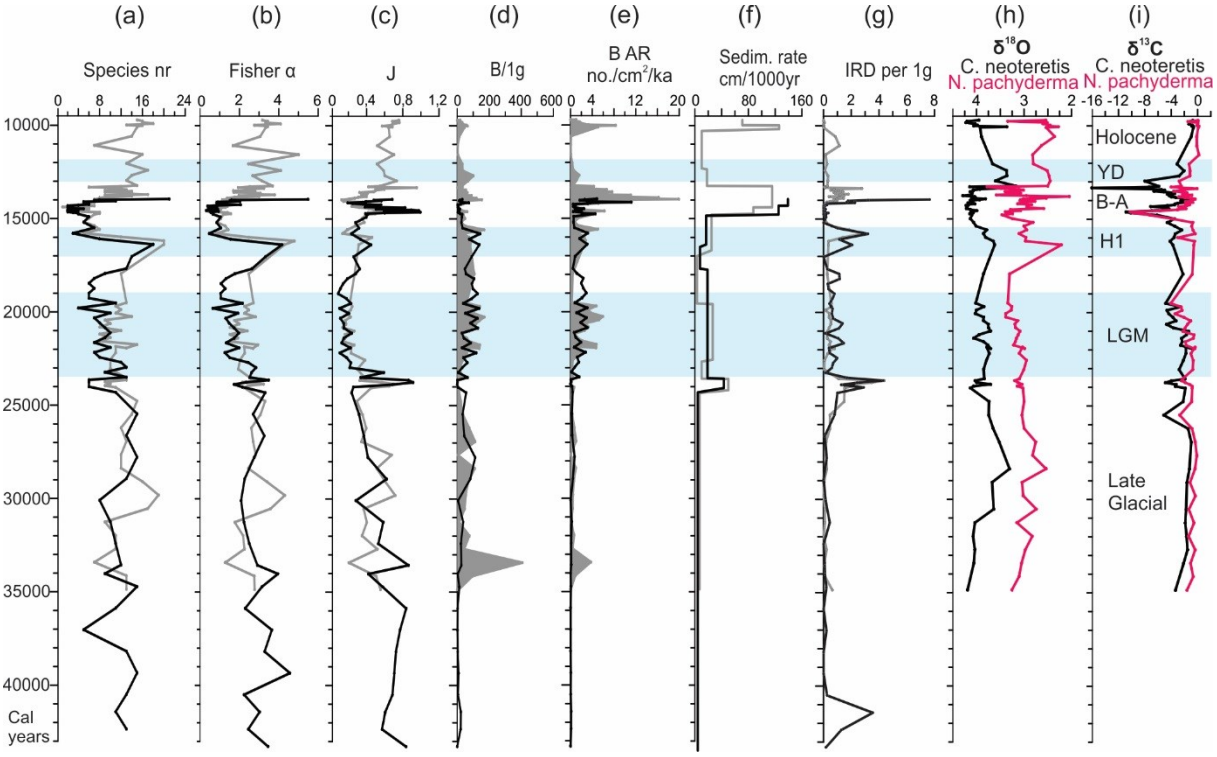

Figure 3. Records for core JM10-333GC (grey) and JM10-335GC (black) plotted versus age (cal yr BP). (a) number of species, (b) Fischer α index, (c) Pielou index (J), (d) benthic foraminifera per gram dry weight sediment, (e) benthic foraminiferal accumulation rate, (f) average sedimentation rates, (g) number of IRD >1mm per gram dry weight sediment. (h) Planktonic (*N. pachyderma,* red) and benthic (*C. neoteretis,* black) $\delta^{18}O$ values corrected for ice volume measured in core JM10-335GC. (i) Planktonic (*N. pachyderma,* red) and benthic (*C. neoteretis,* black) $\delta^{13}C$ values measured in core JM10-335GC. Abbreviations: YD, Younger Dryas; B-A, Bølling-Allerød interstadials; H1, Heinrich event H1; LGM, last glacial maximum.

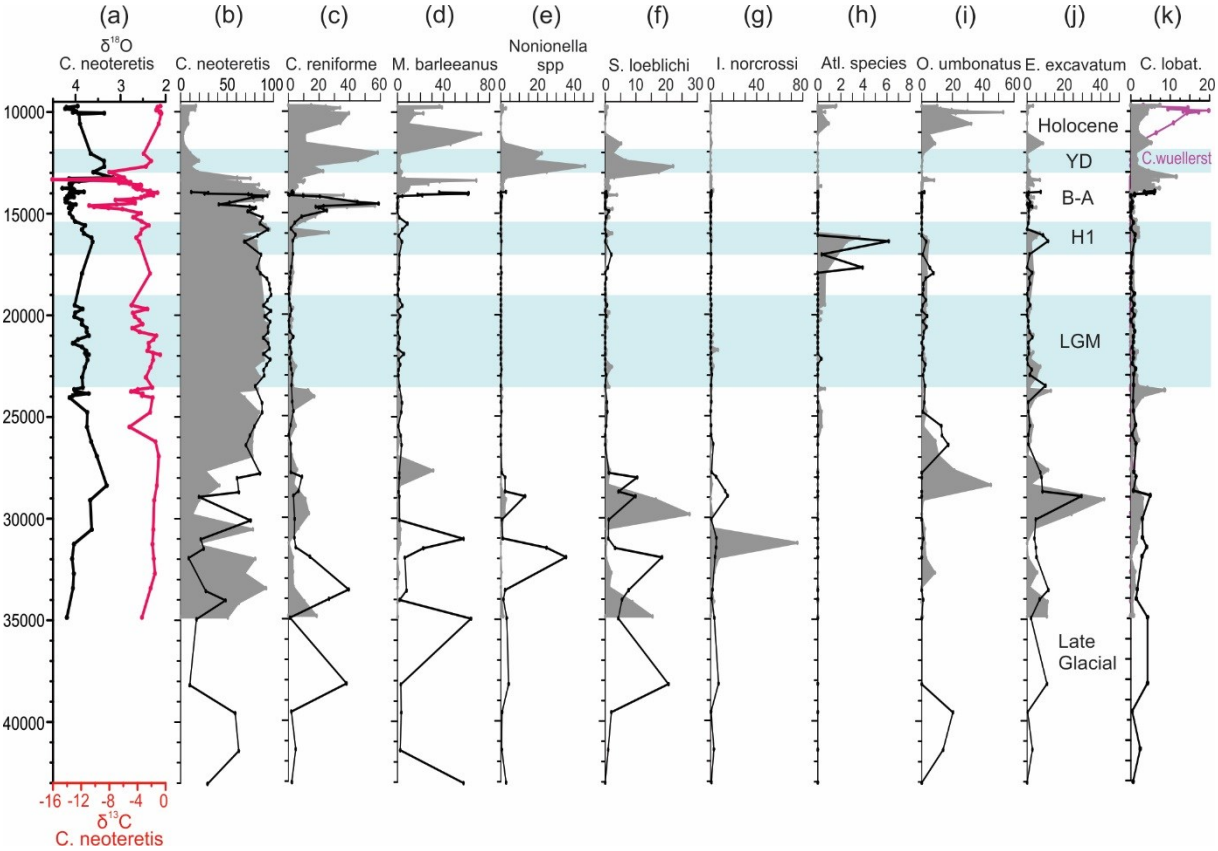

Figure. 4. (a) Benthic $\delta^{18}O$ (black) and $\delta^{13}C$ (red) values measured on *C. neoteretis* in core JM10-335GC. (b–k) Records of relative abundance of benthic foraminiferal species in percentages of total benthic fauna for core JM10-333GC (grey) and JM10-335GC (black) plotted versus age (cal yr BP), (b) *Cassidulina neoteretis*, (c) *Cassidulina reniforme*, (d) *Melonis barleeanus*, (e) *Nonionella* spp, (f) *Stainfortia loeblichi*, (g) *Islandiella norcrossi*, (h) 'Atlantic species' group, (i) *Oridorsalis umbonatus*, (j) *Elphidium excavatum*, (k) *Cibicides lobatulus*\ *Cibicidoides wuellerstorfi*. Abbreviations: YD, Younger Dryas; B-A, Bølling-Allerød interstadials; H1, Heinrich event H1; LGM, last glacial maximum.

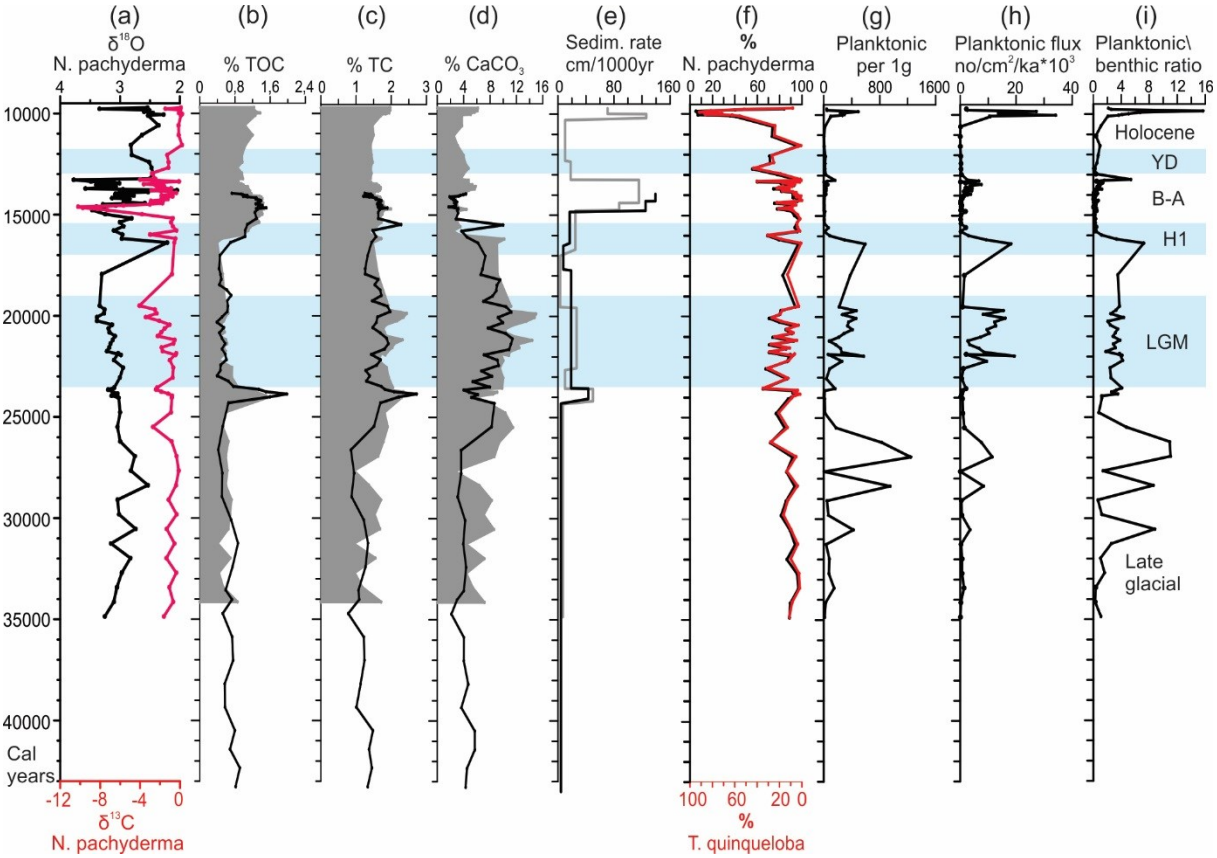

Figure 5. (a) Planktonic $\delta^{18}O$ (black) and $\delta^{13}C$ (red) values measured on *N. pachyderma,* in core JM10-335GC. (b–e) Records for core JM10-333GC (grey) and JM10-335GC (black) plotted versus age (cal yr BP), (b) % TOC, (c) % TC, (d) % $CaCO_3$, (e) sedimentation rates. (f-i) Planktonic records from core JM10-225GC. (f) Relative abundance of planktonic foraminifera species in percentages of total planktonic fauna, *N. pachyderma* (black) and *T. quinqueloba* (red, inverse scale), (g) planktonic foraminifera per gram dry weight sediment, (h) flux of planktonic foraminifera, (i) planktonic\benthic foraminifera ratio. Abbreviations: YD, Younger Dryas; B-A, Bølling-Allerød interstadials; H1, Heinrich event H1; LGM, last glacial maximum.

Paper 3

"Excess sulfur" in sediments from western Svalbard margin as indication for the efficiency of the microbial filter in paleo-anaerobic oxidation of methane (AOM)

Kamila Sztybor, Tine Lander Rasmussen and Troels Laier

In preparation for submission to Chemical Geology

“Excess sulfur” in sediments from western Svalbard margin as indication for the efficiency of the microbial filter in paleo-anaerobic oxidation of methane (AOM)

Kamila Sztybor[1]*, Tine L. Rasmussen[1], Troels Laier[2]

[1]CAGE - Centre for Arctic Gas Hydrate, Environment and Climate, Department of Geology, UiT The Arctic University of Norway, Dramsveien 201, N-9037 Tromsø, Norway,

[2]Geological Survey of Denmark and Greenland, Department of Geochemistry, Øster Voldgade 10, DK-1350 Copenhagen K, Denmark

**Corresponding author. Email: kamila.sztybor@uit.no*

Abstract:

Anaerobic oxidation of methane (AOM) in near-surface sediments is an important process in significantly limiting methane emissions from the seafloor. Sediments with low content of organic carbon are known as those of highest capacity and efficiency of AOM. In this study, we focus on the relationship between AOM, stable isotopes, concentrations of pyrite particles and their texture, magnetic susceptibility, carbon and sulfur content and carbon-sulfur ratios in three cores. Two cores are from a pockmark with active methane seepage and one core from outside the pockmark. The records are from the western Svalbard margin, from ca 1200 m water depth. The cores are characterized by similar lithofacies, sedimentation rates and organic carbon content (TOC). However, the pockmark cores show much higher concentration of pyrite particles, sulfur content and higher sulfur-carbon ratios. Sulfur vs. carbon plots, usually used to characterize the type of depositional environments, here show diagenetically produced “excess” sulfide in the process of AOM. Highest sulfur flux correlates with extremely low $\delta^{13}C$ values in foraminiferal shells and is taken as strong evidence that sulfate reduction is coupled to the anaerobic oxidation of methane. Based on “excess” sulfide, AOM rates and consumed methane flux are estimated here for the Last Glacial Maximum and the deglaciation period. The calculated methane flux correspond to low

to medium methane fluxes at modern seeps. Furthermore, different pyrite textures were observed in high excess sulfide core intervals, from the low excess sulfide intervals and in the control core, which most likely is connected to different precipitation mechanisms. Moreover, the low and nearly constant magnetic susceptibility values and high content of pyrite in pockmark cores compared to high and highly variable susceptibility values and low pyrite in the control core is probably the result of dissolution of magnetic minerals in the reducing methane seep sediments and the formation of paramagnetic minerals, mainly pyrite.

1. Introduction

Cold methane seeps are common on continental margins worldwide (Judd and Hovland, 2007). Methane from deeper geological sources is migrating towards the seafloor through conduits like faults and cracks. The methane may reach the atmosphere or be oxidized aerobically in the water column, but the major part is usually oxidized anaerobically in the sediment and before it reaches the sediment-water interface (Hinrichs and Boetius, 2003; Treude et al., 2005). The sulfate-dependent process of anaerobic methane oxidation (AOM) is mediated by a consortium of methane-oxidizing archaea and sulfate-reducing bacteria (Boetius et al., 2000; Hinrichs et al., 2000) and works as a filter that significantly limits the emissions of methane to the water column (Treude et al., 2003; Niemann et al., 2006). The AOM takes place at the sulfate-methane transition zone (SMTZ), a sediment interval separating methane bearing sediments from sulfate bearing sediments (Borowski et al., 1996), where upward migrating methane reacts with downward diffusing sulfate to produce dissolved bicarbonate and hydrogen sulfide (e.g. Reeburgh, 1976). The dissolved bicarbonate increases the alkalinity of the pore water. In addition, the $\delta^{13}C$ values of the dissolved inorganic carbon (DIC) decrease, because methane is strongly depleted in ^{13}C relative to seawater DIC (Luff and Wallmann, 2003; Chen et al., 2010). Low $\delta^{13}C$ values of

pore water DIC derived from AOM can mix with the DIC of fluids from greater depths migrating upwards and the bicarbonate produced from fermentation of buried organic matter (Snyder et al., 2007; Chatterjee et al., 2011). The hydrogen sulfide can be oxidized by chemosynthetic communities (Hovland and Thomsen, 1989; MacDonald et al., 1990; Levin, 2005) or stored as iron sulfides, mostly pyrite (Novosel et al., 2005; Zhang et al., 2014; Lin et al., 2016).

Sulfur reduction (SR) in marine sediments is normally coupled to degradation of organic matter at the seafloor (Berner, 1982; Thomsen and Vorren, 1984). Total sulfur (TS) vs total organic carbon (TOC) plots and TS/TOC ratios are useful for characterizing ancient and modern sedimentary depositional environments (Berner and Raiswell, 1983; Leventhal, 1983, 1995). For marine sediments deposited in normal oxygenated seawater the TS/TOC ratio is constant and is about ~0.36 (or ~2.8 if showed as TOC/TS) (Berner, 1982; Berner and Raiswell, 1983). Lower ratios occurs in freshwater sediments because of limited sulfate availability, higher ratios are attributed to euxinic environments (Berner and Raiswell, 1984). In methane seep environments SR includes two processes: fermentation of buried organic matter and AOM (e.g. Snyder et al., 2007). Because both processes are sulfate consuming, sediments with lower content of organic matter have higher capacity for AOM, because more of the sulfate flux is available for AOM (Pohlman et al., 2013). In seep sediments poor in organic matter, almost all sulfate is consumed in AOM (Pohlman et al., 2013). Sulfate reduction not connected to decomposition of organic material leads to elevated sulfide sulfur in the sediment in relation to organic carbon and disequilibrium from the normal TS/TOC ratio (Leventhal, 1995).

Here we investigate the relationship between higher sulfur content in the sediment and higher sulfur flux as evidence for enhanced AOM. From the total sulfur content of the seep core the sulfur content of the control core covering the same time interval was subtracted, so the fluxes

shows only the sulfur coming from the process of AOM. Several studies showed that paleo-AOM can be inferred by the presence of authigenic carbonates (Judd and Hovland, 2007; Magalhães et al., 2012) and microfossils with very low $\delta^{13}C$ values (Hill et al., 2011; Consolaro et al., 2015). Unfortunately, neither carbonates nor isotopic signatures reflect how much of the methane has been consumed in the process of AOM. The efficiency of the microbial filter was estimated from experiments (e.g. Treude et al., 2003; Joye et al., 2004; Sommer et al., 2006) or modelled based on the pore-water profiles (Aharon and Fu, 2000; Hong et al., 2016). However, these attempts to quantify AOM rates are considered controversial as the measured and calculated fluxes can change significantly on short time-scales (Snyder et al., 2007 and references therein). In this study, we propose the first long term (late glacial and deglaciation) quantitative AOM record based on the flux of "excess sulfur".

3. Material and methods

The study is based on three gravity cores retrieved from a water depth of 1200 m at Vestnesa Ridge, eastern Fram Strait: JM10-333GC and -335GC in June 2010 and HH12-929GC in August 2012 during a cruise with *RV Jan Mayen* (now *RV Helmer Hanssen*) (Fig. 1a). Pockmarks at the eastern part of the ridge are characterized by active gas discharge into the water column (Bünz et al., 2012; Plaza-Faverola et al., 2015). Cores JM10-335GC and HH12-929GC were taken from the same active pockmark, while core JM10-333GC was taken outside the pockmark field as a control (Fig. 1b).

Details of core handling have been published previously (Sztybor and Rasmussen, 2016). For this study, samples at 5 cm intervals were used in all three records. Total organic carbon (TOC) and total sulfur (TS) were measured in bulk samples using a Leco CS-200 induction furnace instrument. The excess sulfur was calculated as TS of the pockmark core

minus TS of the control core outside pockmark, for samples of same age in the cores. The sulfur fluxes (mg/cm^2/1000 yr) were calculated using the formula:

mg S/g x Mass Accumulation Rate (MAR)

where, MAR=Linear Sedimentation Rate (LSR) (cm/1000 yr) x Dry Bulk Density (DBD) (g/cm^3). The AOM:SR ratio used in methane flux calculations was 1:1 as in sediments with low TOC content (Joye et al., 2004; Pohlman et al., 2013) according to the equation of (Reeburgh, 2007):

$CH_4 + SO_4^{2-} \rightarrow HS^- + HCO_3^- + H_2O$

Pyrite particles were counted in aliquots of the 0.1-1 mm grain-size fractions and concentrations calculated as number per gram dwt (dry weight) sediment. Pyrite fluxes were calculated using the same formula as for calculating of the sulfur fluxes. The diversity of pyrite textures were documented by using a Hitachi TM3000 scanning electron microscope (SEM) at the Department of Geology, UiT Arctic University of Norway. Details about the stratigraphy and age models of cores JM10-333GC and JM10-335GC and stable isotopes measured in several foraminiferal species have been described by Sztybor and Rasmussen (2016) (see Supplementary information and Fig. S1). Here we present the published age models, magnetic susceptibility (MS) records and $\delta^{13}C$ values measured in the planktonic foraminiferal species *Neogloboquadrina pachyderma* and benthic species *Cassidulina neoteretis*.

4. Results

Samples from the control core JM10-333GC show low TS/TOC (0.09– 0.68; average 0.22) ratios with values typical for sediments deposited in normal marine environments (Fig. 2). Results from the seep core JM10-335GC are more scattered, with predominantly high values (0.41–2.35; average 1.12) typical for euxinic environments (Fig. 2). All samples from the seep

core HH12-929GC containing gas hydrates show very high "euxinic" TS/TOC ratios (0.57–2.30; average 1.45) (Fig. 2).

Because of problems with generating a precise age model for core HH12-929GC (Sztybor and Rasmussen, 2016), data plotted against age scale are presented only for cores JM10-333GC and -335GC (Fig. 3). Both the seep and the control core show the same pattern in the distribution of total organic carbon (TOC) *vs* sediment age, also seen in other non-seep records from the western Svalbard margin (e.g. Birgel and Hass, 2004; Zamelczyk et al., 2014) (Fig. 3c). The content is generally low during the glacial interval with average ~0.6 % with one peak at 24,000 yr reaching up to 2%. This peak occurs in both cores at the level of the dark coarse sediments belonging to mass transport deposits (see Sztybor and Rasmussen, 2016 and references therein and Fig. S1 in Supplementary information). The interval is characterized by similar TS/TOC ratios in both cores (Fig. 3b). The TOC values are higher (~0.9–1.3 %) during the deglaciation 16,000–13,500 yr and early Holocene 11,500–9000 yr (~1%) (Fig 3b). During the Bølling and Allerød interstadials c. 15,000–13,000 yr and at 24,000 yr a correlation between increase in %TOC and higher sedimentation rates is clearly visible (Fig. 3c, e).

The total sulfur (TS) content in the control core JM10-333GC (Fig. 3d) co-varies with the TOC (Fig. 3e). In the pockmark core JM10-335GC the TS is high (0.52–1.89 %) throughout the entire core (Fig. 3d). The only interval where TS is similar for both cores is the layer of mass transport deposits mentioned above, which in both cores reach 16 mg S/g (1.6 %).
The magnetic susceptibility (MS) of the control core JM10-333GC show lowest values around 24,000 and 15,000 yr. The MS of the seep core JM10-335GC is very low and nearly constant. The values in both cores are similar in the time intervals of maximum sedimentation rates at 24,000 and 15,000 yr (Fig 3e, f).

The $\delta^{13}C$ values of planktic and benthic foraminifera in the seep core JM10-335GC are characterized by low (0.2– -2 ‰) and nearly constant values in the lowest part of the core

covering the time interval 35,000–26,000 yr and the Holocene. Minor excursions towards slightly lower $\delta^{13}C$ (-3– -5 ‰) occurred between 26,000 and 15,000 yr. Two major excursions towards very low $\delta^{13}C$ (-10– -16 ‰) values occurred between 15,000 and 13,000 yr (Fig 3a). This interval correlates with a significant increase in 'excess' sulfur flux and estimated methane flux (Fig. 3i, j). Because the top of control core 333GC dates 13,800 yr it was not possible to calculate the 'excess' sulfur (Fig. 3i) for the interval covering the youngest $\delta^{13}C$ excursion (Fig. 3a) and highest TS peak that occurred ~13,200 yr. The high 'excess' sulfide coincide with a high flux of framboidal pyrite particles in the 0.1-1 mm size-fraction in the seep cores (Fig. 3h, 4ab). In the control core pyrite in a form of euhedral and anhedral particles occurred exclusively in the intervals of high TOC and TS content ~24,000 and 15,000 – 13,500 yr (Fig. 3h, 4c). Those intervals in the seep core JM10-335GC contain also mostly euhedral pyrite crystals (Fig. 4de).

5. Discussion

The deposition of organic carbon (TOC) and sulfur (TS), mainly representing pyrite, in the deep sea is dependent on sedimentation rates and supply of terrigenous mineral material (Berner, 1982; Berner and Raiswell, 1983; Lin et al., 2000). High sedimentation rates (Fig. 3e) on the western Svalbard margin are associated with downslope mass transport and deposition of terrigenous sediment and IRD (Rasmussen et al., 2007; Jessen et al., 2010). The increased sedimentation rates enable preservation of buried TOC, which has escaped complete degradation at the seafloor (Knies and Stein, 1998; Müller and Stein, 2014). Sulfate reduction coupled to organic matter decomposition occurred in both cores in the interval of mass transport deposits and the Bølling-Allerød interstadials marked by temporal increases in TOC and TS in the control core (Fig. 2, 3cd). The hydrogen sulfide produced during degradation of organic matter have been recognized previously to dissolve magnetite and cause formation of pyrite (Canfield and Berner, 1987). As pyrite is a paramagnetic mineral

with magnetic susceptibility values close to zero, this process is the major reason for the loss of magnetostratigraphic records in marine sediments (Canfield and Berner, 1987; Passier et al., 1998). The presence of paramagnetic pyrite (and high TS and TOC content) thus explains the lower MS values in the intervals of high sedimentation rates (Fig. 3). The low MS in these intervals is therefore not only connected with low MS of locally derived material as suggested by Jessen et al. (2010), but could be affected by organoclastic sulfate reduction of the accumulated TOC. The MS signal is very low in the entire seep core probably due to pyrite formation resulting from both processes, the organic matter degradation and AOM. The connection between high upward methane flux and lowering of MS have been described in detail by Novosel et al. (2005). The hydrogen sulphide produced in the process of AOM dissolves highly magnetic iron oxides such as magnetite and generates the nearly non-magnetic pyrite (Novosel et al., 2005; Riedinger et al., 2005; Dewangan et al., 2013). Except of the intervals of high sedimentation rates, the organic matter content is very low in sediments from Vestnesa Ridge (TOC of ~0.5 %; Fig. 3c) and unlikely to sustain a significant organoclastic SR. The study of Pohlman et al. (2013) shows that in sediments with low organic carbon content nearly all pore water sulfate is available for AOM. Pyrite formation can be limited by iron availability (Kao et al., 2004 and references therein), nevertheless the Svalbard margin has a generous supply of this element from multiple glaciated fjords (Rasmussen et al., 2014; Wehrmann et al., 2014). Accumulation of high amounts of pyrite framboids in core JM10-335GC is therefore taken as evidence of enhanced AOM in the shallow sediments (Lin et al., 2016). Textural properties of sedimentary pyrite have been recognized as a result of precipitation mechanisms (Wilkin and Arthur, 2001 and references therein). The framboidal texture in the AOM dominated intervals of the seep core most likely result from rapid nucleation in a highly supersaturated environment (Butler and Rickard, 2000), while occurrence of pyrite predominantly in form of euhedral and anhedral grains in

the intervals of low AOM activity and in the control core is associated with limited nucleation and low supersaturation (Passier et al., 1997; Rickard, 2012).

TS/TOC ratios are prone to diagenesis (Leventhal, 1995). Here we demonstrate that the high TS content and following high TS/TOC ratios are a result of past AOM derived pyrite in the sediment. The post-depositional diagenetic processes caused accumulation of pyrite sulfur and enabled estimation of intensity of the paleo-AOM. The calculated methane flux is in the range of up to ~0.8 mmol m^{-2} d^{-1} (Fig. 3i), which corresponds to low and medium advective flows (Treude et al., 2003; Sommer et al., 2006). This corresponds to consumption of ~5 kg of methane per 1000 yr from just a single m^2 spot inside a pockmark of 500 m in diameter. The value is representative of site JM10-335GC with medium to low influence of methane (Sztybor and Rasmussen, 2016). Other sites (e.g. HH12-929GC) probably would record higher values. The pockmark environment is very heterogeneous and estimation of total flux from the pockmark is difficult. Nevertheless, our findings emphasize the importance of the capacity of the microbial filter to convert high quantities of methane into alkalinity and authigenic minerals, before it reaches the water column or the atmosphere.

6. Conclusions

Our results show a close correlation between higher TS flux, high TS/TOC ratios and very low $\delta^{13}C$ values in benthic and planktic foraminifera indicating increase in past seep activity. The content of TOC vs age in the seep core shows the same pattern and values as in non-seep records. The higher content of TOC during events of increased sedimentation rates correlate with lower AOM rates in the seep core, showing lower capacity of the microbial filter in sediments with higher organic carbon content. The previously reported low MS values seen in seep cores (Sztybor and Rasmussen, 2016) are here confirmed to be associated

with AOM induced pyrite formation based on the correlation of low MS values with elevated TS concentrations and high pyrite particles counts in the samples.

Our results show that estimates of the long-term AOM rates over geologic timescales are of fundamental importance for paleoceanographic and paleoenvironmeantal reconstructions and should be incorporated into the models of the global carbon cycle.

Acknowledgements

The study was supported by the Research Council of Norway through its Centre of Excellence funding scheme for CAGE, project number 223259. We thank S. Vadakkepuliyambatta and T. Grytå for help with preparing Fig. 1b.

Figure captions:

Figure 1. (a) Bathymetric map (IBCAO; Jakobsson et al., 2000) of the West Svalbard margin. Red box marks the location of Vestnesa Ridge. (b) Detailed bathymetric map of the pockmark on the southern part of Vestnesa Ridge with location of the three studied gravity cores (JM10-335GC and HH12-929GC inside the pockmark and JM10-333GC outside the pockmark). Map based on data from Bünz et al. (2012).

Figure 2. Plot of weight percent total organic carbon versus weight percent total sulfur for two seep cores and a control core. Region enclosed by dashed line represents present-day normal marine sediments. Adapted from Berner and Raiswell (1983).

Figure 3. (a) Planktic (*Neogloboquadrina pachyderma*, black) and benthic (*Cassidulina neoteretis*, red) $\delta^{13}C$ values measured in core JM10-335GC. (b–g) Records for core JM10-

333GC (black) and JM10-335GC (gray), (b) TS/TOC ratio, (c) % TOC, (d) mg S/g and %TS, (e) average sedimentation rates, (f) magnetic susceptibility, (g) flux of sulfur. (h) Excess sulfur flux (grey) and estimated AOM rates (green). (i) Flux of pyrite grains and aggregates in core JM10-333GC (black) and JM10-335GC (green) and pyritized burrows in core JM10-335GC (red), (j) estimated methane flux.

Figure 4. Scanning electron microscope images with examples of pyrite textures: (a–b) framboidal pyrite from core JM10-335GC, (c–e) euhedral and anhedral pyrite from core JM10-333GC (c) and core JM10-335GC (d–e).

Supplementary material: Lithology and age models of cores JM10-333GC and JM10-335GC (Fig. S1, Table S1).

7. References

Aharon, P., Fu, B., 2000. Microbial sulfate reduction rates and sulfur and oxygen isotope fractionations at oil and gas seeps in deepwater Gulf of Mexico. Geochimica et Cosmochimica Acta, 64(2): 233-246.

Berner, R.A., 1982. Burial of organic carbon and pyrite sulfur in the modern ocean; its geochemical and environmental significance. American Journal of Science, 282(4): 451-473.

Berner, R.A., Raiswell, R., 1983. Burial of organic carbon and pyrite sulfur in sediments over phanerozoic time: a new theory. Geochimica et Cosmochimica Acta, 47(5): 855-862.

Berner, R.A., Raiswell, R., 1984. C/S method for distinguishing freshwater from marine sedimentary rocks. Geology, 12(6): 365-368.

Birgel, D., Hass, H., 2004. Oceanic and atmospheric variations during the last deglaciation in the Fram Strait (Arctic Ocean): a coupled high-resolution organic-geochemical and sedimentological study. Quaternary Science Reviews, 23(1-2): 29-47.

Boetius, A. et al., 2000. A marine microbial consortium apparently mediating anaerobic oxidation of methane. Nature, 407(6804): 623-626.

Borowski, W.S., Paull, C.K., Ussler, W., 1996. Marine pore-water sulfate profiles indicate in situ methane flux from underlying gas hydrate. Geology, 24(7): 655-658.
Butler, I.B., Rickard, D., 2000. Framboidal pyrite formation via the oxidation of iron (II) monosulfide by hydrogen sulphide. Geochimica et Cosmochimica Acta, 64(15): 2665-2672.
Bünz, S., Polyanov, S., Vadakkepuliyambatta, S., Consolaro, C., Mienert, J., 2012. Active gas venting through hydrate-bearing sediments on the Vestnesa Ridge, offshore W-Svalbard. Marine Geology, 332-334: 189-197.
Canfield, D.E., Berner, R.A., 1987. Dissolution and pyritization of magnetite in anoxie marine sediments. Geochimica et Cosmochimica Acta, 51(3): 645-659.
Chatterjee, S. et al., 2011. Pore water sulfate, alkalinity, and carbon isotope profiles in shallow sediment above marine gas hydrate systems: A numerical modeling perspective. Journal of Geophysical Research, 116(B9).
Chen, Y. et al., 2010. Sources of methane inferred from pore-water δ13C of dissolved inorganic carbon in Pockmark G11, offshore Mid-Norway. Chemical Geology, 275(3-4): 127-138.
Consolaro, C. et al., 2015. Carbon isotope (δ13C) excursions suggest times of major methane release during the last 14 kyr in Fram Strait, the deep-water gateway to the Arctic. Climate of the Past, 11(4): 669-685.
Dewangan, P. et al., 2013. Diagenesis of magnetic minerals in a gas hydrate/cold seep environment off the Krishna–Godavari basin, Bay of Bengal. Marine Geology, 340: 57-70.
Hill, T.M., Paull, C.K., Critser, R.B., 2011. Glacial and deglacial seafloor methane emissions from pockmarks on the northern flank of the Storegga Slide complex. Geo-Marine Letters, 32(1): 73-84.
Hinrichs, K.-U., Boetius, A., 2003. The Anaerobic Oxidation of Methane: New Insights in Microbial Ecology and Biogeochemistry. In: Wefer, G. et al. (Eds.), Ocean Margin Systems. Springer Berlin Heidelberg, Berlin, Heidelberg, pp. 457-477.
Hinrichs, K.-U., Summons, R.E., Orphan, V., Sylva, S.P., Hayes, J.M., 2000. Molecular and isotopic analysis of anaerobic methane-oxidizing communities in marine sediments. Organic Geochemistry, 31(12): 1685-1701.
Hong, W.-L. et al., 2016. Removal of methane through hydrological, microbial, and geochemical processes in the shallow sediments of pockmarks along eastern Vestnesa Ridge (Svalbard). Limnology and Oceanography: n/a-n/a.
Hovland, M., Thomsen, E., 1989. Hydrocarbon-based communities in the North Sea? Sarsia, 74(1): 29-42.
Jessen, S.P., Rasmussen, T.L., Nielsen, T., Solheim, A., 2010. A new Late Weichselian and Holocene marine chronology for the western Svalbard slope 30,000–0 cal years BP. Quaternary Science Reviews, 29(9-10): 1301-1312.
Joye, S.B. et al., 2004. The anaerobic oxidation of methane and sulfate reduction in sediments from Gulf of Mexico cold seeps. Chemical Geology, 205(3-4): 219-238.
Judd, A., Hovland, M., 2007. Seabed fluid flow: the impact on geology, biology and the marine environment. Cambridge University Press.
Kao, S.-J., Hsu, S.-C., Horng, C.-S., Liu, K.-K., 2004. Carbon-sulfur-iron relationships in the rapidly accumulating marine sediments off southwestern Taiwan. In: Ronald J. Hill, J.L.Z.A.M.J.B.G.C.R.E.M.G., Kenneth, P. (Eds.), The Geochemical Society Special Publications. Elsevier, pp. 441-457.
Knies, J., Stein, R., 1998. New aspects of organic carbon deposition and its paleoceanographic implications along the Northern Barents Sea Margin during the last 30,000 years. Paleoceanography, 13(4): 384-394.

Leventhal, J.S., 1983. An interpretation of carbon and sulfur relationships in Black Sea sediments as indicators of environments of deposition. Geochimica et Cosmochimica Acta, 47(1): 133-137.
Leventhal, J.S., 1995. Carbon-sulfur plots to show diagenetic and epigenetic sulfidation in sediments. Geochimica et Cosmochimica Acta, 59(6): 1207-1211.
Levin, L.A., 2005. Ecology of cold seep sediments: Interactions of fauna with flow, chemistry and microbes. In: Gibson, R.N., Atkinson, R.J.A., Gordon, J.D.M. (Eds.), Oceanography and Marine Biology - an Annual Review, Vol. 43. Oceanography and Marine Biology. Crc Press-Taylor & Francis Group, Boca Raton, pp. 1-46.
Lin, Q., Wang, J., Algeo, T.J., Sun, F., Lin, R., 2016. Enhanced framboidal pyrite formation related to anaerobic oxidation of methane in the sulfate-methane transition zone of the northern South China Sea. Marine Geology, 379: 100-108.
Lin, S., Huang, K.-M., Chen, S.-K., 2000. Organic carbon deposition and its control on iron sulfide formation of the southern East China Sea continental shelf sediments. Continental Shelf Research, 20(4–5): 619-635.
Luff, R., Wallmann, K., 2003. Fluid flow, methane fluxes, carbonate precipitation and biogeochemical turnover in gas hydrate-bearing sediments at Hydrate Ridge, Cascadia Margin: numerical modeling and mass balances. Geochimica et Cosmochimica Acta, 67(18): 3403-3421.
MacDonald, I.R. et al., 1990. Gulf of Mexico hydrocarbon seep communities: VI. Patterns in community structure and habitat. Geo-Marine Letters, 10(4): 244-252.
Magalhães, V.H. et al., 2012. Formation processes of methane-derived authigenic carbonates from the Gulf of Cadiz. Sedimentary Geology, 243-244: 155-168.
Müller, J., Stein, R., 2014. High-resolution record of late glacial and deglacial sea ice changes in Fram Strait corroborates ice–ocean interactions during abrupt climate shifts. Earth and Planetary Science Letters, 403: 446-455.
Niemann, H. et al., 2006. Novel microbial communities of the Haakon Mosby mud volcano and their role as a methane sink. Nature, 443(7113): 854-8.
Novosel, I., Spence, G.D., Hyndman, R.D., 2005. Reduced magnetization produced by increased methane flux at a gas hydrate vent. Marine Geology, 216(4): 265-274.
Passier, H.F., Dekkers, M.J., de Lange, G.J., 1998. Sediment chemistry and magnetic properties in an anomalously reducing core from the eastern Mediterranean Sea. Chemical Geology, 152(3–4): 287-306.
Passier, H.F., Middelburg, J.J., de Lange, G.J., Böttcher, M.E., 1997. Pyrite contents, microtextures, and sulfur isotopes in relation to formation of the youngest eastern Mediterranean sapropel. Geology, 25(6): 519-522.
Plaza-Faverola, A. et al., 2015. Role of tectonic stress in seepage evolution along the gas hydrate-charged Vestnesa Ridge, Fram Strait. Geophysical Research Letters, 42(3): 733-742.
Pohlman, J.W. et al., 2013. Anaerobic methane oxidation in low-organic content methane seep sediments. Geochimica et Cosmochimica Acta, 108: 184-201.
Rasmussen, T.L., Thomsen, E., Nielsen, T., 2014. Water mass exchange between the Nordic seas and the Arctic Ocean on millennial timescale during MIS 4-MIS 2. Geochemistry, Geophysics, Geosystems, 15(3): 530-544.
Rasmussen, T.L. et al., 2007. Paleoceanographic evolution of the SW Svalbard margin (76°N) since 20,000 14C yr BP. Quaternary Research, 67(1): 100-114.
Reeburgh, W.S., 1976. Methane consumption in Cariaco Trench waters and sediments. Earth and Planetary Science Letters, 28(3): 337-344.
Reeburgh, W.S., 2007. Oceanic methane biogeochemistry. Chem Rev, 107(2): 486-513.
Rickard, D., 2012. Sulfidic sediments and sedimentary rocks, 65. Newnes.

Riedinger, N. et al., 2005. Diagenetic Alteration of Magnetic Signals by Anaerobic Oxidation of Methane Related to a Change in Sedimentation Rate. Geochimica et Cosmochimica Acta, 69(16): 4117-4126.
Snyder, G.T. et al., 2007. Pore water profiles and authigenic mineralization in shallow marine sediments above the methane-charged system on Umitaka Spur, Japan Sea. Deep Sea Research Part II: Topical Studies in Oceanography, 54(11-13): 1216-1239.
Sommer, S. et al., 2006. Efficiency of the benthic filter: Biological control of the emission of dissolved methane from sediments containing shallow gas hydrates at Hydrate Ridge. Global Biogeochemical Cycles, 20(2): n/a-n/a.
Sztybor, K., Rasmussen, T.L., 2016. Diagenetic disturbances of marine sedimentary records from methane-influenced environments in the Fram Strait as indications of variation in seep intensity during the last 35 000 years. Boreas: n/a-n/a.
Thomsen, E., Vorren, T.O., 1984. Pyritization of tubes and burrows from Late Pleistocene continental shelf sediments off North Norway. Sedimentology, 31(4): 481-492.
Treude, T., Boetius, A., Knittel, K., Wallmann, K., Jørgensen, B.B., 2003. Anaerobic oxidation of methane above gas hydrates at Hydrate Ridge, NE Pacific Ocean. Marine Ecology Progress Series, 264: 1-14.
Treude, T. et al., 2005. Anaerobic oxidation of methane and sulfate reduction along the Chilean continental margin. Geochimica et Cosmochimica Acta, 69(11): 2767-2779.
Wehrmann, L.M. et al., 2014. Iron and manganese speciation and cycling in glacially influenced high-latitude fjord sediments (West Spitsbergen, Svalbard): Evidence for a benthic recycling-transport mechanism. Geochimica et Cosmochimica Acta, 141: 628-655.
Wilkin, R.T., Arthur, M.A., 2001. Variations in pyrite texture, sulfur isotope composition, and iron systematics in the Black Sea: evidence for Late Pleistocene to Holocene excursions of the o2-h2s redox transition. Geochimica et Cosmochimica Acta, 65(9): 1399-1416.
Zamelczyk, K., Rasmussen, T.L., Husum, K., Godtliebsen, F., Hald, M., 2014. Surface water conditions and calcium carbonate preservation in the Fram Strait during marine isotope stage 2, 28.8-15.4 kyr. Paleoceanography, 29(1): 1-12.
Zhang, M. et al., 2014. Morphology and formation mechanism of pyrite induced by the anaerobic oxidation of methane from the continental slope of the NE South China Sea. Journal of Asian Earth Sciences, 92: 293-301.

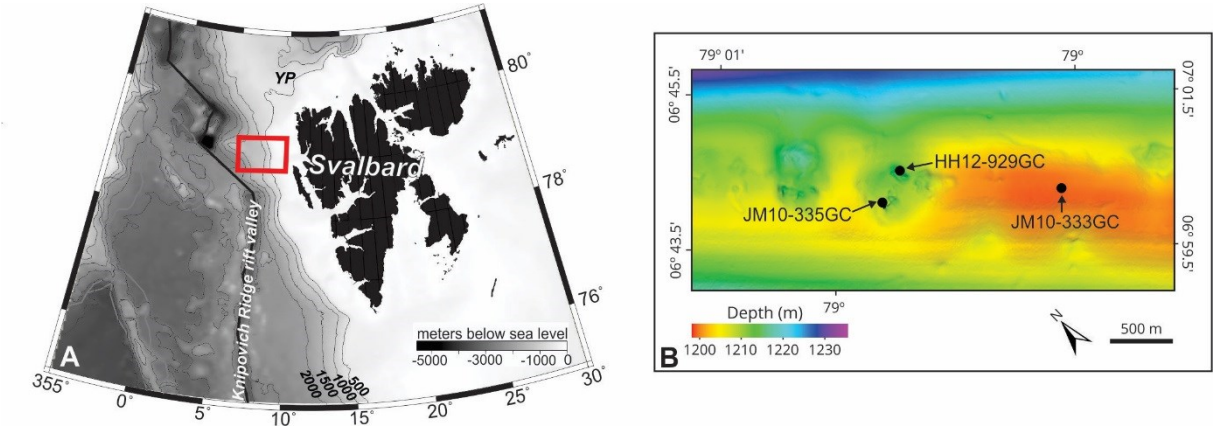

Figure 1. (a) Bathymetric map (IBCAO; Jakobsson et al., 2000) of the West Svalbard margin. Red box marks the location of Vestnesa Ridge. (b) Detailed bathymetric map of the pockmark on the southern part of Vestnesa Ridge with location of the three studied gravity cores (JM10-335GC and HH12-929GC inside the pockmark and JM10-333GC outside the pockmark). Map based on data from Bünz et al. (2012).

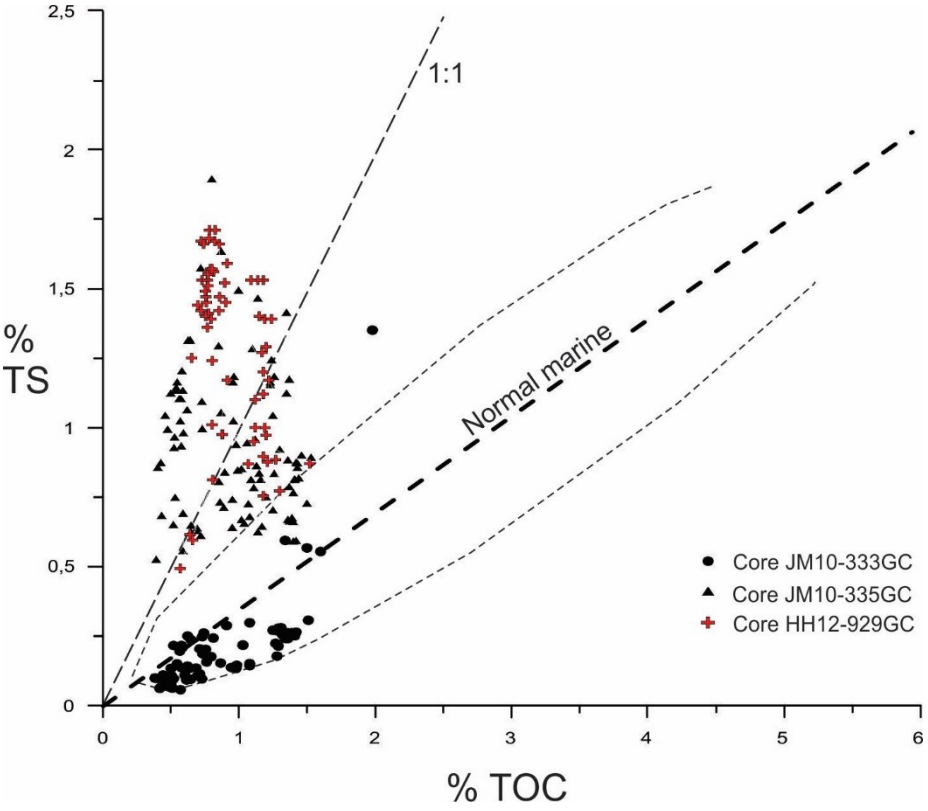

Figure 2. Plot of weight percent total organic carbon versus weight percent total sulfur for two seep cores and a control core. Region enclosed by dashed line represents present-day normal marine sediments. Adapted from Berner and Raiswell (1983).

Figure 3. (a) Planktic (*Neogloboquadrina pachyderma*, black) and benthic (*Cassidulina neoteretis*, red) $\delta^{13}C$ values measured in core JM10-335GC. (b–g) Records for core JM10-333GC (black) and JM10-335GC (gray), (b) TS/TOC ratio, (c) % TOC, (d) mg S/g and %TS, (e) average sedimentation rates, (f) magnetic susceptibility, (g) flux of sulfur. (h) Excess sulfur flux (grey) and estimated AOM rates (green). (i) Flux of pyrite grains and aggregates in core JM10-333GC (black) and JM10-335GC (green) and pyritized burrows in core JM10-335GC (red), (j) estimated methane flux.

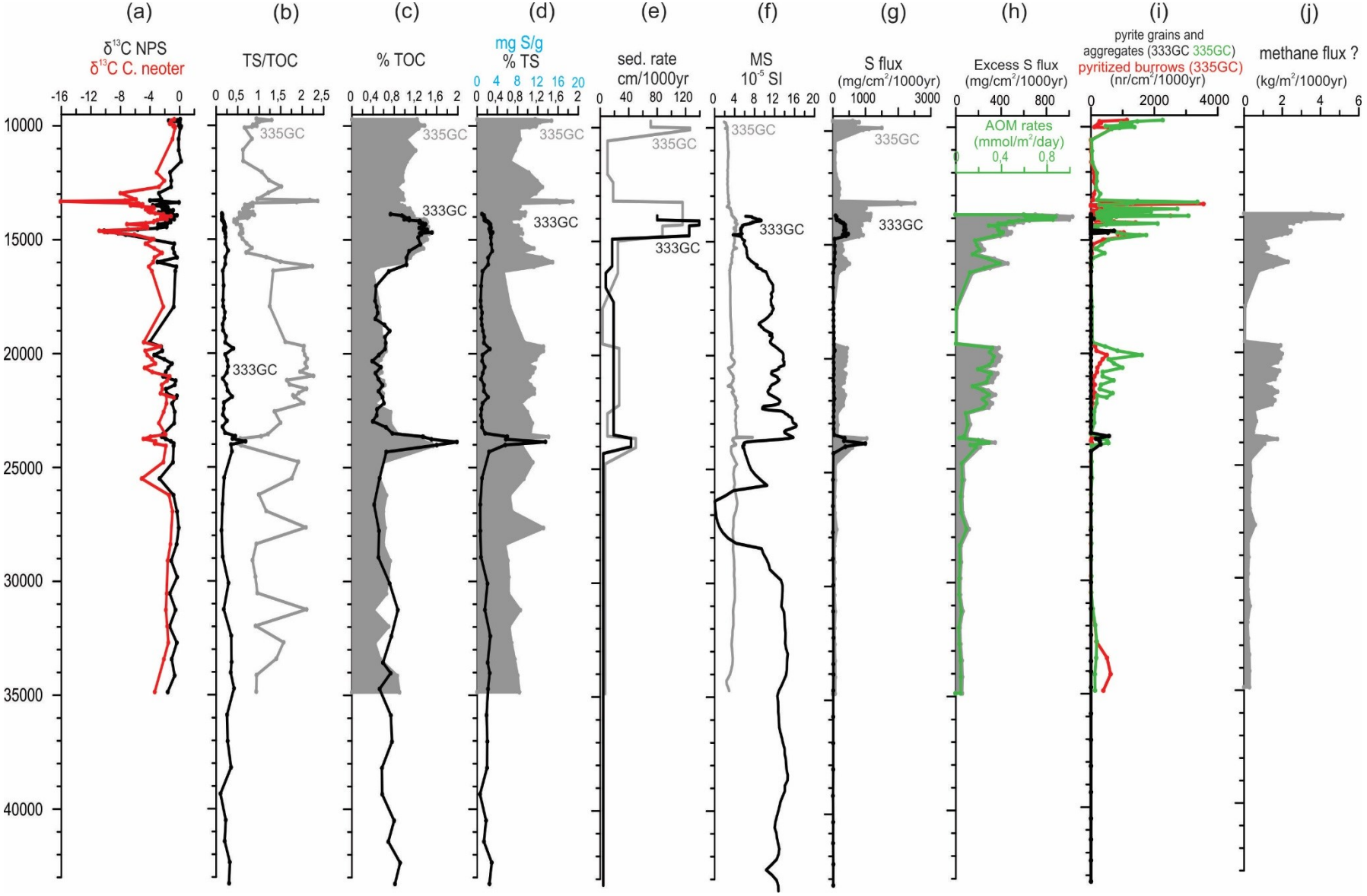
(a)
δ13C NPS
δ13C C. neoter
-16 -12 -8 -4 0
(b)
TS/TOC
0 0,5 1 1,5 2 2,5
335GC
333GC
(c)
% TOC
0 0,4 0,8 1,2 1,6 2
335GC
333GC
(d)
mg S/g
% TS
0 4 8 12 16 20
0 0,4 0,8 1,2 1,6 2
335GC
333GC
(e)
sed. rate
cm/1000yr
0 40 80 120
335GC
333GC
(f)
MS
10-5 SI
0 4 8 12 16 20
335GC
333GC
(g)
S flux
(mg/cm2/1000yr)
0 1000 3000
335GC
333GC
(h)
Excess S flux
(mg/cm2/1000yr)
0 400 800
AOM rates
(mmol/m2/day)
0 0,4 0,8
(i)
pyrite grains and
aggregates (333GC 335GC)
pyritized burrows (335GC)
(nr/cm2/1000yr)
0 2000 4000
(j)
methane flux ?
(kg/m2/1000yr)
0 2 4 6
10000
15000
20000
25000
30000
35000
40000

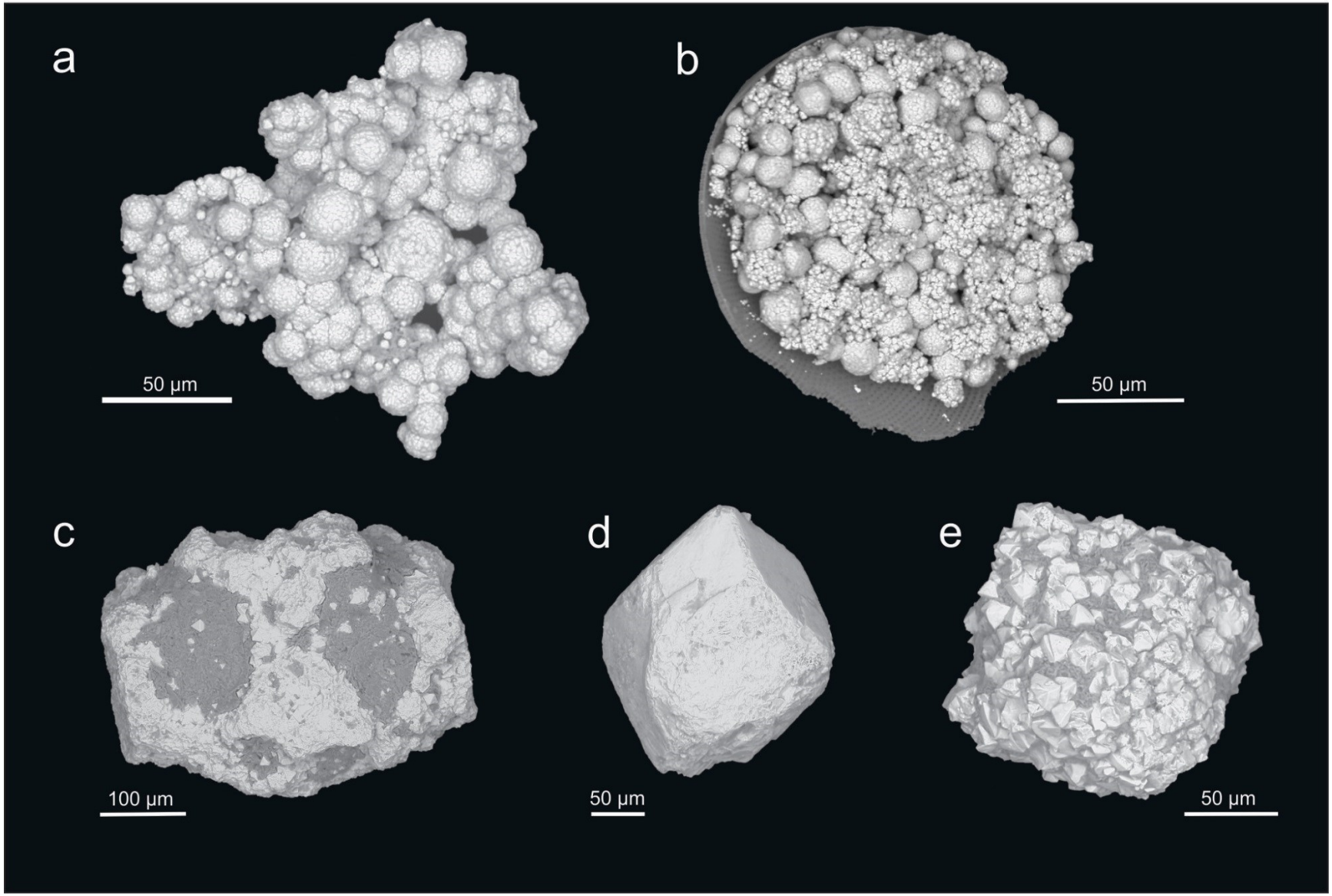

Figure 4. Scanning electron microscope images with examples of pyrite textures: (a–b) framboidal pyrite from core JM10-335GC, (c–e) euhedral and anhedral pyrite from core JM10-333GC (c) and core JM10-335GC (d–e).

Supplementary information for

"Excess sulfur" in sediments from western Svalbard margin as indication for the efficiency of the microbial filter in paleo-anaerobic oxidation of methane (AOM)

Kamila Sztybor, Tine L. Rasmussen and Troels Laier

Lithology and age models of cores JM10-333GC and JM10-335GC

The age models are based on AMS ^{14}C dates, oxygen isotopes, lithology and correlation with the western Svalbard slope MS stack as presented in Fig. S1 and Table S1. Details about age model construction, lithology and stratigraphy were described by Sztybor and Rasmussen (2016). Both cores, the control core JM10-333GC and the pockmark core JM10-335GC contain lithostratigraphic markers typical for the western Svalbard margin: fine silty clay with laminations and a layer of coarse, unsorted sediments (Jessen et al., 2010). Additionally core JM10-335GC contains a layer of fine-grained diatom-rich mud. The fine clay with laminations was interpreted as deposited from deglacial turbid meltwater plumes during the Bølling-Allerød interstadial and the layer of coarse sediments as downslope mass transport deposits formed at the onset of the Last Glacial Maximum (Jessen et al., 2010 and references therein). The horizons were found in other cores from the western Svalbard margin (Jessen et al., 2010; Müller et al., 2009; Müller and Stein, 2014; Rasmussen et al., 2007), and are well dated and together with the magnetic susceptibility signal they can be used as chronostratigraphic markers based on tie-points published by Jessen et al. (2010) (Fig. S1). The age models were calculated assuming linear sedimentation rates between dates and tie-points (Fig. S1, Table S1). All AMS-14C ages were calibrated based on Fairbanks et al. (2005) calibration program.

According to the age models core JM10-333GC dates 43,000 years at the bottom and ~13,800 years at the core top, while core JM10-335GC from the pockmark dates 35,000 years at the bottom and ~9700 years at the top (Fig. S1).

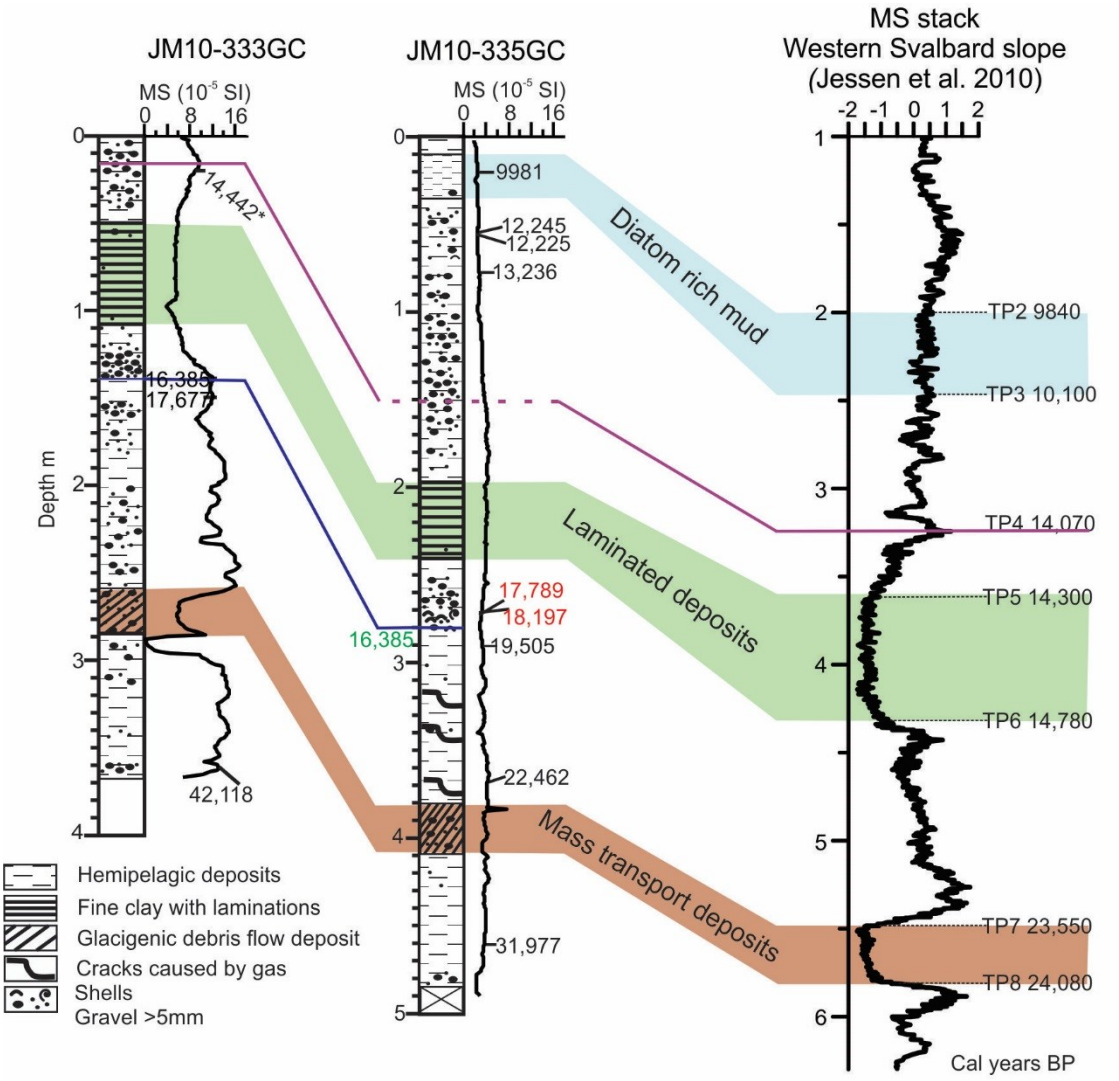

Figure. S1. Correlation between the control core JM10-333GC and pockmark core JM10-335GC and the stacked magnetic susceptibility record for the western Svalbard slope (Jessen et al., 2010), lithological log and calibrated AMS^{14} dates. Three lithological stratigraphic markers are indicated with color shading. Ages in green are based on correlation between the cores, ages in red are considered too old (see Sztybor and Rasmussen, 2016).

Table S1. AMS ^{14}C dates and calibrated ages of cores JM10-333GC and JM10-335GC. Correlation tie points for Western Svalbard slope from Jessen et al. (2010) are shown in italics.

Core	Depth (cm)	Dated material	Laboratory code	Age ($^{14}C \pm 1\sigma$)	Calibrated age $\pm 1\sigma$
Jessen et al., 2010-TP4	18	*N. pachyderma*	—	12,250 ± 150	14,070 ± 210
JM10-333GC	20	mixed benthic foraminifera	Beta-4133010	12,920 ± 40	14,442 ± 119**
Jessen et al., 2010-TP5	50	bivalve	—	12,840 ± 150	14,300 ± 260
Jessen et al., 2010-TP6	110	bivalve	—	13,140 ± 150	14,780 ± 220
JM10-333GC	137	*N. pachyderma*	UBA-23419	14,475 ± 61	16,385 ± 142
JM10-333GC	147	*N. pachyderma*	UBA-23420	15,228 ± 61	17,677 ± 190
Jessen et al., 2010-TP7	258	*N. pachyderma*	—	20,150 ± 130	23,550 ± 185
Jessen et al., 2010-TP8	281	*N. pachyderma*	—	20,580 ± 130	24,080 ± 150
JM10-333GC	359	*N. pachyderma*	Beta-412869	37,420 ± 340	42,118 ± 339
Jessen et al., 2010-TP2	10	planktonic foraminifera	–	9240 ± 100	9840 ± 200
JM10-335GC	20	*N. pachyderma*	UBA-18137	9302 ± 38	9981 ± 111
Jessen et al., 2010-TP3	35	planktonic foraminifera	–	9390 ± 100	10,100 ± 150
JM10-335GC	56	*N. pachyderma*	UBA-23417	10,829 ± 43	12,245 ± 107
JM10-335GC	57	mixed benthic foraminifera	UBA-23418	10,820 ± 43	12,225 ± 106
JM10-335GC	75	*N. pachyderma*	UBA-18138	11,830 ± 44	13,236 ± 69
Jessen et al., 2010-TP5	198	bivalve	—	12,840 ± 150	14,300 ± 260
Jessen et al., 2010-TP6	240	bivalve	—	13,140 ± 150	14,780 ± 220
JM10-335GC	278	*N. pachyderma*	UBA-23197	15,486 ± 73	18,197 ± 189
JM10-335GC	278	bivalve	UBA-18142	15,283 ± 56	17,789 ± 182
JM10-335GC	290	*N. pachyderma*	UBA-18139	16,830 ± 71	19,505 ± 90
JM10-335GC	369	*N. pachyderma*	UBA-18140	19,327 ± 77	22,462 ± 95
Jessen et al., 2010-TP7	380	*N. pachyderma*	—	20,150 ± 130	23,550 ± 185
Jessen et al., 2010-TP8	405	*N. pachyderma*	—	20,580 ± 130	24,080 ± 150
JM10-335GC	460	*N. pachyderma*	UBA-18141	27,132 ± 150	31,977 ± 221
**Unknown reservoir age. Calibrated age may be too old.					